Contributions to the development of active RFID systems at the 433 MHz band

Pere Tuset-Peiró

peretuset@uoc.edu

PhD Thesis Dissertation

Doctoral Programme in Network and Information Technologies

Advisor: Dr. Xavier Vilajosana Guillén

DPCS Research Group

Internet Interdisciplinary Institute

Universitat Oberta de Catalunya

To Esther and Júlia,
joy of my life.

Resum

RFID (Radio Frequency Identification) és una tecnologia d'identificació i seguiment sense fils. Un sistema RFID es compon de tres elements; una etiqueta enganxada a l'objecte a identificar, un interrogador que llegeix les etiquetes dins del seu rang de comunicació, i, finalment, un gestor que interactua amb altres subsistemes dins de la cadena de valor. Les etiquetes contenen un identificador únic i es poden classificar en passives, semi-actives o actives depenent de la font d'energia que els permet comunicar-se. Les etiquetes passives i semi-actives depenen de l'energia proporcionada per l'interrogador per comunicar-se, mentre que les etiquetes actives tenen una bateria que els permet comunicar-se de manera autònoma.

Els sistemes RFID es consideren una alternativa a les tecnologies d'identificació clàssiques, com ara els codis de barres. Els beneficis dels sistemes RFID resideixen en el fet que les etiquetes no requereixen de contacte directe o línia de visió per ser llegides. Avui en dia, els sistemes RFID passius i semi-passius són els més estesos degut el seu menor cost. Els sistemes RFID passius i semi-actius es poden trobar en els sistemes automàtics de seguretat ferroviària o en els sistemes de monitorització de pressió de pneumàtics, entre d'altres. No obstant això, el potencial dels sistemes RFID actius és més alt; a més de comunicar-se de manera autònoma les etiquetes poden dur a terme altres tasques, com ara adquirir i emmagatzemar dades de l'entorn mitjançant sensors, la qual cosa permet noves aplicacions industrials.

Donat el potencial de la tecnologia RFID activa aquesta tesi contribueix al seu desenvolupament centrant-se en les capes més baixes de la pila de protocols, és a dir, la capa física i la capa d'enllaç de dades. Aquestes capes determinen l'abast de la comunicació entre l'interrogador i les etiquetes, el nombre d'etiquetes que un interrogador pot llegir per segon i el consum d'energia que utilitzen les etiquetes en el procés, que són els paràmetres de rendiment clau en un sistema RFID. En particular, la tesi es centra en els sistemes RFID actius que operen a la banda 433 MHz i que estan estandarditzats sota la norma ISO/IEC 18000-7.

A la capa física la tesi avalua els aspectes de propagació de la banda 433 MHz en diferents entorns i els compara amb la banda 2.4 GHz, que s'utilitza en els sistemes RFID actius estandarditzats sota la norma ISO/IEC 18000-4. Els resultats demostren que, per a la mateixa potència de transmissió, els sistemes RFID actius que funcionen a la banda 433 MHz aconsegueixen un millor abast de comunicació gràcies a unes millors característiques de propagació. Els resultats també mostren que la diversitat en freqüència no afegeix fiabilitat als sistemes RFID actius que funcionen a la banda 433 MHz i, per tant, es recomana aplicar altres mecanismes per millorar la robustesa de l'enllaç.

A la capa d'enllaç de dades la tesi proposa un nou protocol d'accés al medi i el compara amb FSA (Frame Slotted ALOHA), el protocol d'accés al medi definit en l'estàndard ISO/IEC 18000-7. LPDQ (Low-Power Distributed Queuing) combina LPL (Low-Power

Listening) per a la sincronització de xarxa i DQ (Distributed Queuing) per a la transmissió de dades. En comparació amb FSA, que només arriba a un rendiment de 36.8% a causa de les col·lisions, LPDQ aconsegueix un rendiment proper a l'òptim (99.5%) independentment del nombre d'etiquetes. A més, LPDQ redueix el consum d'energia de les etiquetes en més d'un 10% respecte el cas òptim de FSA.

Finalment, la tesi presenta una implementació del protocol LPDQ operant a la banda 433 MHz. La implementació utilitza el xip CC430 de Texas Instruments i demostra que LPDQ es pot implementar utilitzant una ràdio comercial i que s'aconsegueix el rendiment i el consum d'energia esperats.

Resumen

RFID (Radio Frequency IDentification) es una tecnología de identificación y seguimiento inalámbrica. Un sistema RFID se compone de tres elementos; una etiqueta pegada al objeto a identificar, un interrogador que lee las etiquetas dentro de su rango de comunicación, y, finalmente, un gestor que interactúa con otros subsistemas dentro de la cadena de valor. Las etiquetas contienen un identificador único y se pueden clasificar en pasivas, semi-activas o activas dependiendo de la fuente de energía que les permite comunicarse. Las etiquetas pasivas y semi-activas dependen de la energía proporcionada por el interrogador para comunicarse, mientras que las etiquetas activas tienen una batería que les permite comunicarse de manera autónoma.

Los sistemas RFID se consideran una alternativa a las tecnologías de identificación clásicas, tales como los códigos de barras. Los beneficios de los sistemas RFID residen en el hecho que las etiquetas no requieren de contacto directo o línea de visión para ser leídas. Hoy en día, los sistemas RFID pasivos y semi-pasivos son los más extendidos debido a su menor coste. Los sistemas RFID pasivos y semi-activos se pueden encontrar en los sistemas automáticos de seguridad ferroviaria y los sistemas de monitorización de presión de neumáticos, entre otros. Sin embargo, el potencial de los sistemas RFID activos es más alto; además de comunicarse de manera autónoma las etiquetas pueden llevar a cabo otras tareas, como por ejemplo adquirir y almacenar datos del entorno mediante sensores, lo que permite nuevas aplicaciones industriales.

Dado el potencial de la tecnología RFID activa esta tesis contribuye a su desarrollo centrándose en las capas más bajas de la pila de protocolos, es decir, la capa física y la capa de enlace de datos. Estas capas determinan el alcance de la comunicación entre el interrogador y las etiquetas, el numero de etiquetas que un interrogador puede leer por segundo y el consumo de energía que emplean las etiquetas en el proceso, que son los parámetros de rendimiento clave en un sistema RFID. En particular, la tesis se centra en los sistemas RFID activos que operan en la banda de 433 MHz y que están estandarizados bajo la norma ISO/IEC 18000-7.

En la capa física la tesis evalua los aspectos de propagación de la banda 433 MHz en diferentes entornos y los compara con la banda 2.4 GHz, que se utiliza en los sistemas RFID activos estandarizados bajo la norma ISO/IEC 18000-4. Los resultados demuestran que, para la misma potencia de transmisión, los sistemas RFID activos que funcionan en la banda 433 MHz logran un mejor alcance debido a sus mejores características de propagación. Los resultados también muestran que la diversidad en frecuencia no añade fiabilidad a los sistemas RFID activos que funcionan en la banda 433 MHz y, por tanto, es recomendado aplicar otros mecanismos para mejorar la robustez del enlace.

En la capa de enlace de datos la tesis propone un nuevo protocolo de acceso al medio y lo compara con FSA (Frame Slotted ALOHA), el protocolo de acceso al medio definido en el estándar ISO/IEC 18000 7. LPDQ (Low-Power Distributed Queuing) combina LPL

(Low-Power Listening) para la sincronización de red y DQ (Distributed Queuing) para la transmisión de datos. En comparación con FSA, que sólo alcanza un rendimiento de 36.8 % debido a las colisiones, LPDQ logra un rendimiento cercano al óptimo (99.5 %) independientemente del número de etiquetas. Además, LPDQ reduce el consumo de energía de las etiquetas más de un 10 % respecto el caso óptimo de FSA.

Por último, la tesis presenta una implementación del protocolo LPDQ operando en la banda 433 MHz. La implementación utiliza el chip CC430 de Texas Instruments y demuestra que LPDQ se puede implementar utilizando una radio comercial y que se consigue el rendimiento y el consumo de energía esperados.

Abstract

RFID (Radio Frequency IDentification) is a wireless identification and tracking technology. A RFID system is composed of three elements; a tag attached to the object to be identified, an interrogator that collects tags within its communication range, and, finally, a manager that interfaces to other subsystems in the application value chain. Tags contain a unique identifier and can be classified into passive, semi-active and active depending on the source of energy that allows it to communicate. Passive and semi-active tags rely on the energy provided by the interrogator to communicate, whereas active tags have a battery that allows them to communicate autonomously.

RFID systems are considered to be an alternative to legacy identification technologies, such as bar codes. The benefits of RFID systems lay in the fact that tags do not require direct contact or line-of-sight to be acquired. Today, passive and semi-passive RFID systems are the most widespread due to its lower cost. Passive and semi-active RFID systems can be found in railway automatic security systems and tire pressure monitoring systems, among others. However, the potential of active RFID systems is higher; in addition to communicate autonomously tags can perform other tasks, e.g., acquire and store environment data using sensors, which enables new industrial applications.

Given the potential of active RFID technology this thesis contributes to its development by focusing on the lowest layers of the stack, i.e., the physical and the data-link layers. These layers determine the tag communication range, packet throughput and energy consumption, which are key performance parameters in an active RFID system. In particular, the thesis focuses on the physical and data-link layer active RFID systems operating at the 433 MHz band, which are standardized under ISO/IEC 18000-7.

At the physical layer the thesis studies propagation aspects of the 433 MHz band in different environments and compares it to the 2.4 GHz band, which is also used in active RFID systems, e.g., ISO/IEC 18000-4. The results demonstrate that active RFID systems operating at the 433 MHz band can achieve better communication range at the same transmit power due its better propagation characteristics. The results also show that channel hopping does not add reliability to active RFID systems operating at the 433 MHz band and, thus, other mechanisms need to be implemented to add robustness.

At the data-link layer the thesis proposes a new MAC (Medium Access Control) protocol and compares it to FSA (Frame Slotted ALOHA), the MAC protocol defined in the ISO/IEC 18000 family. The protocol, named after LPDQ (Low-Power Distributed Queuing), combines LPL (Low-Power Listening) for network synchronization and DQ (Distributed Queuing) for data transmission. Compared to FSA, which only achieves a performance of 36.8% due to the effects of contention, LPDQ can achieve a performance close to the optimal, e.g., 99%, regardless of the number of tags. In addition, LPDQ can reduce tag energy consumption by more than 10% compared to FSA.

Finally, the thesis presents a real-world implementation of LPDQ operating at the 433 MHz band. The implementation uses the Texas Instruments CC430 SoC (System on Chip) and demonstrates that LPDQ can be implemented using off-the-shelf radio transceivers and the performance and energy consumption achieved.

Acknowledgements

Right now I am sitting on a plane on my way back from Santiago de Chile to Barcelona. I have spend a week at Universidad Diego Portales presenting part of the research on active RFID systems that I have conducted over the last three years and that is part of this thesis. I am pretty exhausted and the effects of jet-lag are kicking in, but I will still try to put together a list of acknowledgements without forgetting anyone that has somehow contributed to to its development. If I do, please forgive me in advance.

My first acknowledgement goes to Prof. Diego Dujovne and Prof. Luciano Ahumada, who have invited me to visit Universidad Diego Portales to talk about my research and visit his beautiful country. Also to Dr. Albert Anglès, who I collaborated with in the early stages of my research, and is currently a post-doc researcher at Universidad Diego Portales working in 60 GHz wireless communications. Thank you all for making my visit so interesting from both the technical and the cultural sides. I look forward to meeting you back in Barcelona someday in the near future.

Back in time, my second acknowledgement is for Pere Barberán and Dr. Léonard Janer from Escola Universitària Politècnica de Mataró (EUPMt). Not so long ago they were teaching me the basics of computer communications and operating systems, and are now my work colleagues and friends. I also want to mention the people at the Technology Transfer Section at TecnoCampus Mataró-Maresme: Josep, Roberto, Jordi, Manel, Ariadna, Matias and the others. I kindly remember the two years that I spent working with them on interesting projects related to e-inclusion and e-health.

My next acknowledgement goes to people at the DASH7 Alliance, an organization devoted to the standardization of active RFID technology. I still recall going to Amsterdam on June 2011 and meeting Patrick and JP, which lead the Alliance at that time. Six months later, on December 2011, I was organizing a DASH7 Alliance meeting in Barcelona with more than fifty attendees from all over around the world. Since then I have had the pleasure to meet and work with a lot of interesting people: Chanaka, Yordan, Michäel, Ron, Antti and Maarten among many others.

I am also very grateful to Francisco Vázquez and Dr. Jesús Alonso-Zárate, from Centre Tecnològic de Telecomunicacions de Catalunya (CTTC), and Dr. Luís Alonso, from Universitat Politècnica de Catalunya (UPC). They invited me to spend four months with them back in February 2013 and I recall this as the most productive time of this last three years. Despite they were quite busy with their own research at that time, they found time to discuss theoretical and technical details of my work, which in the end greatly shaped the results presented in this thesis.

A special mention goes to Prof. Kris Pister, who invited me to visit the Swarm-Lab at University of California Berkeley (UCB) for four months back in June 2013, and provided all the *burritos* required to properly conduct research. Also, I want to thank Fabien, David, Michael and all the other people at the SwarmLab who warmly welcomed me and contributed to my research by providing ideas and discussing results. Dr. Thomas Watteyne also deserves a word of gratitude for creating and leading the OpenWSN project. There's only a word for him: poipoi!

Another word of gratitude goes to Marc, David, Enosha, Amna, Guillem, José and the remaining colleagues at the Internet Interdisciplinary Institute (IN3), where I have spent the last three years drinking coffee and working on the thesis. Despite coming from very different countries and knowledge backgrounds they have provided the perfect work environment and very interesting discussions on topics not related to the thesis. Some of them have already finished their journey and some of them are about to complete it, but I am very happy that I have met them.

I also want to thank all people at Hewlett & Packard in Sant Cugat del Vallès who have kindly welcomed me on-board and started to show me the secrets of Thermal InkJet printers. Of them all, I want to have a special word of gratitude to Javier and Anarosa for being brave enough to hire me. to Carles, Fran and Paco for taking the time to bring me up to speed, which is not easy considering the complexity of printers. Finally, to Giorgio, Frederic and Xavier for being the ones that work closer to me in the laboratory and have to endure me on a daily basis.

Last but not least, I want to acknowledge Dr. Xavier Vilajosana, my thesis advisor, as well as Dr. Ferran Adelantado and Dr. Juan Luís Navarro, members of my thesis supervision committee, for their guidance and support these last three years. In particular I want to have a special word of gratitude with Xavier, who has proven to be more than an advisor to me. He has become a good friend and work colleague. I hope that all the endeavours that we have started together over the course of this last year will soon reach a tipping point and make a significant impact.

Finally, and most important, I want to acknowledge the support from my family over the course of my life. My parents, Pere and Ona, who have provided everything that I needed in order to become who I am today and have encouraged me to reach farther. Esther, my wife, who has endured with patience my frustrations and celebrated with enthusiasm my achievements. Without her I probably would not have make it that far. Júlia, my daughter-to-be, who is not yet here but has already make me realize the important things in life. She is the one putting more pressure on me to finish the thesis; she will soon need someone to play with! Also, to my extended and political family: grand-parents, uncles, nieces, cousins and the like. It is needles to say that you also deserve a word of gratitude for being who you are or who you have been.

To all, **thank you!**

Pere Tuset-Peiró
November 2nd, 2014

Table of Contents

List of Figures

List of Tables

1 Introduction

This chapter introduces the topic of the thesis and presents its contributions. In particular, the thesis focuses on active RFID (RadioFrequency IDentification) systems operating at the 433 MHz band and the contributions are at the physical and the data-link layers of the communications stack.

1.1. Overview

RFID (Radio Frequency IDentification) is a wireless communication technology that is used to automatically identify and track objects. RFID constitutes an alternative to traditional identification technologies, such as bar codes, since it is does not require direct line-of-sight. For example, items can be identified while enclosed in a box, thus reducing the time required to identify them. Thanks to its benefits, today RFID technology is ubiquitous in various industrial application domains. For example, RFID technology has been successfully applied to tracking medical items in hospitals and billing of vehicles in road tolls, among many others. However, the cost of RFID technology is higher compared to legacy identification solutions and, thus, its usage is limited to high-value items or when many low-value items are grouped together, e.g., in a container.

In general terms, an RFID system is composed of three types of devices: a manager, an interrogator and one or more tags. Tags are the devices that are attached to the physical items that need to be identified and tracked. Tags contain a unique identifier that is transmitted to the interrogator upon receiving a query. In turn, the interrogator is the device that is responsible of collecting the data from the tags that are located within its communication range. The interrogator can either be fixed or mobile depending on the application requirements. Finally, the manager is the device responsible of collecting the tag inventory and offering it to other subsystems in the application value chain. For example, the tag inventory can be provided through a web service to allow real-time product tracking in a supply chain.

RFID systems can be classified into passive, semi-active and active depending on the source of energy that is available to tags in order to operate and communicate with the interrogator.

Passive RFID tags do not have any means of energy and, thus, rely on the energy provided by the interrogator to operate and communicate. To provide energy to tags the interrogator employs inductive coupling for close range communications, e.g., centimetres, and capacitive coupling for far-field communications, e.g., meters. In turn, tags use backscatter modulation to transmit their unique identifier back to the interrogator, a technique that is based on modulating the power reflected on the receiving antenna. Being passive allows tags to be inexpensive and remain operative without any time restriction, but it limits the communication distance that can be achieved and the amount of information that can be transmitted.

In contrast, semi-active RFID tags are equipped with a battery that enables them to operate without the presence of an interrogator. That is, semi-active tags can use the energy available in the battery to periodically capture information using sensors, e.g., temperature, and store it in an internal memory. Such information can then be retrieved when the collection process is triggered by the interrogator. Thus, semi-active tags allow new applications to be deployed, e.g., tracking temperature in freight containers. However, semi-active tags are still limited by the presence of an interrogator to provide energy for the communication process, which ultimately limits the distance at which tags can be read.

Finally, active RFID tags are also equipped with a battery but do not rely on the interrogator to provide energy through inductive/capacitive coupling and use backscatter modulation to communicate. Instead, active RFID tags have a radio transceiver capable of modulating a carrier to transmit information using the energy from the battery. Such approach increases communication range, e.g., hundreds of meters, and allows active RFID tags to operate in two modes. First, as beacons, transmitting their unique identifier periodically to signal their presence. Second, as passive tags, relying on the interrogator to trigger the collection process. The downside of active RFID is the limited lifetime of tags due to battery self-discharge and the higher price of tags due to the a greater number of components.

RFID technology is defined in various standards ratified by ISO/IEC (International Organization for Standardization / International Electrotechnical Commission). Each standard focuses on a particular aspect of the technology. For instance, the wireless communication interface between an interrogator and tags, e.g., physical and data-link layers in the OSI (Open Systems Interconnect) model, is standardized under the

ISO/IEC 18000 family. The ISO/IEC 18000 family is composed of six parts depending on the operation frequency band and operation mode, e.g., passive, semi-active or active. ISO/IEC 18000-1 [1] defines a reference system architecture and the set of physical and data-link layer parameters to be standardized. Passive and semi-active RFID systems operating at the 135 kHz band, 868/915 MHz band and 2.4 GHz band are standardized under ISO/IEC 18000-2 [2], ISO/IEC 18000-6 [3] and ISO/IEC 18000-4 [4] respectively, whereas active RFID systems operating at the 433 MHz band are standardized under ISO/IEC 18000-7 [5].

At the physical layer ISO/IEC 18000-7 focuses on the 433 MHz band because it is available worldwide as an ISM (Industrial, Scientific and Medical) band, meaning that it can be used without a specific license. The standard defines the number of channels, the modulation scheme and the data rate parameters used by the interrogator and the tags to communicate. In particular, it defines a single 100 kHz channel centred at 433.92 MHz that uses a wide-band FSK (Frequency Shift Keying) modulation scheme with a data rate of 27.7 kbps. The physical layer also defines the signal that is used by the interrogator to wake-up the tags that are within its communication range. The wake-up signal is a 31.25 kHz square wave that lasts between 2.35 to 4.8 seconds. The wake-up signal is transmitted by the interrogator while tags are in a preamble-sampling state, in which they periodically turn on the radio transceiver for a short amount of time to detect a wake-up signal from any interrogator within its communication range. Right after receiving the wake-up signal all tags within the interrogator communication range are expected to remain in a ready state, waiting for a collection command from the interrogator, for a minimum of 30 seconds. If tags do not receive a collection command they go back to the preamble sampling state until the next wake-up signal is successfully received and the data collection process starts again.

At the data-link layer the ISO/IEC 18000-7 standard defines the format of the different packet types, e.g., collection or sleep command, and the channel access mechanism to enable tags communicate with the interrogator. In particular the standard defines the use of FSA (Frame Slotted ALOHA), a random access MAC (Medium Access Control) protocol, as the channel access mechanism. The data collection process using FSA is as follows. Time is divided into fixed-length frames and each frame contains a given number of slots, which are the minimum communication unit between tags and the interrogator. To communicate with the interrogator each tag selects one of the slots in the current frame at random, e.g., using a uniform distribution, and transmit their data. Since two or more tags can transmit their data in the same slot of a given frame a collision between tags may occur, rendering the data of the tags unusable. To recover from a collision event the interrogator provides feedback to tags at the end of each frame. Tags that have been successfully read by the interrogator in the current frame go back to the preamble sampling state, whereas tags that have collided in the current frame remain in the ready state. The process is then repeated with the remaining tags until the interrogator detects that all the slots in the current frame are empty. Such an event indicates that all tags within its communication range have been successfully collected.

As described earlier, active RFID systems operating at the 433 MHz band can achieve a greater communication distance between the interrogator and the tags thanks to the radio transceiver and the batteries, which enables new applications in industrial domains. However, the current synchronization and data transmission mechanisms defined in ISO/IEC 18000-7 are suboptimal in terms of energy consumption, which impacts the overall tag lifetime. Regarding synchronization, the current mechanism is suboptimal in terms of energy consumption because it requires that tags remain in receive mode right after they receive the wake-up signal. Regarding data transmission, the current mechanism is suboptimal in terms of energy consumption because the maximum network utilization is bounded to 37.6% of its theoretical capacity due to the collision probability and the packet retransmissions.

Thus, given the potential impact of active RFID technology in industrial applications and the opportunity to improve the current synchronization and data transmission mechanisms defined in the ISO/IEC 18000-7 standard, this thesis focuses on contributing to its development with two main objectives. First, study the physical layer properties of the 433 MHz band to understand its benefits and drawbacks when compared to the

2.4 GHz band, which is typically used today in other low-power wireless communication technologies, e.g., IEEE 802.15.4 [6]. Second, propose new channel access mechanisms for active RFID systems operating at the 433 MHz band that advance the current state of the art, e.g., ISO/IEC 18000-7, in terms of network utilization and energy consumption.

1.2. Contributions

The object of this thesis is to contribute to the development of active RFID systems operating at the 433 MHz band. Given the relevance of the physical and the data-link layers in active RFID systems to achieve long communication distance, high network utilization and low energy consumption, the contributions made in this thesis are focused on these two layers. The contributions of this dissertation are presented as a collection of five articles that have been published in international peer-reviewed conferences and journals. The first two articles deal with physical layer aspects of active RFID systems operating at the 433 MHz band. Specifically, they investigate the suitability of the 433 MHz band as an alternative to the 2.4 GHz band, which is widely used in other wireless technologies. The next two articles deal with data-link layer aspects of active RFID systems. Specifically, they investigate the combination of LPL (Low-Power Listening) and DQ (Distributed Queuing) as a high performance and low power MAC protocol for active RFID systems. The fifth and final paper leverages on the research conducted in the previous articles to present a demonstrator of an active RFID system that operates at the 433 MHz band and uses a MAC protocol based on LPL and DQ. The list of the articles that are part of this thesis can be found next. The remaining of this section is devoted to summarize the specific contributions made by each paper.

- **Pere Tuset**, Ferran Adelantado, Xavier Vilajosana, Francisco Vázquez, Jesús Alonso. "On the use of the 433 MHz band to Improve the Energy Efficiency of M2M Communications". 24th Anual IEEE Symposium on Personal, Indoor and Mobile Radio Communications (PIMRC 2013). London, United Kingdom. September, 2013.

- **Pere Tuset**, Albert Anglès, José López, Xavier Vilajosana. “On the suitability of the the 433 MHz band for M2M wireless communications: propagation aspects”. Transactions on Emerging Telecommunications Technologies. April 2013 (IF=1.049, 2nd quartile).

- **Pere Tuset**, Francisco Vázquez, Jesus Alonso, Luis Alonso, Xavier Vilajosana. “LPDQ: a self-scheduled TDMA MAC protocol for one-hop dynamic low-power wireless networks”. Special Issue on “Internet of Things”. Elsevier Pervasive and Mobile Computing. November 2013 (IF=1.629, 1st quartile).

- **Pere Tuset**, Francisco Vázquez, Jesus Alonso, Luis Alonso, Xavier Vilajosana. “Experimental energy consumption of FSA and DQ for data collection scenarios”. Special Issue on “Wireless Sensor Networks and the Internet of Things”. MDPI Sensors. June 2014 (IF=1.953, 1st quartile).

- **Pere Tuset**, Francisco Vázquez, Jesus Alonso, Luis Alonso, Xavier Vilajosana. “Demonstrating Low-Power Distributed Queuing for Active RFID Communications at 433 MHz”. IEEE International Conference on Computer Communications (INFOCOM 2014). Toronto, Canada. May, 2014.

The first paper, ”*On the use of the 433 MHz band to Improve the Energy Efficiency of M2M Communications*”, compares the 433 MHz and 2.4 GHz bands in terms of energy consumption. The contribution of the paper is demonstrating that single-hop communications at 433 MHz can be more energy efficient than multi-hop communications at 2.4 GHz. In particular, using the 433 MHz band enables to reduce the number of hops between a device and the gateway, thus leading to a reduction in the overall network energy consumption. Moreover, by reducing the effective data rate of communications it is possible to further reducing the need for multi-hop communications, further reducing the overall network energy consumption.

The second paper, ”*On the suitability of the the 433 MHz band for M2M wireless communications: propagation aspects*”, goes further to investigate the suitability of the

433 MHz band for low-power wireless communications. The paper presents two major contributions. First, it presents an empirical propagation model at 433 MHz for both indoor and outdoor environments that enables to predict link budget depending on node height from ground. Such propagation models are valuable to planning the deployment of networks in these environments because they enable to estimate the overall network coverage. Second, it presents LoS (Line-of-Sight) and NLoS (Non-Line-of-Sight) measurements to determine the effects of multi-path propagation at the 433 MHz band. The results show that, contrarily to the 2.4 GHz band, channel hopping at the 433 MHz band is not able to combat multi-path propagation because the channels are highly correlated. For that reason, the paper proposes that antenna diversity is introduced in order to cope with the effects of multi-path propagation.

The third paper, "*LPDQ: a self-scheduled TDMA MAC protocol for one-hop dynamic low-power wireless networks*", presents LPDQ (Low-Power Distributed Queuing). LPDQ is a MAC protocol targeted at data-collection scenarios using low-power wireless communications. The paper starts by presenting the operation fundamentals of LPDQ, which combines LPL (Low-Power Listening) for network synchronization and DQ (Distributed Queuing) for data transmission. The paper then moves on to discuss the implementation details of LPDQ using off-the-shelf low-power radio transceivers. After that, the paper conducts a series of experiments that demonstrates how LPDQ is able to synchronize the network and create an ad hoc network schedule that operates as a random access protocol under light traffic conditions and smoothly converges to a deterministic access protocol under congestion. Under both traffic conditions LPDQ can achieve an efficiency close to 99%, that is, there are no collisions for data packet transmissions. In addition, LPDQ has two additional features that are interesting for data collection scenarios; it is stable regardless of the number of devices that are present in the network and is fair in terms of resource assignment to nodes.

The fourth paper, "*Experimental energy consumption of FSA and DQ for data collection scenarios*", contributes to the body of knowledge by presenting an energy consumption analysis of DQ (Distributed Queuing). The paper compares the obtained results to FSA (Frame Slotted ALOHA), which is the protocol currently used in standards for data-collection scenarios using low-power wireless communications. The paper starts by modelling both FSA an DQ as a finite-state machine. The paper then conducts empirical measurements to determine the probability of being in each state and the average energy consumption in each state in order to determine the average energy consumption of each protocol. The results show that DQ is less energy efficient when compared to the optimal case for FSA, that is, when the number of slots per frame is equal to the number of devices. This is due to the fact that DQ requires to listen to feedback packets in order to maintain synchronization. However, if an optimization to avoid listening to unnecessary feedback packet protocols is implemented, then DQ becomes more energy efficient than FSA. Thus, the paper concludes that DQ is a suitable protocol for data-collections scenarios using low-power wireless communications.

Finally, the fifth paper "*Demonstrating Low-Power Distributed Queuing for Active RFID Communications At 433 MHz*", demonstrates an active RFID system that operates at the 433 MHz band to minimize the need for multi-hop communications and uses LPDQ at the data-link layer to achieve an improved performance and reduced energy consumption. This demonstrator was successfully presented at IEEE INFOCOM 2104 in Toronto, Canada, and won the Best Demo Runner-up Award.

2 On the use of the 433 MHz band to Improve the Energy Efficiency of M2M Communications

***Abstract**: Due to propagation and interference effects at the 2.4 GHz band, Machine-to-Machine (M2M) wireless communications based on the IEEE 802.15.4 standard typically need multi-hop communications to connect end devices with a gateway. Unfortunately, multi-hop transmissions pose some challenges that are not trivial to solve and may slow down the deployment of M2M networks. For this reason, the IEEE 802.15.4f Working Group (WG) is currently defining the specifications of a new physical layer operating at the 433 MHz band, which offers better propagation conditions and suffers from lower interference levels. In this paper, we analyze the energy consumption of single-hop and multi-hop communications at both 433 MHz and 2.4 GHz. We use realistic propagation models and accurate energy consumption models to conduct a comprehensive assessment of the energy performance at the two frequency bands. The results presented in this paper show that operating at 433 MHz instead of 2.4 GHz can significantly reduce the number of hops between the end device and the gateway, which can be translated into a reduction of the overall network energy consumption.*

2.1. Introduction

The main factor that determines the lifespan of a battery-operated end device in Machine-to-Machine (M2M) wireless communications is the time that the radio transceiver is on, either to transmit or receive a packet, or in idle listening. This time depends basically on two factors: the application requirements, i.e., how often does the device need to communicate, and the Medium Access Control (MAC) protocol, which manages the access to the shared physical medium [7]. While the amount of M2M applications are very diverse and pose a great variety of requirements, the MAC protocols suitable for M2M deployments rely on a small subset of technologies. Among other candidate technologies, both the IEEE 802.15.4 Standard for Low-Rate Wireless Personal Area Networks (WPAN) [6] and the IEEE 802.11 Standard for Wireless Local Area Networks (WLAN) [8] are becoming very strong players into the M2M area. These standards define the specifications of the physical (PHY) and MAC layers for short and medium-range wireless communications and, although they can operate in different license-free bands, they typically operate at the worldwide license-free 2.4 GHz band.

Unfortunately, real-life experience has shown that radio propagation conditions at 2.4 GHz are heavily influenced by the environment, and thus the strength of a transmitted radio signal is severely degraded with the distance and the presence of obstacles [9]. For this reason, wireless M2M networks operating at 2.4 GHz typically require multi-hop communications to connect an end device with its intended destination, e.g., an M2M gateway. Unfortunately, multi-hop links are complex to manage because: i) they require some degree of synchronization among the involved devices, and ii) the execution of routing protocols to determine and update the routes between any end device and its intended destination becomes necessary [10]. Moreover, multi-hop transmissions also lead to lower effective data rates and longer transmission delays. In addition, the amount of networks that today use the 2.4 GHz band with very different transmission power profiles is growing every day, leading to unacceptable cross-standard interference levels that limit their performance [11] and can even block each other.

For all these reasons, the world-wide available license-free Sub-1 GHz bands, i.e., 433 MHz and 868/915 MHz, are gaining interest for M2M Applications as an alternative to overcome the propagation and interferences issues at the 2.4 GHz [12]. Particularly, the path-loss at 433MHz is lower than at 2.4 GHz, and thus transmissions at 433 MHz can be typically done in a single-hop fashion. This makes communications simpler, faster, and more energy-efficient. For this reason, the IEEE 802.15.4f Working Group (WG) has started to define a new amendment to the legacy IEEE 802.15.4 standard that includes a narrowband PHY layer for the 433 MHz band [13]. Several authors have already studied the 433 MHz and 2.4 GHz bands focusing on its propagation properties in different environments. For instance, Tanghe et al. [14] present empirical path loss models at 433 MHz, 868 MHz and 2.4 GHz in a stacked shipping containers environment. However, to the best of our knowledge, there is no study available that focuses on the suitability of the 433 MHz band for M2M communications from an energy perspective. This is the main motivation for the work presented in this paper.

The main contribution of this paper is the analytical comparison between the energy efficiency of wireless communications at 433 MHz and 2.4 GHz bands using single-hop and multi-hop communications. Towards this end, we use two well-known channel propagation and realistic energy consumption models. The results presented in this paper show that the reduction of the number of hops at 433 MHz translate into a reduction of the overall network energy consumption. In addition, in harsh radio environments, i.e., where the path-loss exponent is high, it is possible to extend the coverage and maintain a low power profile without resorting to multi-hop communications even when using low transmission rates. This is mainly due to the fact that the power consumption of the radio transceiver circuitry dominates over the actual transmitted power. For example, for the CC1101 radio transceiver [15], increasing the transmitted power from -30 dBm to +10 dBm (a factor of 10^4) only represents an increase in the current consumption from 12 mA to 30 mA (a factor of 2.5).

The remainder of this paper is organized as follows. Section II presents an overview of the narrowband PHY layer being developed by the IEEE 802.15.4f WG for the 433 MHz band. In Section III, we describe the wireless propagation model used for the analysis presented in this paper, as well as the energy model for single-hop and multi-hop communications. Section IV presents and discusses the obtained results and identifies the conditions for which the overall energy consumption of the wireless devices can be reduced by transmitting in a single-hop fashion. Finally, Section V concludes the paper and outlines future lines of research.

2.2. The IEEE 8021.5.4f Standard: An Overview

The new IEEE 802.15.4f Standard [13] defines three optional PHY layers targeted at low-power wireless communications. Two different narrowband PHY layers are defined to operate at the 433 MHz and 2.4 GHz bands, respectively, and an Ultra-Wide Band (UWB) PHY layer is also defined to operate at the 6-9 GHz band.

The channel organization of the IEEE 802.15.4f Standard at the 433MHz band is depicted in Figure 2.1. The overall bandwidth of 1.74 MHz is split into 15 basic channels of 108 kHz each. The modulation used is Binary Minimum Shift Keying (BMSK) modulation. However, the total available bandwidth, and thus the transmission rate, depends on the number of basic channels used. According to the achievable data transmission rate, three channels can be defined: (*i*) the 31.25 kbps channel, which uses a single 108 kHz basic channel and, therefore, all the 15 channels are available (0 to 14), (*ii*) the 100 kbps channel type is formed of 3 consecutive basic channels and, therefore, only 5 channels of 324 kHz are available (1, 4, 7, 10 and 13), and finally, (*iii*) the 250 kbps channel type is formed of 5 consecutive basic channels and, therefore, only 3 channels of 540 kHz are available (2, 7 and 12). The standard also defines 2 guard bands of 110 kHz at the beginning and the end of the band to avoid interfering with adjacent wireless systems.

Finally, all channel types are orthogonal among channels of the same type, but non-orthogonal between different channel types, as depicted in Figure 2.1. For example, the 250 kbps channel centered at channel 2 interferes with all channels types centered at channels 0, 1, 2, 3 and 4, but not with all the remaining channels.

Type	**Channels**	**Bandwidth**	**Modulation**	**Data rate**
31.25	15	108 kHz	BMSK	31.25 kbps
100	5	324 kHz	BMSK	100 kbps
250	3	540 kHz	BMSK	250 kbps

Table 2.1: IEEE 802.15.4f: physical layer channel properties at 433 MHz.

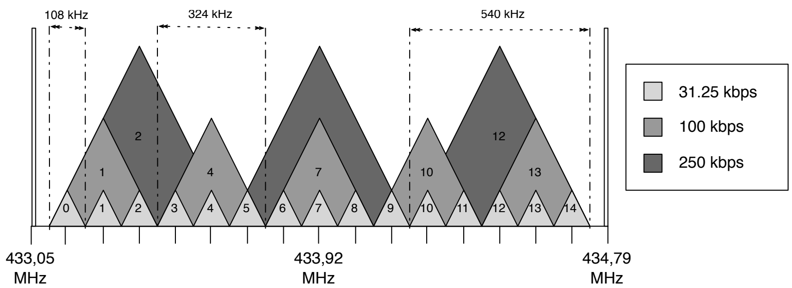

Figure 2.1: IEEE 802.15.4f: physical layer channel organization at 433 MHz.

2.3. System model

The energy efficiency, i.e., the energy measured in Joules required to transmit a single bit, is denoted by E_{bit} and can be defined as (2.1),

$$E_{bit} = \frac{P^m_{TX} + P^m_{RX}}{R_B}[J/bit], \tag{2.1}$$

where R_B is the data rate (bps), and P^m_{TX} and P^m_{RX} are the power consumption of the radio transceiver in transmission and reception modes (mW), respectively.

The energy spent at the receiver depends on the duration of the packet transmission and it is constant for a specific modulation and data rate. However, the power consumed by the transmitter includes both the radio frequency (RF) transmission power and the consumption of the circuitry associated to the transmission chain, referred to as base consumption. While the base consumption is constant and has a nominal value when the radio is on, the transmission power is adjusted, depending on the channel conditions and the receiver sensitivity, to guarantee a given transmission reliability.

The sensitivity (S_{RX}) of the receiver can be defined as the minimum received power (P_{RX}) required to decode a packet with a given reliability, measured in terms of Packet Delivery Ratio (PDR). The sensitivity of a receiver depends on the modulation scheme and the data rate [16]. A robust modulation, i.e., frequency or phase modulation, leads to a higher sensitivity because the signal is less affected by noise and interferences. Similarly, lower data rates lead to higher values of the sensitivity because the amount of energy transmitted per bit is higher.

The average received power between two devices at a distance d can be approximated with the Free Space Propagation Loss (FSPL) model as [17],

$$P_{RX} = \frac{P_{TX}}{L} = P_{TX}\left(\frac{c}{4\pi f d}\right)^{\gamma}, \tag{2.2}$$

where P_{TX} and P_{RX} are the transmitted and received power respectively, and L is attenuation introduced by the channel. The average received power depends on the distance between transmitter and receiver (d), the central frequency of the transmitted signal (f), and the path-loss exponent (γ). The value of this exponent depends on the environment [18]. For example, in free-space, the path-loss exponent is $\gamma = 2$, while $\gamma = 3.6 - 5.1$ in a Non-Line-of-Sight (NLoS) mobile-to-mobile environment [19]. However, in real wireless channels, the instantaneous received power is affected also by small- and large-scale effects, called fast fading (due to multi-path transmissions) and shadowing (due to obstacles and clutter). However, in this paper we focus on coverage, which can be estimated from the average received power obtained considering only the path-loss.

In order to ensure that a packet is received with a certain probability, it must hold that $P_{RX} \geq S_{RX}$. According to (2.2), it is then possible to write that the maximum distance D_{MAX} at which two devices can communicate with a single-hop is:

$$D_{MAX} \leq \left(\frac{P_{TX}}{S_{RX}}\right)^{\frac{1}{\gamma}}\left(\frac{c}{4\pi f}\right). \tag{2.3}$$

If two devices are separated by more than D_{MAX}, then multi-hop transmissions will be needed. If this is the case, the devices that lie in between the source and the destination will act as relays, forwarding the packets to the subsequent device until it reaches the destination. The specific devices used for forwarding are selected by a routing protocol at the network layer which can have either static or dynamic routes. In this paper, we will consider that if more than one hop is required, the distance between two contiguous devices is constant and equal to $d_{hop} = D/N$, with N the number of equally-spaced hops between source and destination. With this assumption, it is possible to compute the minimum number of hops as

$$N_{min} = \left\lceil \frac{D}{D_{MAX}} \right\rceil = \left\lceil D \left(\frac{S_{RX}}{P_{TX}} \right)^{\frac{1}{\gamma}} \left(\frac{4\pi f}{c} \right) \right\rceil . \tag{2.4}$$

Combining (2.1) and (2.4), the energy to transmit a bit E_{bit} between two devices considering the minimum number of hops N_{min} can be written as

$$E_{bit} = \left\lceil D \left(\frac{S_{RX}}{P_{TX}} \right)^{\frac{1}{\gamma}} \left(\frac{4\pi f}{c} \right) \right\rceil \left(\frac{P_{TX}^{m} + P_{RX}^{m}}{R_B} \right) . \tag{2.5}$$

It is worth noting that E_{bit} has discontinuities as the distance D increases due to the ceil function used to model energy consumption in (2.5).

2.4. Numerical results

In this section, the achievable energy efficiency operating at both the 433 MHz and the 2.4 GHz bands is presented considering different channel conditions, i.e., path-loss exponent, and radio transceiver characteristics, i.e., sensitivity and power consumption. Specifically, two sets of numerical evaluations have been conducted. The first set of results is based on theoretical values obtained for all the input parameters (path-loss, sensitivity and energy consumption), while the second set of results is based on a combination of parameters obtained from real-world measurements (path-loss and sensitivity) and the transceivers' data-sheets (energy consumption).

The values of the parameters used for the numerical evaluation are summarized in Table 2.2, Table 2.3, and Table 2.4 respectively. They have been selected according to the specifications of two real radio transceivers operating with the IEEE 802.15.4 standard at 2.4 GHz and the IEEE 802.15.4f standard at 433 MHz. These are the Atmel AT86RF230 [20] and the Texas Instruments CC1101 [15] radio transceivers, respectively. Note that the minimum transmission power for the AT86RF230 radio at 2.4 GHz is -17 dBm, whereas for the CC1101 radio at 433 MHz is -30 dBm.

Finally, it is important to mention that the results presented only take into account the energy required for the radio transmissions at the PHY layer, without considering higher layers of the protocol stack. For example, in the case of multi-hop transmissions, the energy required to exchange control messages required for the routing protocol has not been taken into account. Therefore, the energy consumption analyzed herein for the multi-hop case is only a lower-bound of the actual energy consumption.

2.4.1. Theoretical results

Numerical results have been obtained for 3 different values of the path-loss exponent, i.e., $\gamma = 2$, $\gamma = 3$ and $\gamma = 4$. The results are presented in Figure 2.2 and show that the path-loss exponent γ has a great influence on the overall energy consumption of the network. Higher path-loss exponents lead to a higher number of hops (i.e., more relays are needed to enable end-to-end communications) thus leading to higher overall network energy consumption. However, this behavior is tightly bound to the data transmission rate.

For example, when $\gamma = 3$ and the distance between source and destination is $d =$ 100 m communications at 2.4 GHz and 250 kbps require a total of 8 hops. This translates into an energy efficiency of 40 nJ/bit. In its turn, at 433 MHz and 250 kbps, only 1 hop is required to enable end-to-end communications. This translates into an energy efficiency of 0.55 nJ/bit, which is 72 times lower than at 2.4 GHz. However, when considering a lower transmission rate, for example 100 kbps or 31.25 kbps, the energy efficiency at 433 MHz becomes 15 nJ/bit and 40 nJ/bit, respectively, becoming very close to the

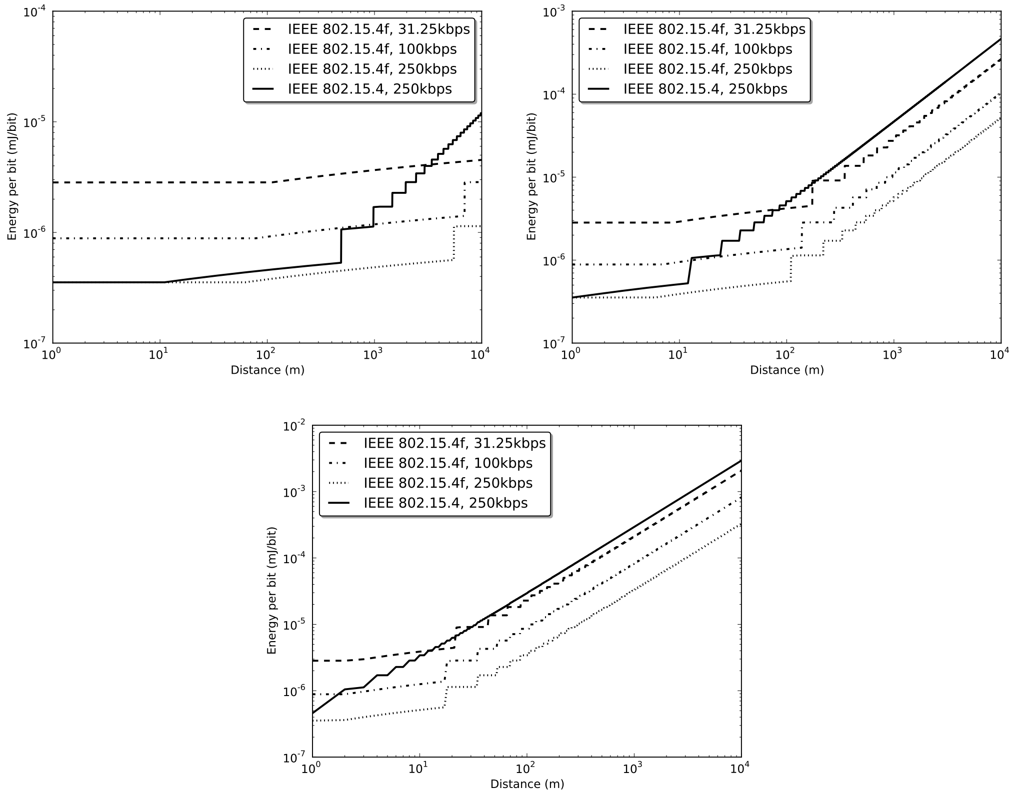

Figure 2.2: Energy efficiency of IEEE 802.15.4 at 2.4 GHz and IEEE 802.15.4f at 433 MHz for different theoretical γ. From left to right $\gamma = 2, 3, 4$.

values achieved at 2.4 GHz.

Therefore, in those environments where high γ values are expected, e.g., city-wise or indoor deployments, the 433 MHz band yields a significant reduction in the number of hops and, thus, increases the overall network energy efficiency and lifespan, even for lower data rates.

2.4.2. Measured results

In this subsection, we present the results based on real-world measurements of sensitivity and path-loss, as well as the transceiver parameters specified by the manufacturers in its data-sheet. These results enable to compare the real energy consumption at these frequencies under single-hop and multi-hop communications.

The sensitivity S_{RX} is a parameter that is not provided for the different IEEE 802.15.4f channel types, i.e. 31.25 kbps, 100 kbps and 250 kbps, in the CC1101 data-sheet [15]. Therefore, we have characterized it by experimentally measuring it for both CC1101 and AT86RF230 transceivers and each channel type at 433 MHz and 2.4 GHz respectively. The procedure to determine the sensitivity has been the following: a transmitter and receiver have been connected with wires through a JWF 50PA-51 [21] programmable channel attenuator. For each value of the channel attenuation, from 70 dB to 100 dB in steps of 6 dB, the transmitter sends a total of 1024 packets with a length of 34 bytes (4 bytes of PHY layer preamble, 4 bytes for synchronization information, 24 bytes of payload, and 2 bytes for redundancy in the form of Cyclic Redundancy Check) and a transmission power of 0 dBm. The nominal value of the transmission power has also been characterized using a Rigol DSA815 [22] spectrum analyzer, and the result is that the actual transmission power is -1.2 dBm in the 3 dB bandwidth. For each value of the channel attenuation, the value of the sensitivity for a target value of a $PDR > 0.9$ has been obtained. The sensitivity for both standards is presented in Figure 2.3 and summarized in Table 2.2 for the different channel types.

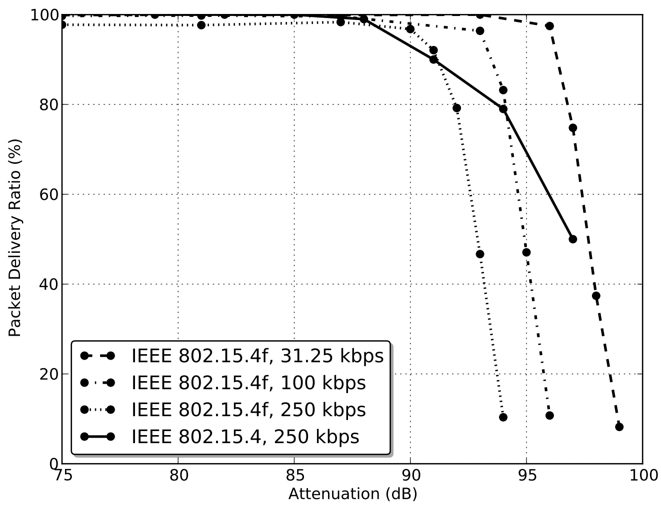

Figure 2.3: Sensitivity measurements for IEEE 802.15.4 at 2.4 GHz and IEEE 802.15.4f at 433 MHz.

The values of the path-loss exponent γ have been measured for the 433 MHz and

Standard	Channel	Modulation	Sensitivity
IEEE 802.15.4f	31 kbps	MSK	-96 dBm
IEEE 802.15.4f	100 kbps	MSK	-93 dBm
IEEE 802.15.4f	250 kbps	MSK	-91 dBm
IEEE 802.15.4	250 kbps	OQPSK	-91 dBm

Table 2.2: Sensitivity summary for IEEE 802.15.4f at 433 MHz and IEEE 802.15.4 at 2.4 GHz.

2.4 GHz bands using two different antenna heights of $h = 70$ cm and $h = 210$ cm. Note that the transmitter and receiver have been placed at the same height in both cases. The measurements have been conducted outdoors in Line of Sight (LoS) conditions using the following procedure: a for each distance from 1 to 100 meters, in steps of 10 meters, the transmitter transmits a total of 1024 packets with the same format used for the characterization of the sensitivity. The Received Signal Strength (RSS) has been measured for of each incoming packet, and the results have been averaged. Finally, the the path-loss exponent has been calculated by using a linear regression method. The values of γ obtained for the two considered frequencies and heights are presented in Table 2.3 and the measurement of the RSS is depicted in Figure 2.4. It is worth noting that when $h = 70$ cm, the path-loss exponent γ at 433 MHz is larger than at 2.4 GHz, i.e., $\gamma_{433} = 2.75$ and $\gamma_{2.4} = 2.29$, respectively. At $h = 70$ cm the first Fresnel zone is clear at 2.4 GHz but not at 433 MHz. Thus, additional power losses are introduced at 433 MHz due to the diffraction effects introduced by the channel.

Band	$h = 70$ cm	$h = 210$ cm
433 MHz	$\gamma = 2.75$	$\gamma = 2.29$
2.4 GHz	$\gamma = 2.29$	$\gamma = 2.29$

Table 2.3: Path-loss exponents (γ) at $h = 70$ cm and $h = 210$ cm for the 433 MHz and 2.4 GHz bands.

The values of the transmission and reception power consumptions for the two transceivers have been obtained from the respective data-sheets considering a supply voltage $V = 3$ V. The current consumption in both cases can be considered constant regardless of the modulation and the data rate. Contrarily, the current consumption in transmit mode depends on the current required to power the transceiver circuitry (I_{BASE}) and the current re-

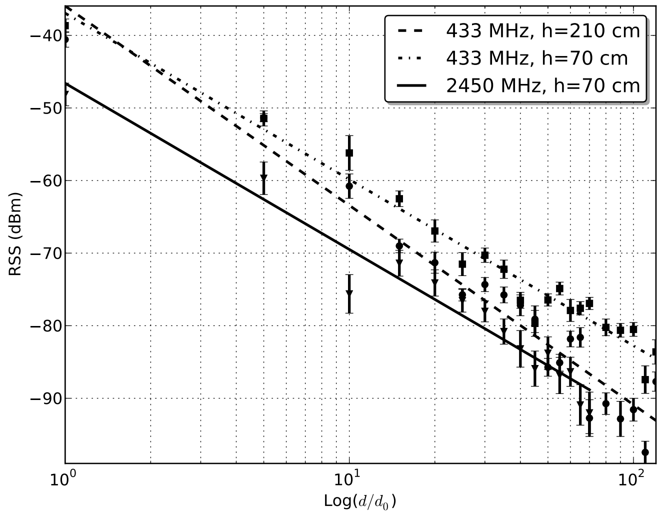

Figure 2.4: Propagation measurements for IEEE 802.15.4 at 2.4 GHz and IEEE 802.15.4f at 433 MHz.

quired to output a certain power ($I_{TX}(dBm)$), e.g., 0 dBm. Using the data available in the data-sheet for the two transceivers, the power in transmit mode depending on the actual transmit power has been approximated using the following linear function,

$$P_{TX}^m = V \cdot (I_{BASE} + I_{TX}(dBm)), P_{RX}^m = cte. \tag{2.6}$$

The values of the receive and transmit power consumption for the two transceivers are summarized in Table 2.4.

Transceiver	P_{RX}^m **(mW)**	P_{TX}^m **(mW)**
CC1101	52.5	$3 \cdot (10.0 + 0.45 * (P_{TX} + 30))$
AT86RF230	46.5	$3 \cdot (9.5 + 0.3 * (P_{TX} + 17))$

Table 2.4: Transmit and receive power for the Atmel AT86RF230 and the Texas Instruments CC1101 radio transceivers.

The energy consumption for the values of γ in Table 2.3 depending on node height ($h = 70$ cm, $h = 210$ cm) and operating frequency (433 MHz and 2.4 GHz) are presented in Figure 2.5. The results have been obtained using the transceiver parameters for the different channel configurations presented in Table 2.2 and Table 2.4, respectively.

For $h = 70$ cm ($\gamma_{433} = 2.75$, $\gamma_{2450} = 2.29$), transmissions at the 2.4 GHz band at

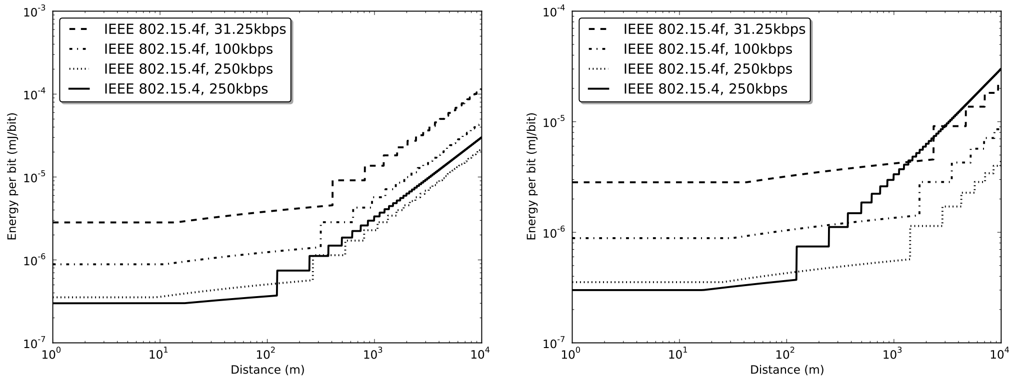

Figure 2.5: Energy consumption of IEEE 802.15.4 at 2.4 GHz and IEEE 802.15.4f at 433 MHz for real values of γ. Left $\gamma_{433} = 2.75$ and $\gamma_{2.4} = 2.29$. Right $\gamma_{433} = 2.29$ and $\gamma_{2.4} = 2.29$.

250 kbps are more energy efficient than at 433 MHz up to a distance of $d = 130$ m. This is due to fact that the AT86RF230 transceiver utilizes less power than the CC1101 in transmit and receive modes, as presented in Table 2.4. When the distance between transmitter and receiver increases transmissions at the 2.4 GHz band require multi-hop communications. However, when transmitting at 433 MHz and at 250 kbps single-hop communications can be maintained up to a distance of $d = 280$ m. When the distance is greater than $d = 280$ m, transmissions at 433 MHz band and at 250 kbps also require multi-hop communications. However, in this case, the energy efficiency is still better than at 2.4 GHz (30%), due to the fact that less hops are required for end-to-end communications. In contrast, at 100 kbps and 31 kbps the energy efficiency at 433 MHz is lower than at 250 kbps, either at 433 MHz or at 2.4 GHz, because the increase in the sensitivity does not compensate the higher energy per bit required to enable end-to-end communications.

For $h = 210$ cm ($\gamma_{433} = \gamma_{2450} = 2.29$) transmission at 2.4 GHz and 250 kbps are more efficient than at 433 MHz and 250 kbps up to a distance of $d = 130$ m. When the distance is greater than $d = 130$ m, transmissions at the 2.4 GHz band require two or more hops, thus increasing the energy consumption per bit despite the fact that each device can reduce its transmit power. Contrarily, at the 433 MHz band and at 250 kbps, single hop communications can be maintained up to a distance of $d = 1$ km for the same data rate, thus increasing the energy efficiency of the network. Furthermore, as the distance increases, even lower data rates, i.e., 31 kbps and 100 kbps, become more energy efficient than at 2.4 GHz in spite of the higher initial energy per bit and the longer transmission time. This effect is caused by the fact that the overall energy consumption is dominated by the energy required to power each transceiver, either in transmit or receive mode, and not the actual energy required to transmit a bit with a certain transmit power.

Therefore, from the numerical results based on real path-loss and sensitivity measurements it is possible to conclude that transmitting at the 433 MHz band can reduce the energy per bit required for end-to-end communications compared to doing so at 2.4 GHz, thus increasing the energy efficiency and lifespan of a network. This holds true even when considering a worse path-loss exponent $\gamma_{433} > \gamma_{2.4}$ caused by the diffraction effects introduced by the larger Fresnel zone.

2.5. Conclusions

In this paper, we have used well-known propagation and energy consumption models to determine the energy efficiency of single-hop and multi-hop communications at the 433 MHz and 2.4 GHz bands using both theoretical and realistic path-loss exponents, power consumption and sensitivity values. Results show that communications at 433 MHz minimize the need for multi-hop communications and thus reduce the energy consumption of the overall network.

Nevertheless, there are several aspects that remain open to be analyzed in order to determine the suitability of using the 433 MHz band for Machine-to-Machine (M2M) communications. In particular, our future work will be aimed at including the effects of shadowing and fading in the propagation model, as these effects largely impact the communication performance [23]. In addition, we will also investigate the effects of interference on the Packet Delivery Ratio (PDR). The fact that the transmission range at 433 MHz is larger than at 2.4 GHz, as well as the fact that it uses narrowband channels instead of spread spectrum, makes systems operating at 433 MHz more prone to interference from other wireless systems.

3 On the suitability of the 433 MHz band for M2M low-power wireless communications: propagation aspects

Abstract: *The 433 MHz band is gaining relevance as an alternative to the 2.4 GHz band for M2M communications using low-power wireless technologies. Currently two standards are being developed that use the 433 MHz band, DASH7 Mode 2 and IEEE 802.15.4f. The article presents propagation models based on measurements conducted at the 433 MHz and 2.4 GHz bands that can be used for link budget calculations in both outdoor and indoor environments depending on node height. The results obtained show that the 433 MHz band has a better communication range both in indoor and outdoor environments despite the negative effects of having a larger Fresnel zone. In addition, indoor propagation measurements are conducted in LoS and NLoS conditions to determine the suitability of channel hopping to combat the effects of multi-path propagation. Contrarily to the 2.4 GHz band, the results show that channel hopping at the 433 MHz does not provide any link robustness advantage because the channel coherence bandwidth is larger than the whole 433 MHz band bandwidth and, thus, all channels are highly correlated.*

3.1. Introduction

Machine-to-Machine (M2M) communications refer to the set of technologies that are used to connect systems for the purpose of remote monitoring and control without human intervention. To connect end devices with the surrounding infrastructure, M2M communications typically rely on cellular or low-power wireless technologies. For low-power wireless technologies the 2.4 GHz band is commonly used for two main reasons. First, the 2.4 GHz band is part of the ISM (Industrial, Scientific and Medical) bands meaning that it is available world-wide without requiring a license. Second, the IEEE 802.15.4 standard [6] defines the use of the 2.4 GHz band for Low-Rate Wireless Personal Area Networks (LR-WPAN) and, thus, many off-the-shelf transceivers are readily available from different manufacturers. Today IEEE 802.15.4 networks have already been successfully deployed in various environments, i.e. industrial monitoring, but there are several factors that may limit its suitability. For example, in industrial environments IEEE 802.15.4 suffers from high attenuations caused by concrete walls and metallic surfaces. In addition, in such scenarios IEEE 802.15.4 networks have to cope with interferences coming from other narrowband and broadband wireless technologies operating at the same band with higher transmit power [24, 25], e.g. IEEE 802.11 and IEEE 802.15.1.

To overcome these limitations two approaches are used in IEEE 802.15.4 networks. First, the use of DSSS (Direct-Sequence Spread Spectrum) helps improving coexistence with narrowband and broadband interferences. Second, channel hopping also contributes to mitigate the effects of interferences, either narrowband or broadband, and also combats the effects of multi-path propagation [26]. In that sense IEEE 802.15.4e [27] has recently been approved as part of the IEEE 802.15.4 standard and an open source reference implementation already exists [28]. In addition to spread spectrum techniques, the use of the 868 MHz and 915 MHz bands has also been devised as an alternative to overcome the limitations of the 2.4 GHz band in certain environments. These bands are also part of the IEEE 802.15.4 standard and offer better propagation and interference characteristics thanks to its lower operating frequency and data rate, as well as because fewer wireless systems currently make use of these bands. However, these bands do not represent a true alternative to the 2.4 GHz band because ubiquitous deployment is limited by existing regulations [29, 30]. The 868 MHz band allows a transmit power up to 14 dBm (25 mW) but is not a part of the ISM bands and, thus, it is only available in the European Union (EU). Moreover, channel hopping is not available at the 868 MHz band because only one channel is available. On its behalf, the 915 MHz band enables transmit powers up to 30 dBm (1 W) and is part of the ISM bands, but usage is limited to the United States (US).

Recently the 433 MHz band has re-gained momentum as an alternative to the 868/915 MHz and 2.4 GHz bands. Compared to the former, the 433 MHz band is a true ISM band and, thus, it is available (almost) world-wide without requiring a license. Compared to latter, the 433 MHz band has better propagation characteristics due to its lower operating frequency and is currently less affected by external interferences due to the lower number of systems operating at the band. Given its interesting properties and the possible impact in M2M communications, there are two standardization organizations that are currently defining physical layers that operate at the 433 MHz band, e.g. DASH7 Mode 2 [5] and IEEE 802.15.4f [13]. Nevertheless, despite the efforts that have already been conducted, there are still aspects at the physical layer that require further investigation in order to understand its properties and determine which frequency band is more suitable depending on application requirements. Thus, we currently focus in evaluating the physical layer characteristics of the 433 MHz band and compare it to the 2.4 GHz band. Specifically, we focus this article in evaluating and comparing the propagation aspects of both bands in different environments, e.g. indoor and outdoor, to determine its suitability for M2M communications using low-power wireless technologies. For example, better propagation may lead to a reduction in the requirements of multi-hop communications and, thus, decrease the overhead introduced by routing protocols [31].

The contributions of the article are the following. First, it presents an overview of the low-power standards currently being developed at the 433 MHz band for M2M wireless communications. Second, it conducts empirical measurements to demonstrate the benefits and drawbacks of the 433 MHz band compared to the 2.4 GHz band in both outdoor and indoor scenarios at different node heights from ground level. Third, it evaluates the behavior of channel hopping against multi-path propagation at the 433 MHz band both in LoS (Line of Sight) and NLoS (Non-Line Of Sight) indoor environments. Therefore, our results contribute to the understanding of the propagation properties of the 433 MHz band and demonstrate that, under similar conditions, 433 MHz propagation is better in terms of range than 2.4 GHz. In addition, the obtained empiric propagation models can be useful for the deployment of M2M wireless communications in both outdoor and indoor environments where nodes have to be deployed at different heights.

The remainder of the article is organized as follows. Section 2 presents the work related to propagation at the 433 MHz and 2.4 GHz bands and introduces the different low-power wireless communication standards that are currently developed at the 433 MHz band. Section 3 presents the theoretical background related to the propagation aspects of wireless communications. Section 4 presents the experimental methodology that we have used to evaluate and compare the propagation aspects of the 433 MHz band with the 2.4 GHz band. The corresponding results of the experiments are presented and discussed in Section 5. Finally, Section 6 concludes the article.

3.2. Theoretical propagation models

The main characteristics that determine the performance of any wireless communication system are interference and propagation. Interference determines how noise and other wireless systems operating at or near the carrier frequency affect the performance of the system under consideration. On its behalf, propagation determines how the power of an electromagnetic wave that propagates through space falls off depending on the distance between the transmitter and the receiver, as well as the characteristics of the surrounding environment. This phenomenon is well modeled with the log-normal propagation model described in Equation 3.1 [32, 33, 17, 34].

$$\begin{aligned} RSS(d,h) &= RSS(d_0,h) - 10\gamma(h)log_{10}(d/d_0)+ \\ &+\psi_{shad};\ d \geq d_0 \\ RSS(d_0,h) &= P_t + G_{TX} + G_{RX} - A - L_g(h) \end{aligned} \tag{3.1}$$

where $P_t(dBm)$ is the transmit power, G_{TX} and G_{RX} in dBi are the transmitter and receiver antenna gains, and A is a constant called intercept factor, expressed in dB, which depends on the receiver antenna effective area (and hence the wavelength) as well as the average channel attenuation at a given initial distance d_0, as shown in Equation 3.2 [17]. $L_g(h)(dB)$ models the diffraction losses, i.e. the power losses attributed to the first Fresnel zone obstruction. The Fresnel zone is a concept related to the diffraction of waves that determines the region of the space that defines the condition of visibility between the transmitter and receiver antennas. In Line Of Sight (LoS) conditions, the first Fresnel zone is free and thus the received power is proportional to the propagation losses. In Non-Line Of Sight (NLoS) conditions, the first Fresnel zone is obstructed by an obstacle that causes diffraction.

All the parameters presented above are combined by $RSS(d_0,h)$ at $d = d_0$. γ is known as path loss exponent which represents the falloff of the received power with the distance, i.e. the slope. The path loss exponent is frequency independent and environment specific. For environments close to free space $\gamma = 2$, which in turn transforms Equation 3.1 to the free space propagation model [17]. For more complex environments such as near ground, it is best to estimate γ together with $RSS(d_0,h)$ to minimize the mean square error between the model and the empirical measurements. In such environments the value of γ is typically between 2 and 4, or more, depending on whether the path is LoS or NLoS [33, 32]. Finally, $\psi_{shad}(dB) \sim N(0,\sigma_{shad})$ is a zero mean log-normally distributed random variable with standard deviation $\sigma_{shad}(dB)$ which models the received power variations around the propagation model caused by multipath propagation [35], either shadowing or fading. Most empirical studies show standard deviations between $0.4dB$ and $4dB$ [33, 36].

$$A = 20log_{10}(\frac{4\pi d_0}{\lambda}) \tag{3.2}$$

3.3. Related work

3.3.1. Propagation models at 433 MHz and 2.4 GHz

There are some studies that have already conducted experimental propagation measurements at the 433 MHz band and 2.4 GHz bands. Thelen et al. [37] carried out measurements in a potato field at the 433 MHz band. In their study they took two series of measurements that expanded over a two week period each and checked three main aspects. First, the reception rate depending on the received power to determine the receiver sensitivity. Second, the variation of the received power according to the distance between the transmitter and the receiver with the growth stage of the potato crop. Third, the influence of micro-climate (temperature, relative humidity and rain) on the received power. Whilst the paper verifies that the foliage and micro-climate has an impact on the propagation of radio waves, it fails to validate how well the proposed model fits the empiric data in the specific environment. At the 2.4 GHz band, Holland et al. [38] investigated radio propagation aspects using Tmote Sky motes. In the experiments they measured received power, signal quality and packet reception as a function of distance, angle and transmit power, in both indoor and outdoor environments taking into account environmental conditions. The results show that mote position and height have a great impact on received power and link quality, but the authors do not present any propagation model that can be useful for link budget planning. Finally, in [39] the authors conduct propagation measurements in the military UHF bands, which include the 433 MHz band, to characterize path loss of narrowband channels in urban terrain for ground based communications. The results, obtained using RF equipment, show that the mean received power in LoS conditions matches two-ray propagation theory and is not affected by street width.

More recently, Zhang et al. [40] measured propagation characteristics at the 433 MHz and the 2.4 GHz bands in an orchard environment with different peach tree heights and fruit densities. Specifically, they evaluated the channel fading and the packet loss rate for different antenna heights. From the results they conclude that the antenna height influence at the 433 MHz band is slightly larger, but the initial path loss at the 2.4 GHz band is greater. In addition, they found that for their particular environment the optimal antenna height is 3.5 m. Nevertheless, they also fail to present a propagation model that can be useful for link budget planning. Wennerström et al. [41] focused on the PRR (Packet Received Ratio) and RSS (Received Signal Strength) behavior against meteorological conditions (temperature and humidity) in a two week period using TelosB motes. Their experimental results demonstrate that temperature and humidity variations influence the PRR. They assume that the RSS variations are correlated with temperature and humidity variations but fail to take into account that the RSS variation can be also attributed to multipath propagation (shadowing and fading). Finally, in [14] the authors present empirical path loss models at different frequencies for an environment of stacked shipping containers. In particular, they conducted measurements for intra- and inter-container communications at the IEEE 802.15.4 bands, e.g. 433 MHz, 868 MHz and 2.4 GHz, as well as for extra-container communications using the GSM/UMTS bands, e.g. 900 MHz, 1850 MHz and 2100 MHz. For the inter-container measurements the results show that path loss is lowest at 433 MHz band in the pathways between container rows, and lowest at 2.4 GHz band in the small gaps between adjacent containers.

Other interesting articles related to propagation aspects at the 433 MHz and the 2.4 GHz bands in different environments include [42, 43, 44, 45].

3.3.2. Overview of 433 MHz standards

As stated earlier, the 433 MHz band has recently gained relevance as an alternative to the 868/915 MHz and 2.4 GHz bands for different reasons. First, compared to 868/915 MHz it is available (almost) world-wide without the need of a license. Second, compared to 2.4 GHz it has better propagation characteristics due to its lower operating frequency. Nevertheless the 433 MHz band has some downsides as well. The band is not harmonized, e.g. different regulations in different countries. In the European Union (EU) the transmission power is 10 dBm with a 10% duty cycle or 0 dBm with a 100% duty cycle [29], whereas in the United States (US) the transmission power is -14 dBm for periodic control applications and -23 dBm for other periodic applications [30]. However, a Duty Cycle Correction (DCC) of up to 20 dB can be applied to enable higher transmit powers as long as the average transmit power during the averaging time frame, i.e. pulse train or worst case 100 ms, is kept within the regulatory limits. Furthermore, the 433 MHz band is more limited in terms of bandwidth than the 2.4 GHz band is, e.g. 1.74 MHz and 100 MHz respectively. Finally, the optimal antenna size for the 433 MHz band is larger compared to an equivalent antenna for the 2.4 GHz band.

The 433 MHz band extends from 433.05 MHz to 434.79 MHz and is organized into fifteen 108 kHz narrowband channels for two reasons. First, support for multiple channels enables different systems located in the same physical domain to coexist, e.g. a narrowband channel can be allocated between two consecutive narrowband or broadband systems without either causing or receiving interference. Second, using narrowband channels enables to comply with specific regional regulations that have more strict bandwidth limitations, e.g. China. Currently two standards are being developed that use the 433 MHz band for low-power wireless communications: DASH7 Mode 2 and IEEE 802.15.4f. Considering the scope of our work, the following subsections present the physical layer characteristics of both standards. For a detailed overview of the remaining layers refer to the related standards [5, 13].

DASH7 Mode 2

DASH7 Mode 2 [5] is a new version of the ISO/IEC 18000-7:2009 standard developed by the DASH7 Alliance for active RFID (RadioFrequency IDentification) applications. The physical layer of DASH7 Mode 2 operates at the 433 MHz band and is organized into fifteen 108 kHz channels, including two 6 kHz guard bands at the beginning and the end of the spectrum to avoid interference with/from other wireless systems operating in adjacent bands. The fifteen channels are combined to form five different channel types –Base, Legacy, Normal, Hi-Rate and Blink– that have different bandwidth and use different modulation schemes. The Normal class provides eight 216 kHz channels that use a broadband BFSK (Binary Frequency Shift Keying) or GFSK (Gaussian Frequency Shift Keying) modulation scheme with a data rate of 55 kbps. The Hi-Rate class provides four 432 kHz channels that use a narrowband BFSK or GFSK modulation scheme with a data rate of 200 kbps. The Blink class provides two 648 kHz channels that use the same modulation and data rate than the Hi-rate channel class. Finally, the Base and Legacy classes provide a single 432 kHz channel, centered at 433.92 MHz, that uses a modulation and data rate similar to the Normal class. An overview of the different channel classes is shown in Table 3.1 and depicted in Figure 3.1.

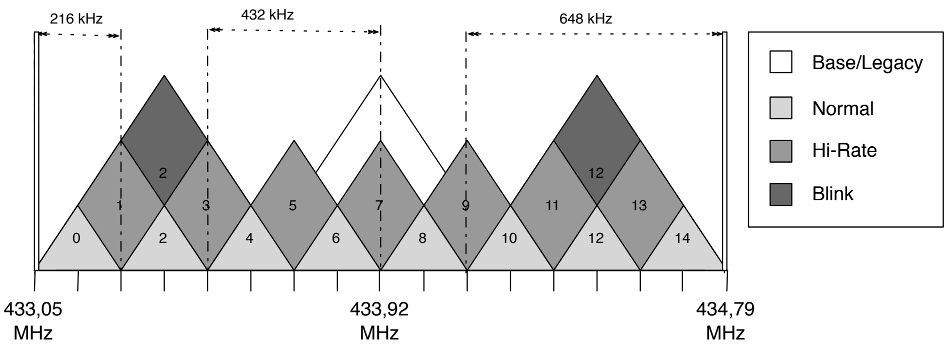

Figure 3.1: DASH7 Mode 2 physical layer channel organization. In DASH7 Mode 2 only the Normal and Blink channel types are orthogonal, that is, neighboring channels of the same type do not cause and receive interference to/from each other. The remaining channel types are non-orthogonal and, thus, neighbor channels cause and receive interference to/from each other and also to the Normal and Hi-Rate channel types. For example, the Blink channel type centered at channel 2 interferes with Normal and Hi-Rate channel types centered at channels 0, 2, and 4.

IEEE 802.15.4f

IEEE 802.15.4f [13] is an amendment of the IEEE 802.15.4-2011 standard that defines three new optional physical layers targeted at active RFID (RadioFrequency IDentification) applications. The first two physical layers are narrowband and located at the

Name	Channels	Bandwidth	Modulation	Data rate
Base	1	432 kHz	1.8-BFSK	55 kbps
Normal	8	216 kHz	1.8-BFSK	55 kbps
Hi-Rate	4	432 kHz	0.5-BFSK	200 kbps
Blink	2	648 kHz	0.5-BFSK	200 kbps

Table 3.1: DASH7 Mode 2 physical layer channel organization. Each channel class has different bandwidth, modulation scheme, data rate and available number of channels, which enables to use them according to the application and regulation requirements. Optionally a GFSK modulation scheme can be used instead of BFSK to improve bandwidth utilization at the expense of decreasing the receiver sensitivity by around 3 dB.

433 MHz and 2.4 GHz bands respectively, whereas the third physical layer is Ultra-Wide Band (UWB) and is located at the 6-9 GHz band. Similarly to DASH7 Mode 2, the whole 433 MHz bandwidth is divided into fifteen 108 kHz narrowband channels. These fifteen narrowband channels are combined together, as shown in Table 3.2 and in Figure 3.2, in order to provide three different channel types with different available bandwidths that are capable of offering different data rates. The 31.25 kbps channel type uses the basic narrowband 108 kHz channel and, thus, all the fifteen channels are available (0 to 14). The 100 kbps channel type is formed of three consecutive basic narrowband channels and, thus, only five 324 kHz channels are available (i.e. 1, 4, 7, 10 and 13). Finally, the 250 kbps channel type is formed of five consecutive basic narrowband channels and, thus, only three 540 kHz channels are available (2, 7 and 12). IEEE 802.15.4f also includes two 110 kHz guard bands at the beginning and the end of the band to avoid interfering and interference with/from other wireless systems operating in adjacent bands.

Name	Channels	Bandwidth	Modulation	Data rate
31.25	15	108 kHz	BMSK	31.25 kbps
100	5	324 kHz	BMSK	100 kbps
250	3	540 kHz	BMSK	250 kbps

Table 3.2: IEEE 802.15.4f physical layer channel organization. Each channel class has different bandwidth and available number of channels, which enables to use them according to the application and regulation requirements. Compared to the BFSK modulation scheme of DASH7 Mode 2, the MSK modulation scheme provides better spectral efficiency while maintaining an acceptable bit error rate.

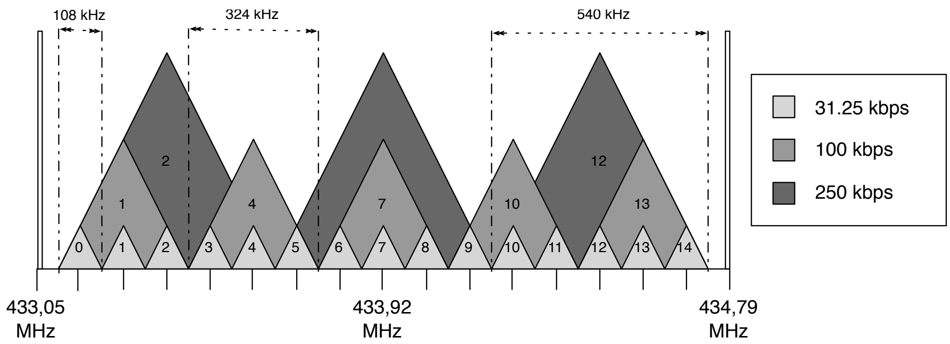

Figure 3.2: IEEE 802.15.4f physical layer channel organization. In IEEE 802.15.4f operating at the 433 MHz band all channel types are orthogonal with channels of the same type but non-orthogonal between different channel types. For example, the 250 kbps channel centered at channel 2 will cause and receive interference to/from all channels types centered at channels 0, 1, 2, 3 and 4 but not to/from all the remaining channels.

3.4. Experimental setup

Given the theoretical propagation models described in Section 3.2, our experiments aim to evaluate the propagation aspects of the 433 MHz band and compare it to the 2.4 GHz band in different environments, e.g. indoor and outdoor. In order to conduct these experiments we use COTS (Custom Off The Shelf) devices, namely COU24-A2 and OpenMote-433 motes. For that reason in the current section we present a detailed description of the devices and the configuration parameters (e.g. transmit power, receiver sensitivity, signal modulation, data rate, etc.) that have been used to conduct the different experiments. Finally, as we use COTS devices, we also present the procedure that we have used to calibrate the motes and ensure they operate under the configured parameters.

3.4.1. Equipment

The set of experiments at the 2.4 GHz band are conducted using two COU24-A2 motes, as depicted in Figure 3.3. The COU24-A2 motes are equipped with an Atmel 8-bit ATmega-1281 microcontroller and an Atmel AT86RF230 transceiver. The microcontroller operates at 4 MHz and features 8 Kbytes RAM, 128 Kbytes of Flash and 4 Kbytes EEPROM memory respectively. The transceiver is fully compliant with IEEE 802.15.4-2006 standard, e.g. 250 kbps with OQPSK modulation and DSSS, and is connected to an onboard 0 dBi chip antenna.

Figure 3.3: A COU24-A2 development board. The COU24-A2 board features an Atmel ATmega-1281 microcontroller and an Atmel AT86RF20 transceiver.

To conduct the experiments at the 433 MHz band we use two OpenMote-433, as depicted in Figure 3.4. OpenMote-433 boards feature a 32-bit ARM Cortex-M3 STM32F103 microcontroller from ST Microelectronics and a Texas Instruments CC1101 transceiver. The microcontroller operates at 72 MHz with 20 kBytes of RAM and 128 kBytes of Flash memory respectively. The transceiver operates at the Sub-1 GHz band with full support for both DASH7 Mode 2 and IEEE 802.15.4f standards, e.g. FSK/GFSK/MSK modulations with bit-rates up to 250 kbps, and is connected to a 0 dBi $\lambda/2$ helix antenna using a SMA connector.

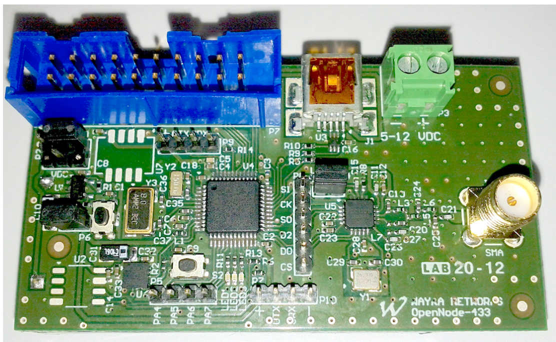

Figure 3.4: An OpenMote-433 development board. The OpenMote-433 features a ST Microelectronics STM32F103 microcontroller and a Texas Instruments CC1101 transceiver.

3.4.2. Configuration

The configuration parameters of both devices used in the experimental measurements campaign are presented in Table 3.3. The chosen data rate and modulation scheme for the OpenMote-433 are in accordance with DASH7 Mode 2 Normal channel type, as presented in Section 3.3. In both cases the transmit power is configured to be the same, e.g. 0 dBm, for comparison purposes.

	COU24-A2	**OpenMote-433**
Standard	IEEE 802.15.4	DASH7 Mode 2
Modulation	OQPSK	GFSK
Data rate (kbps)	250	200
Transmit power (dBm)	0	0
Channel number (MHz)	18 (2450)	7 (433.92)
Channel bandwidth	5 MHz	432 kHz
Antenna type	0 dBi $\lambda/2$ chip	0 dBi $\lambda/2$ helix
RSSI resolution (dB)	3	0.5

Table 3.3: Configuration parameters for the COU24-A2 and the OpenMote-433 motes.

Two metrics have been used throughout the measurement camping to evaluate the propagation aspects of the 433 MHz and the 2.4 GHz bands, the RSS (Received Signal Strength) and the PDR (Packet Delivery Ratio). The RSS measures the received power level at the input of the signal demodulator given the receiver filter bandwidth and Low Noise Amplifier (LNA) gain. On its behalf, the PDR indicates the percentage of packets that have been successfully received at the receiver normalized to one.

3.4.3. Calibration

Prior to start the measurements campaign we have conducted a set of preliminary measurements to calibrate the transmitter and receiver used during the experiments campaign at the 433 MHz and 2.4 GHz bands to ensure that they operate under the configuration parameters, e.g. transmit power, modulation scheme and channel bandwidth, presented in Table 3.3.

At the 433 MHz band we have connected the OpenMote-433 board to a Rigol DSA-815 spectrum analyzer. The peak output power, measured at the output of the SMA connector, is about -3 dBm and the overall power in the given bandwidth, i.e. 432 kHz for a DASH7 Mode 2 Hi-Rate channel, is 0 dBm. In addition, we have also calibrated the receiver node. In particular, we have measured the linearity of the RSS according to a known transmit power, e.g. $P_t = 0\ dBm$, and channel attenuation using a JWF 50PA-51 programmable attenuator. The obtained results are in accordance with the configured parameters in Table 3.3 and, thus, the transmitter node configuration is validated. Despite, the results are not shown due to lack of space.

At the 2.4 GHz band an extensive calibration of the COU24-A2 has not been possible because the motes use an integrated chip antenna and, thus, it is not possible to connect them to any measurement equipment. Therefore to ensure that node operation is consistent with configured parameters we have compared the RSS at a distance of 1 m in outdoor with other available motes. In all the devices the measured signal is quasi identical regardless of the selected. Hence we consider that the COU24-A2 motes used for the experimentation campaign are calibrated.

Finally, we have also conducted measurements to determine the sensitivity of the DASH7 Mode 2 and IEEE 802.15.4f standards at 433 MHz using the OpenMote-433 motes and the IEEE 802.15.4 standard at 2.4 GHz using the COU24-A2 motes. The measurements have been conducted sending 1024 packets with a 23 byte payload for each channel type. Notice that the sensitivity parameter is defined as the RSS value such that the $PDR >= 90\%$. The results of the measurements are depicted in Figure 3.5

and summarized in Table 3.4.

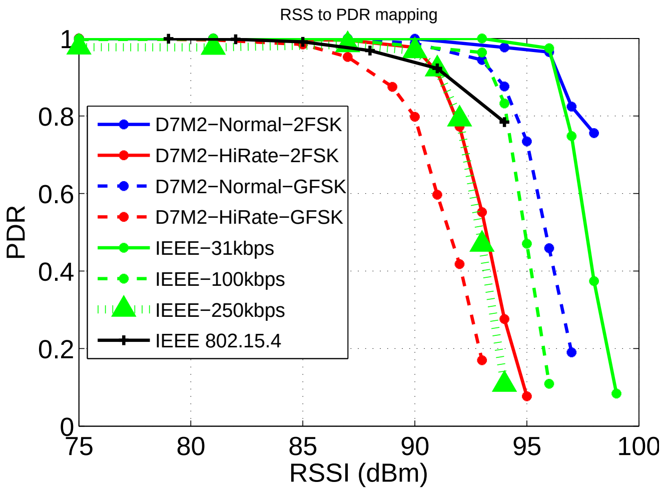

Figure 3.5: RSS to PDR mapping for COU24-A2 and OpenMote-433 motes. For the IEEE 802.15.4 standard operating at 2.4 GHz the COU24-A2 achieves a sensitivity of -91 dBm. On its behalf, using DASH7 Mode 2 Hi-Rate channel type at 433 MHz with a GFSK modulation the OpenMote-433 achieves a sensitivity of -88 dBm.

Standard	**Channel type**	**Modulation**	**Sensitivity**
DASH7 Mode 2	Normal	2FSK	-97 dBm
DASH7 Mode 2	Normal	GFSK	-94 dBm
DASH7 Mode 2	Hi-Rate	2FSK	-91 dBm
DASH7 Mode 2	Hi-Rate	GFSK	-88 dBm
IEEE 802.15.4f	31 kbps	MSK	-96 dBm
IEEE 802.15.4f	100 kbps	MSK	-93 dBm
IEEE 802.15.4f	250 kbps	MSK	-91 dBm
IEEE 802.15.4	250 kbps	OQPSK	-91 dBm

Table 3.4: Sensitivity summary for DASH7 Mode 2 and IEEE 802.15.4f at 433 MHz and for IEEE 802.15.4 at 2.4 GHz. These figures combined with the propagation models presented in Section 3.5 enable to estimate the effective communication range for each standard and channel type.

3.5. Experiments and results

In this section we first experimentally evaluate the diffraction phenomenon for 433 MHz and 2.4 GHz, i.e. from which height the Fresnel zone is not obstructed by the effect of being close to the ground. With the knowledge of the height such that the first Fresnel zone is free, we then experimentally validate the large scale propagation for both bands. Additionally, we validate the dependence of height to the propagation characteristics, $(RSS(d0,h), \gamma(h))$ according to the propagation model described in Equation 3.1, since the closer to the ground, the more obstructed the Fresnel zone is and, hence, the higher the power losses are. Finally, we also validate the small scale propagation effects (known as multipath) for the 433 MHz band and compare it with the results at the 2.4 GHz band obtained in [26]. The goal is to validate if channel hopping can combat multipath at the 433 MHz band since the band is flat fading, i.e. the coherence bandwidth of the wireless channel is higher than the bandwidth of the transmitted signal. It is important to mention that in all the experiments the antennas were positioned to ensure proper polarization and the locations were carefully measured to ensure repeatability.

3.5.1. Diffraction modeling

First we focus in obtaining and evaluating the diffraction models for the 433 MHz and 2.4 GHz bands. The diffraction models are useful to analyze the power losses attributed to the penetration of a certain obstacle inside the first Fresnel zone [17]. In our case we analyze the power losses attributed to the penetration by ground, modeled by the parameter $L_g(dB)$. As we are interested in finding the variation of the RSS with the height with respect from ground, we fix the distance between the transmitter and the receiver, for instance $d0 = 5$ m, and we vary the height of nodes. For this scenario the model in Equation 3.1 simplifies to Equation 3.3 taking into account that $\overline{\psi_{shad}} = 0$ dB and $h0 = h_{free}$.

$$\overline{RSS(d0,h)} = \overline{RSS(d0,h0)} - Lg(h);\ h \leq h0 \tag{3.3}$$

The corresponding diffraction models for the 433 MHz and 2.4 GHz bands are depicted in Figure 3.6 for two environments, outdoor and indoor. In general terms it is possible to see that the 433 MHz band is less affected by diffraction losses when compared to the 2.4 GHz band in both environments. The diffraction results are combined with the effects of multi-path propagation and the 9-16 dB deltas are expected from the Friis equation dependence on the wavelength. Despite, it is possible to observe that the first Fresnel zone becomes free after a height of $h = 2.1$ m for 433 MHz and a height of $h = 36$ cm for 2.4 GHz. Hence, the rule of thumb $h_{free} = 3\lambda$ to ensure a free first Fresnel zone is satisfied for both bands. In addition, it is possible to see that in the outdoor environment the magnitude of this interference is lower than in indoor.

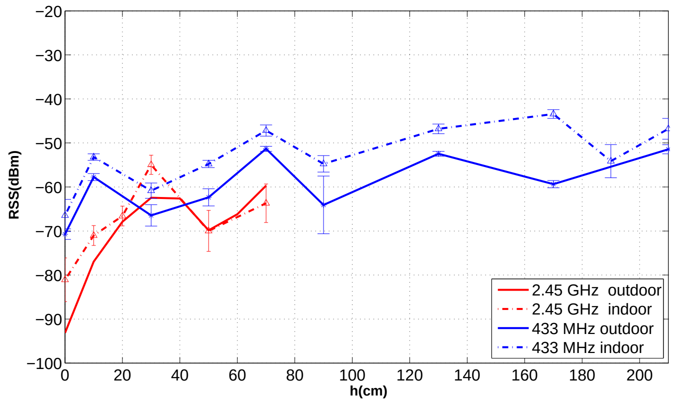

Figure 3.6: Diffraction modelling for the 433 MHz and 2.4 GHz bands in indoor and outdoor environments. The error bars represent the temporal RSS variation attributed to diffraction and multipath, i.e. reflections from ground and other surrounding objects. Also, the rule of thumb $h_{free} = 3\lambda$ to ensure a free first Fresnel zone is satisfied for both bands.

3.5.2. Large-scale propagation

This section deals with the empirical evaluation of the large scale propagation characteristics of the 433 MHz and 2.4 GHz bands in outdoor and indoor environments. For each measurement the transmitter sends 1024 packets of 33 bytes (including a preamble of 4 bytes, a synchronization word of 4 bytes, 23 bytes of data and a 2-byte CRC) to the receiver at the configured channel, while the receiver is continuously listening for incoming packets.

Outdoor

This section is devoted to analyze the propagation effects and compare the wireless range between the 433 MHz and the 2.4 GHz bands in an outdoor environment. This environment is depicted in Figure 3.7 and is found at the GPS coordinates $(+41°31'39.27''; +2°26'7.92'')$. The ground is asphalt and the environment did not have obstructions in the path. The measurements were taken along the yellow line.

Figure 3.7: Outdoor propagation environment. The measurements were taken along the yellow line and the columns are not obstructions.

The methodology to conduct the measurements is the following: RSS measurements are taken for each received packet at the following distances, where the notation (x:z:y) means from x meters to y meters every z meters.

- For heights from $h = 0$ cm to $h = 70$ cm: [1 m:1 m:10 m, 15 m:5 m:70 m, 80 m:10 m:120 m].
- For heights from $h = 70$ cm to $h = 2.10$ m: [1 m, 5 m:5 m:70 m, 80 m:10 m:120 m].

The results of the RSS over distance for the 433 MHz and 2.4 GHz bands are depicted in Figure 3.8. As expected the RSS falls off linearly with $log10(d/d0)$ and γ increases when the height with respect to ground decreases due to the Fresnel zone obstruction caused by ground. The $RSS(d0, h0)$ of the propagation model at 433 MHz is 10 dB higher than $RSS(d0, h0)$ of the 2.4 GHz propagation model. Also, for $h = 0$ and

$log10(d/d0) = 0$, the RSS for 433 MHz is 28 dB higher than 2.4 GHz. This is traduced to a higher wireless range at 433 MHz. To find the wireless range in meters using the propagation models the following procedure is used. First, according to Table 3.4, the PDR is $> 90\%$ when $RSS > -91$ dBm for 2.4 GHz and when $RSS > -88$ dBm for 433 MHz. Then, for a height of $h = 10$ cm, the maximum range at 2.4 GHz such that the $RSS > -91$ dBm is $log10(d/d0) = 0.8 \Rightarrow d = 8$ m, and the maximum range at 433 MHz such that the $RSS > -88$ dBm is $log10(d/d0) = 1.65 \Rightarrow d = 45$ m. Similarly, for a height of $h = 70$ cm at 2.4 GHz and a height of $h = 2.10$ m at 433 MHz the maximum range is 70 m and 160 m respectively.

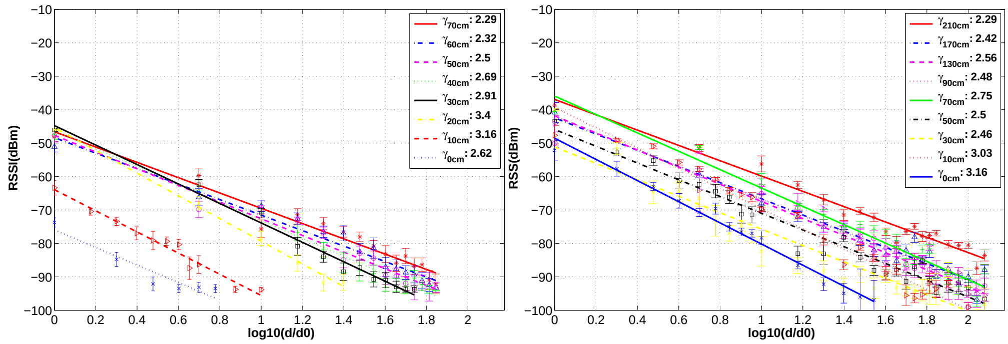

(a) (b)

Figure 3.8: Propagation models for 2.4 GHz and 433 MHz in an outdoor environment.

The corresponding values for $RSS(d0, h)$, $\gamma(h)$ and σ_{shad} for all the propagation models are presented in Table 3.5 and Table 3.6 respectively. Additionally we include the coefficient of determination R^2 which is a statistical measure of how well the regression line approximates to the measurements. An R^2 of 1.0 indicates that the regression line perfectly fits the data. As observed, the path loss exponents are more or less similar. However, a significant difference is shown by $RSS(d0, h)$. This effect is because, according to Equation 3.1, $RSS(d0, h)$ is proportional to the intercept factor which is inversely proportional to λ (Equation 3.2) and, thus, the lower the λ the higher the received power. Moreover as A is related to the effective area of the receiver antenna, the larger it is the more energy it can pick up. An average gain of 11.6 dB is given by the 433 MHz band which is close to the theoretical value of 14.87 dB obtained from the difference of Equation 3.2 between both frequency bands.

Concerning the shadowing, the respective statistical distributions are shown in Figure 3.9 and Figure 3.10 for both bands. We only show the shadowing distribution for near ground and away from ground heights, due to space constraints. As illustrated, the distribution of the shadowing follows approximately a Gaussian distribution.

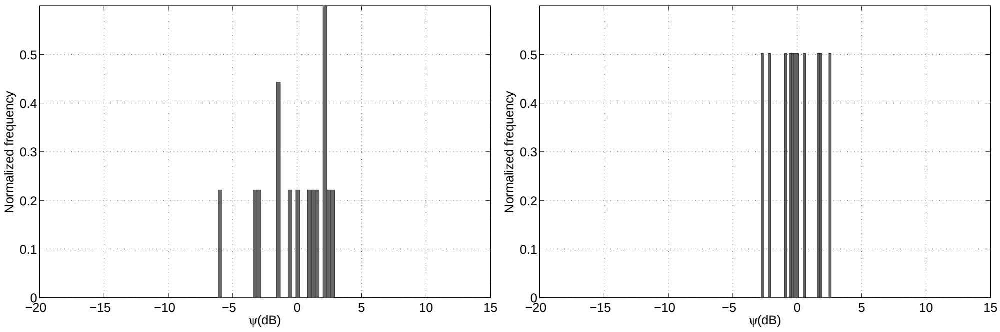

(a) (b)

Figure 3.9: Shadowing distribution for 2.4 GHz in outdoor environment, 3.9a: $h = 0.7$ m with σ_{shad} :2.58 dB, 3.9b: $h = 0.1$ m with σ_{shad} : 1.64 dB.

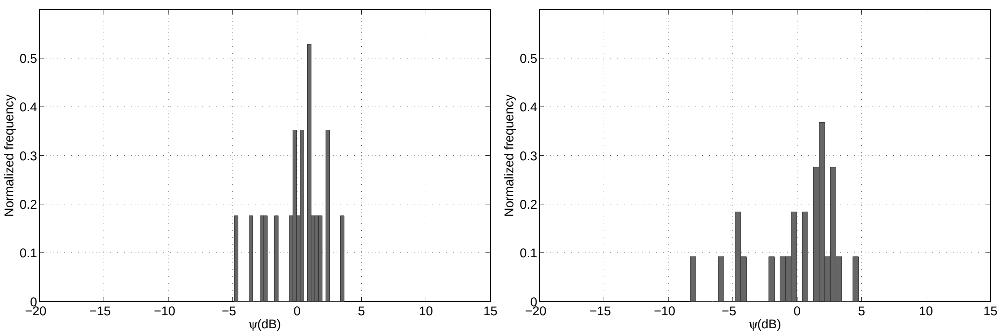

(a) (b)

Figure 3.10: Shadowing distribution for 433 MHz in outdoor environment, 3.10a: $h =$ 2.10 m with σ_{shad} : 2.18 dB, 3.10b: $h = 0.1m$ with σ_{shad} : 3.27 dB.

$h(m)$	0.7	0.6	0.5	0.4	0.3	0.2	0.1	0
$RSS(d0,h)$(dBm)	-46.6	-48.36	-47.67	-46.26	-44.77	-45.39	-63.92	-75.97
γ	2.29	2.32	2.5	2.69	2.91	3.4	3.16	2.62
$\sigma_{shad}(dB)$	2.58	2.21	2.37	1.95	1.82	1.34	1.64	2.52
R^2	0.95	0.97	0.97	0.98	0.98	0.99	0.97	0.9

Table 3.5: Propagation model characteristics at 2.4 GHz in an outdoor environment.

$h(m)$	2.1	1.7	1.3	0.9	0.7	0.5	0.3	0.1	0
$RSS(d0,h)$(dBm)	-36.94	-42.4	-41.83	-42.02	-35.95	-45.93	-51.15	-39.35	-48.55
γ	2.29	2.42	2.56	2.48	2.75	2.5	2.46	3.03	3.16
$\sigma_{shad}(dB)$	2.18	2.82	3.54	3.03	3.4	2.93	4.85	3.27	1.80
R^2	0.97	0.95	0.93	0.95	0.94	0.96	0.9	0.97	0.98

Table 3.6: Propagation model characteristics at 433 MHz in an outdoor environment.

Indoor

The large-scale propagation measurements in an indoor environment were taken in a 80 m corridor at the same measurement distances of outdoor measurements. An illustration of the indoor scenario, including a brief description of the environment, is shown in Figure 3.11.

Figure 3.11: Indoor propagation environment. The outer of the building and the floor partitions are made by reinforced concrete, whereas the wall partitions are made by plaster and the floor is made of stoneware. Finally, it is important to mention that there are metal structure in the ceilings used to conduct the electricity and communications wiring.

The corresponding propagation models for this environment are depicted in Figure 3.12. The waveguide effects can be observed at the 2.4 GHz band since the path loss exponent γ is smaller than 2. In fact $1.2 < \gamma < 2$ [46, 47]), that is, the actual path loss exponent is lower than the free space path loss exponent. However the waveguide effects cannot be appreciated in the 433 MHz band due to two reasons. First, the reflection of an electromagnetic wave in an obstacle only occurs when the size of the obstacle is large compared to the wavelength [48]. Thus, as the wavelength at 433 MHz is around 69 cm the waves are not reflected but propagate along the objects. Second, the size of a waveguide depends on the wavelength of the electromagnetic wave [49]. Hence, the required dimension of the corridor to act as a waveguide is larger at the 433 MHz band.

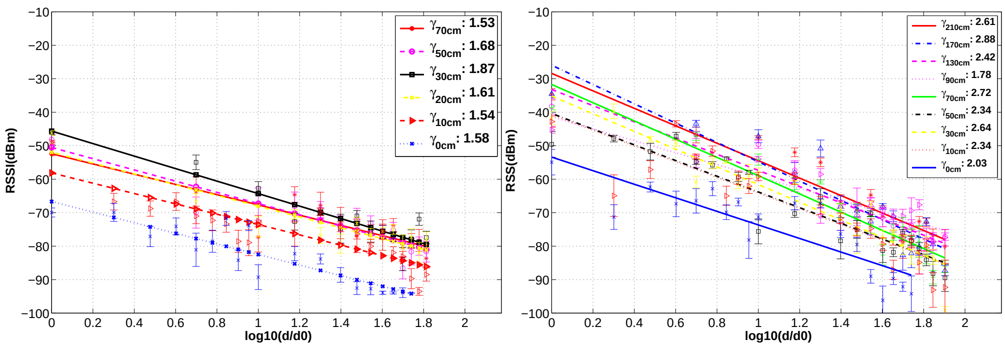

(a) (b)

Figure 3.12: Propagation models for 2.4 GHz and 433 MHz in and indoor environment.

The results of $RSS(d0, h)$, $\gamma(h)$, σ_{shad} and R^2 for this environment are depicted in Table 3.7 and Table 3.8. Again, a significant difference can be observed for the values of $RSS(d0, h)$ between both bands. The average gain at the distance $d0$ is 14.4 dB which matches with the value obtained using Equation 3.2. The corresponding distributions of the shadowing for the 2.4 GHz and 433 MHz bands are illustrated in Figure 3.13 and Figure 3.14. Again, most of the distributions demonstrates that the shadowing approximates to a Gaussian distribution, which in turns validates the theory presented in Section 3.2. Therefore, the 433 MHz band provides an increase of the received power with respect to 2.4 GHz by around 14 dB which approximately means doubling the wireless range, despite of the waveguide effects not being contemplated.

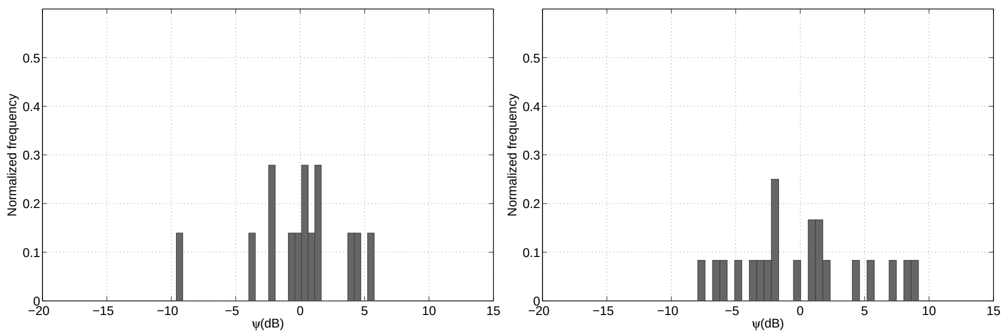

(a) (b)

Figure 3.13: Shadowing distribution for 2.4 GHz in indoor environment, 3.13a: $h = 0.7$ m with σ_{shad} :3.78 dB, 3.13b: $h = 0.1$ m with σ_{shad} : 4.89 dB.

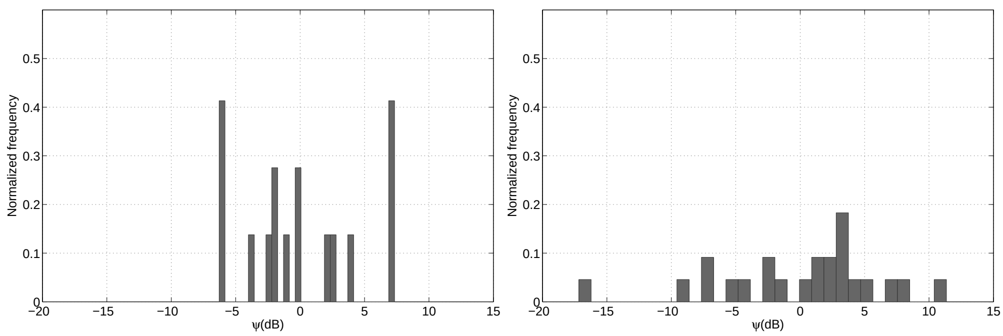

(a) (b)

Figure 3.14: Shadowing distribution for 433 MHz in indoor environment, 3.14a: $h =$ 2.10 m with σ_{shad} : 4.64 dB, 3.14b: $h = 0.1$ m with σ_{shad} : 6.37 dB.

$h(m)$	0.7	0.5	0.3	0.2	0.1	0
$RSS(d0, h)$(dBm)	-52.39	-50.53	-45.64	-51.98	-58.12	-66.68
γ	1.53	1.68	1.87	1.61	1.54	1.58
$\sigma_{shad}(dB)$	3.78	3.69	3.44	3.55	4.89	3.80
R^2	0.81	0.84	0.88	0.84	0.74	0.82

Table 3.7: Propagation model characteristics at 2.4 GHz in an indoor environment.

3.5.3. Small-scale propagation

This subsection analyzes the effects of multipath propagation at the 433 MHz band and evaluates if multipath can be combated using channel hopping, as presented in [26] for the 2.4 GHz band. In their experiments the receiver is fixed at a certain location

$h(m)$	2.1	1.7	1.3	0.9	0.7	0.5	0.3	0.1	0
$RSS(d0,h)$(dBm)	-28.42	-25.96	-33.21	-41.4	-31.72	-40.37	-35.15	-40.7	-53.41
γ	2.61	2.88	2.42	1.78	2.72	2.34	2.64	2.34	2.03
$\sigma_{shad}(dB)$	4.64	5.83	3.77	4.06	4.23	5	4.78	6.38	6.37
R^2	0.89	0.86	0.91	0.83	0.91	0.87	0.90	0.80	0.72

Table 3.8: Propagation model characteristics at 433 MHz in an indoor environment.

and the transmitter is displaced every 1 cm on a 20 cm x 35 cm area, corresponding to $\lambda/12.24$. According to the results, multipath propagation at 2.4 GHz can be combated with channel hopping, since the channel is frequency selective, or with antenna diversity.

In our case, the methodology to conduct the experiments is similar but with a displacement of 5.66 cm corresponding to the same order of magnitude of λ for the 433 MHz band. The receiver is fixed and the transmitter is placed at the appropriate location in a 113.2 cm x 198 cm square. For each position 1024 packets with the same structure of the large scale propagation measurements are transmitted over the first channel with an inter-packet delay of 3 ms. Upon finishing a channel the transmitter waits for 10 ms and changes to the following channel and the process is repeated until all channels are completed. Once all the channels are completed the process is repeated for all the remaining positions in the square. Using such setup, two different experiments have been conducted to evaluate the suitability of channel hopping at the 433 MHz band, one in Line-of-Sight (LoS) conditions and the other in Non-Line-of-Sight (NLoS) conditions. Both experiments have been conducted in a domestic environment with concrete floor and plaster walls and ceilings, as depicted in Figure 3.15.

Line of Sight (LoS)

In this experiment the transmitter and the receiver are located in the same room at a distance of 5 meters and with clear line of sight as illustrated in Figure 3.15. The results in terms of RSS depending on node position and channel are shown in Figure 3.16. Due to space constraints only results from channels 1, 7 and 14 are presented.

In LoS conditions the PDR (not shown) is always the maximum because the received signal is well-above the receiver sensitivity. As observed in Figure 3.16, there are fadings

Figure 3.15: Indoor domestic environment. The transmitter and the receiver are in Line-of-Sight.

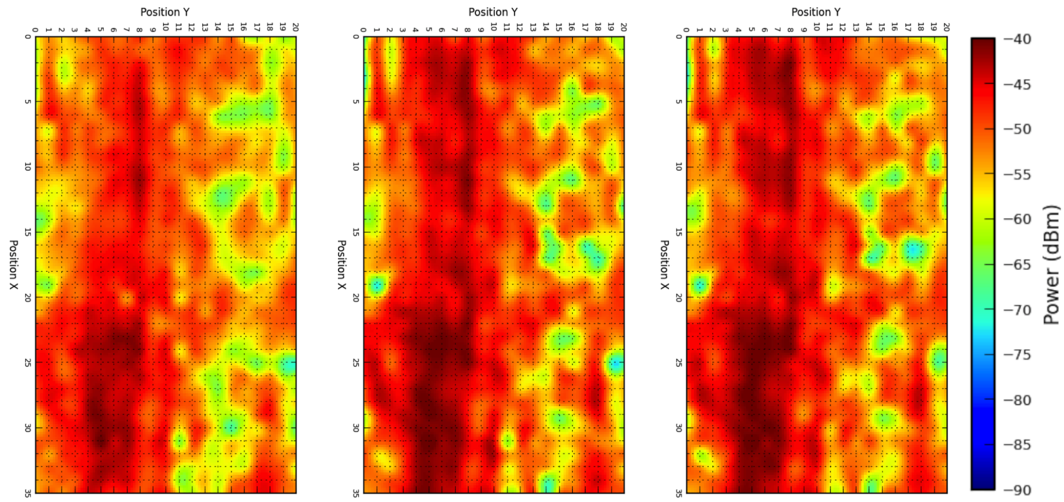

Figure 3.16: RSS in LOS conditions. From left to right: channels 1, 7 and 14 respectively.

with a magnitude of 20-25 dB approximately in some positions. These fadings are caused by multipath propagation. Moreover, it is possible to see that the magnitude of the RSS is more or less constant within the different channels regardless of node position. This is because the wireless channel is flat fading (the channels are narrowband). Flat fading channels occur when the channel delay spread (the order of τ_s =10 ns, 100 ns for indoor environments) is much lower than the time delay of the transmitted signal or the channel coherence bandwidth B_{wc} is larger than the bandwidth of the transmitted signal B_s. Mathematically this is expressed as $B_s^{-1} = 1/108KHz = 9.26\mu s >> \tau_s$. In comparison to the results presented in [26], at the 2.4 GHz band the wireless channel is frequency selective ($B_{wc} << B_s$ or $\tau_s >> B_s^{-1}$) and hence the magnitude of the wireless channel is different for each single channel (5 MHz of bandwidth) and, thus, channel hopping can combat multipath. However in our case, the wireless channel is not frequency selective but flat fading $B_{wc} >> B_s$ or $\tau_s << B_s^{-1}$) and the magnitude of the wireless channel is almost the same for each single channel. Thus, channel hopping cannot combat multipath.

Non-Line of Sight (NLoS)

In this second experiment the transmitter is located in the same place as in the previous experiment and the receiver is located at the furthest room of the building, where NLoS conditions exist. The experiments presented above are repeated to verify the effects of multipath propagation in NLoS conditions.

The results obtained from this experiment are depicted in Figure 3.17 for channels 1, 7, and 14. Contrarily to the previous results, PDR in NLoS conditions (not shown) greatly varies from one hundred percent to zero percent depending on the transmitter positions due to the effects of fadings, which are caused by multipath propagation. The magnitude of the RSS is more or less constant within the different channel regardless of node position. This is because the wireless channel is flat fading and, thus, in NLoS conditions channel hopping cannot combat the negative effects of multipath either.

Finally, if we average the PDR for the different positions, over all deep fades in the data set where the PDR $\leq 5\%$ we obtain the results shown in Figure 3.18. As it is possible to observe, in the case of NLoS the transition from a deep fade (PDR $\leq 5\%$) to a *good* position (PDR $\geq 95\%$) the node has to move an average of 30 cm. This is *quasi* the half wavelength $\lambda/2$ or the coherence length, and confirms the theory and results given by [26, 17]. Therefore the only way to combat multipath at the 433 MHz band is by means of a spatial displacement of $\lambda/2$ to any direction or by means of using antenna diversity.

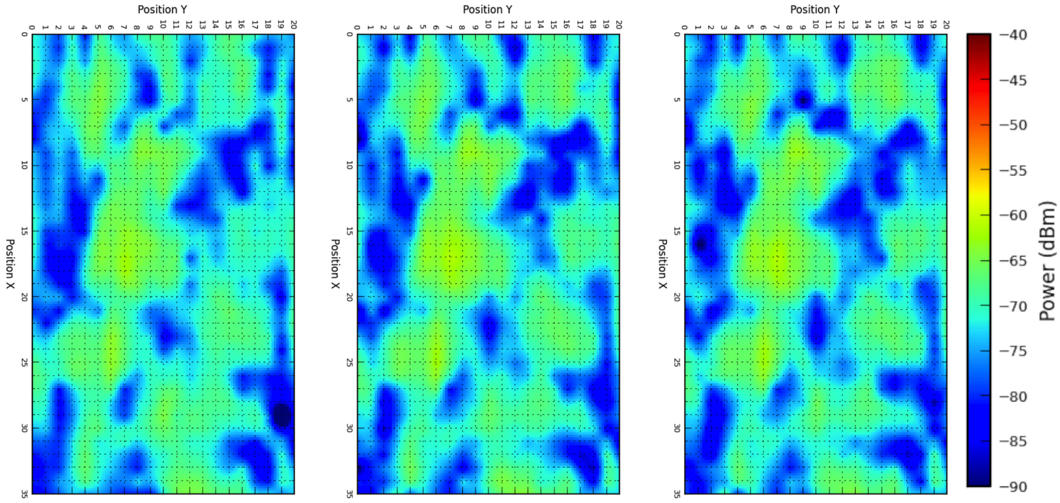

Figure 3.17: RSS in NLOS conditions. From left to right: channels 1, 7 and 14 respectively.

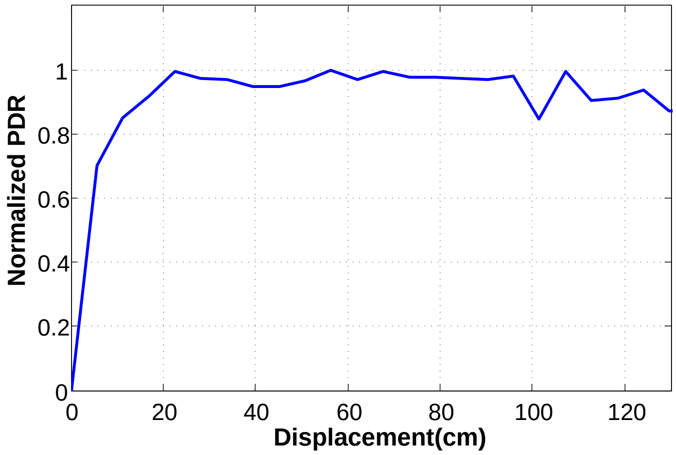

Figure 3.18: Channel coherence length obtained from the averaged PDR for all channels and node displacements.

3.5.4. Discussion

From the diffraction results presented in Section 3.5.1 we confirm that the received power at 433 MHz is well above 2.4 GHz despite of the larger Fresnel zone. At ground level, the RSS at 433 MHz is 20 dB above the RSS at 2.4 GHz, whereas in LoS the RSS is 10 dB above.

Regarding the propagation results presented in Section 3.5.2, the results confirm that the wireless range is dependent both on the frequency, node height and the environment. The adopted propagation model in Equation 3.1 demonstrates that the path loss exponent γ is height dependent and that $RSS(d_0, h)$ is frequency band dependent because of the intercept factor. We find the corresponding model parameters ($RSS(d0, h)$, $\gamma(h)$ and σ_{shad}) by line fitting for the 433 MHz and 2.4 GHz bands. The obtained propagation models depicted in Figure 3.8 and Figure 3.12 are useful to compare the different frequency bands.

In addition, it is important to mention that in indoor environments there is less contribution due to multipath propagation at 433 MHz. The path loss exponent at the 433 MHz band is higher than at 2.4 GHz because the larger wavelength reduces the effects of multipath propagation, e.g. waveguide phenomenon in corridors. Despite of a higher γ, the 433 MHz band has an advantage of 14 dB at $d = d0$ with respect to the 2.4 GHz band. If we assume that both 2.4 GHz and 433 MHz receivers have the same sensitivity, at the distance where both 433 MHz and 2.4 GHz propagation models crosses, the RSS at the 2.4 GHz band may be below the receiver sensitivity and hence $PDR << 1$, whereas the RSS at the 433 MHz band will be above with $PDR = 1$. Moreover, the propagation model characteristics are height dependent and the shadowing follows a Gaussian distribution.

Finally, from the small-scale results presented in Section 3.5.3 we confirm that, contrarily to the results presented by Watteyne et al. [26] for the 2.4 GHz band, channel hopping does not improve robustness against multipath propagation for the 433 MHz band. The rationale behind that fact is that, as expected, the channel coherence bandwidth, the inverse of the channel delay spread, at the 433 MHz band is larger than the whole bandwidth itself and, thus, all the channels are highly correlated.

3.6. Conclusions

This article has presented a short overview of the low-power wireless standards currently being developed at 433 MHz for M2M communications, namely DASH7 Mode

2 and IEEE 802.15.4f, and extensively evaluated the propagation characteristics of the 433 MHz and the 2.4 GHz bands in both indoor and outdoor environments. The results obtained show that the communication range at 433 MHz is better than at 2.4 GHz despite the effects of having a larger Fresnel zone. The results also demonstrate that, contrarily to the 2.4 GHz band, the use of channel hopping does not combat the effects of multipath propagation because the channel coherence bandwidth is larger than the whole 433 MHz band bandwidth and, thus, all channels are highly correlated.

From the obtained results we conclude that the 433 MHz band has a great potential for M2M communications using low-power wireless technologies. Besides being available world-wide, for a similar environment the better propagation characteristics enable to reduce multi-hop communication requirements, which in turn has a direct impact on the node and network energy consumption and, thus, its overall battery life. Nevertheless, the fact that multipath propagation cannot be combated through channel hopping needs to be taken into account when designing low-power wireless systems for M2M communications that operate at the 433 MHz band. For example, antenna diversity may need to be considered to improve link robustness against multipath propagation. Similarly, despite the better range it is still advisable to incorporate packet routing mechanisms at the network layer that are capable of sending packets over disjoint paths to circumvent the effects of multipath propagation. In addition, there are other important physical layer aspects that need to be considered to design upper layer protocols, e.g. Media Access Control (MAC) protocols, that operate at the 433 MHz band. For example, better signal propagation also leads to an increased level of interference to/from adjacent wireless systems operating at the same band and, thus, dynamic power allocation mechanisms may be required to improve spatial coexistence and further reduce node and network energy consumption.

4 LPDQ: a self-scheduled TDMA MAC protocol for one-hop dynamic low-power wireless networks

Abstract: *Current Medium Access Control (MAC) protocols for data collection scenarios with a large number of nodes that generate bursty traffic are based on Low-Power Listening (LPL) for network synchronization and Frame Slotted ALOHA (FSA) as the channel access mechanism. However, FSA has an efficiency bounded to 36.8% due to contention effects, which reduces packet throughput and increases energy consumption. In this paper, we target such scenarios by presenting Low-Power Distributed Queuing (LPDQ), a highly efficient and low-power MAC protocol. LPDQ is able to self-schedule data transmissions, acting as a FSA MAC under light traffic and seamlessly converging to a Time Division Multiple Access (TDMA) MAC under congestion. The paper presents the design principles and the implementation details of LPDQ using low-power commercial radio transceivers. Experiments demonstrate an efficiency close to 99% that is independent of the number of nodes and is fair in terms of resource allocation.*

4.1. Introduction

The Internet of Things (IoT) [50] is a paradigm in which objects are augmented with sensors and actuators and integrated to the Internet through low-power wireless communications and standardized protocols [51] to enable interaction with humans and other machines in an Machine to Machine (M2M) context. Integrating objects with the Internet may be challenging due to available energy constraints and the need to have long-lasting network deployments [52]. It is widely known that the radio transceiver is the element that dominates energy consumption in wireless communication devices [53]. In particular, it is the Medium Access Control (MAC) layer that controls when the radio transceiver has to be powered on, either to transmit or receive, and thus determines the overall energy consumption. According to [54], the energy waste at the MAC layer comes from four sources: packet collisions, packet overhearing, idle listening, and protocol overhead. For that reason, it is key to design MAC protocols that are efficient in these terms.

Two aspects need to be tackled in the design of an efficient MAC protocol [55]: network synchronization and channel access. Regarding the former, MAC protocols can be classified into synchronous or asynchronous depending on whether nodes have a common notion of time that determines the action to take, e.g., receive or transmit. Regarding the latter, MAC protocols can be classified into reservation-based, random access and hybrid according to the availability of a network schedule that determines which node should transmit at each instant. The decision between the different alternatives depends on the application requirements and certain trade-offs exist between network performance and energy consumption. For networks with fixed nodes and periodic traffic it has been shown that a time-synchronized approach combined with schedule-based communications, e.g., IEEE 802.15.4e [27] based on Time Slotted Channel Hopping (TSCH), leads to high network efficiency and low energy consumption [56, 57, 58].

However, for networks with a large number of nodes, either fixed or mobile, that are collected on demand and generate bursty traffic patterns, such approach is suboptimal due to the energy required to create, distribute and maintain the network schedule. In these scenarios, which are common in the IoT domain, a better approach is to combine Low-Power Listening (LPL) for network synchronization [59] with a random channel access mechanism to enable data transmission [60]. However, current random channel access mechanisms, e.g., those based on Frame Slotted ALOHA (FSA), are suboptimal in terms of both network performance and energy consumption due to the effects of contention. Several authors have presented mechanisms to minimize collision probability in FSA-based protocols [61], which typically rely on discovering how many nodes are present in the network, either a priori (building a tree previous to data transmission) or a posteriori (inferring the number of collisions in the current frame), and adapting the number of slots per frame based on the feedback. Yet, when nodes generate bursty traffic patterns both approaches are not optimal because the discovery process either reduces network data throughput (due to time required to build the tree) or increases node energy consumption (due to data packet collisions in subsequent frames).

Due to the limitations of existing MAC protocols for such scenarios, in this paper we focus on the design, implementation and evaluation of Low-Power Distributed Queuing (LPDQ). LPDQ is based on LPL for network synchronization and DQ for channel access, and includes Channel Hopping (CH) to add robustness against multi-path propagation and external interference. The paper also presents the implementation of LPDQ using off-the-shelf hardware and a custom software stack, and discusses its main challenges and the solutions that have been adopted. Finally, an experimental evaluation is also presented, demonstrating LPDQ performance and comparing it to FSA in terms of packet throughput. The main benefits of the LPDQ compared to FSA are: a) No collisions during data packet transmission, b) Performance is independent on the number of nodes, and c) Resources are evenly distributed among nodes. To the best of our knowledge, this is the first paper that presents and evaluates the performance of a MAC protocol based on the principles described above for the IoT. Moreover, as far as we know, none of the current research includes experimental evaluation showing the feasibility of the MAC protocol when implemented using low-power commercial radio transceivers.

The remainder of the paper is organized as follows. Section 2 presents the research related to improving the performance of FSA, as well as the research related to DQ. Section 3 presents the design principles and operational details of LPDQ. Section 4 discusses the implementation of LPDQ using off-the-shelf hardware and a custom software stack. Section 5 evaluates the performance of LPDQ and compares it to FSA. Finally, Section 6 concludes the paper.

4.2. Related work

This section presents the work related to our research and is divided into two subsections. The first subsection presents the research related to improving the performance of FSA, whereas the second subsection introduces DQ and presents the existing research. As introduced earlier, MAC protocols can be classified into reservation based, random access and hybrid. In that sense, FSA can be classified as random access, whereas DQ can be classified as hybrid. Other examples of hybrid channel access protocols are ZMAC and Crankshaft, which are extensively reviewed in Bachir et al. [55] together with other reservation based and random access MAC protocols.

4.2.1. Frame Slotted ALOHA

FSA is the channel access mechanism used by standards that need to support data collection scenarios where nodes generate bursty traffic, e.g., ISO 18000 [5]. ISO 18000 is a family of standards targeted at Radio-Frequency IDentification (RFID), e.g., item identification and management applications. The ISO 18000-1 standard defines the generic system architecture, whereas the remaining parts of the standard, e.g., ISO 18000-2 to ISO 18000-7, define the physical layer and data-link layer parameters to operate at different frequency bands, e.g., 135 kHz, 13.56 MHz, 2.45 GHz, 868-915 MHz, and 433 MHz. In particular, the data-link layer of ISO 18000-7 [5], which is targeted at active RFID operating in the 433 MHz band, uses LPL to wake-up nodes and FSA to enable data transmission. However, due to the effects of contention, e.g., two nodes transmitting in the same slot, the maximum performance of FSA is 36.8% only when the number of slots per frame is equal to the number of contending nodes [61].

To improve the performance of FSA, several authors have proposed various methods based on two principles. First, using a tree splitting algorithm to detect the number of nodes present in the network a priori, e.g., previous to data transmission. Second, determining the optimal number of slots per frame a posteriori, e.g., based on the information extracted from collisions in the current slot. The different proposals that are available in the literature are summarized next.

Yoon et. al. [62] propose two mechanisms to improve the tag anti-collision protocol. The first is based on a dynamic approach to enable the reader select the optimal slot size. The second is based on a broadcast command that enables to put tags to sleep more effectively. The results, based on real-world experiments, show that the collection time is directly proportional to the number of tags. In [63], Yeh et al. present Adaptive Splitting and Pre-Signaling (ASPS), a counter-based tag anti-collision protocol that uses adaptive splitting and pre-signaling to reduce tag collision. First, by means of predicting the number of tags it can split them into groups to reduce collision probability. Second, by means of using pre-signaling it is possible to reduce tag identification delay. The results obtained show that the MAC protocol achieves a maximum efficiency of 55%. Nilsson et al. [64] present and evaluate a contention-based MAC protocol for active RFID that uses a non-persistent Carrier Sense Multiple Access / Collision Avoidance (CSMA/CA) with a dynamic back-off window in a non-slotted channel. The paper studies energy consumption, read-out delay and message throughput based on computer simulations. The results show that it is possible to reduce the average energy consumption, leading to a 50 % increase in tag battery lifetime. In [65], Chin et al. present E^2MAC, an energy efficient MAC that uses a dynamic FSA with three different frame types to read and monitor tags. The results show that the protocol reduces the number of collisions and the energy wasted to resolve them.

More recently, Namboodiri et al. investigate in [61] the effects of collisions in slotted ALOHA-based protocols for RFID and show that collisions have an impact on both the transaction time and the energy required to complete it. The authors derive a mathematical model of the protocol performance, validate it using simulations and, finally, evaluate it using an experimental setup. In the experimental phase the energy consumption of both the reader and the tags is evaluated, confirming that the consumption is directly proportional to the number of tags present in the reader field. In [66], Qian et al. present Adaptively Splitting-based Arbitration Protocol (ASAP), a protocol that creates groups of tags on demand and estimates the cardinality of each group during this process. The authors perform both theoretical analysis and simulation evaluation to show that the performance of ASAP is better than other existing collision-arbitration protocols and the efficiency is close to the theoretically optimal values. Finally, Wu et al. [67] present a novel anti-collision protocol based on a binary tree slotted ALOHA, which allows to adjust the number of slots per frame to a value close to the number of tags. The results show that the MAC performance can be increased to 42%.

4.2.2. Distributed Queuing

DQ is a channel access mechanism that evolves from Collision Tree Algorithm (CTA) [68]. In CTA, the ternary feedback (e.g., empty, collision and success) obtained from the transmission of data packets in a given slot is used to subsequently split nodes into sub-groups to reduce the collision probability of future data packet transmissions. Empty feedback is provided when no station transmits a data packet in a given slot, collision feedback is provided when two or more stations transmit a data packet, and success feedback is provided when only one station transmits a data packet. Using such approach it is possible to ensure that after a certain number of transmissions, which depends on the number of slots per frame and the number of nodes in the network, each node will be able to transmit without contention. In that sense, DQ improves over CTA in three different ways. First, DQ interleaves the contention resolution process with the transmission of data packets. Second, DQ uses smaller packets to obtain ternary feedback from nodes requesting access to the network. Third, DQ uses the feedback obtained to organize the nodes in two different queues, one to manage the subsequent resolution of collisions and the other to manage the transmission of data packets. Compared to CTA, using such approach enables DQ to minimize the effects of contention, thus leading to an increase in network performance and a reduction in the energy consumption of nodes.

Originally, DQ was designed for the distribution of digital signals over wired networks, e.g., CAble TeleVision (CATV) [69]. However, over the years DQ has been adapted to the specific requirements of other types of networks, both wired and wireless. Regarding the latter, in DQRAP/CDMA [70] it was adapted for third generation cellular networks based on Code Division Multiple Access (CDMA). In DQCA [71, 72] it was adapted for Wireless Local Area Networks (WLANs). In DQMAN [73] it was adapted for Mobile Ad Hoc Networks (MANETs). Finally, in DQBAN [74] it was adapted for Body Area Networks (BANETs). In all cases DQ has been able to ensure collision-free data transmissions and offer a near optimum performance that is independent of the offered traffic and the number of nodes present in the network. This is specially interesting for data collection scenarios in the IoT, where a large number of nodes generate bursty traffic patterns.

4.3. Protocol design

In this section we present and describe the operation principles of LPDQ, a MAC protocol specifically suited for scenarios where nodes, either static or mobile, are collected on demand and generate bursty traffic patterns. Such requirements makes the use of both reservation based and random access protocols either impractical or inefficient. First, reservation based protocols are not suitable because the number of nodes is unknown a priori and, thus, a network schedule cannot be pre-calculated. Second, random access protocols are not suitable because the bursty traffic pattern saturates the network, leading to packet collisions and an increased energy consumption due to retransmissions. A particular example of such scenario are active RFID networks, where the goal is to collect data from devices present within the coordinator communication range. Active RFID networks can be been used to create real-time inventory of items in

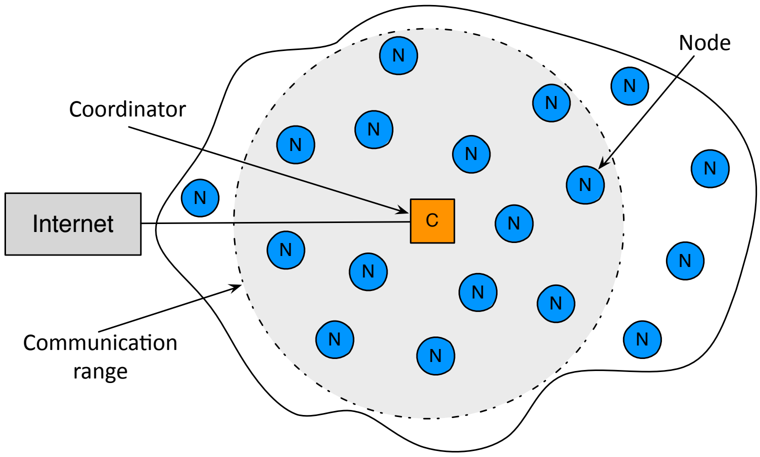

Figure 4.1: Network topology with a coordinator and multiple nodes.

a warehouse or collecting data sensor from nodes in a smart city.

4.3.1. Reference topology and design principles

LPDQ uses a single-hop star topology with two device types, node and coordinator, as depicted in Figure 4.1. A node (or device) is a battery-operated device that includes a low-power radio transceiver that enables it to communicate with the coordinator. In addition, a node may contain sensors and actuators to monitor physical parameters or actuate over physical elements. On its behalf, a coordinator (or gateway) is the device responsible for triggering communications with nodes and interfacing with other networks, e.g., the Internet.

As introduced earlier, LPDQ is based on three design principles: Low-Power Listening (LPL), Distributed Queuing (DQ) and Channel Hopping (CH). First, LPL is used for network synchronization and enables the coordinator to wake up nodes that are within its communication range. Second, DQ is used as the channel access mechanism and ensures that all each node knows exactly which action to take in each frame, e.g., receive or transmit a packet, and that all data transmissions in the network are collision free despite there is no network schedule. Third, CH is used to add robustness to the network against the effects of multi-path propagation and external interferences from other networks operating in the same band. Using these principles, the operation of LPDQ is divided in two phases: network synchronization and data transmission. These two phases are described in detail in the following subsections.

4.3.2. Network synchronization

In LPDQ, communications are triggered by the coordinator, as depicted in Figure 4.2. The network synchronization phase is responsible for waking up all nodes that are within the coordinator communication range and synchronizing them to enable data transmission. By default, nodes are in a low-power listening mode in which they periodically wake up and turn on the radio transceiver for a short period of time to detect communication requests from surrounding coordinators. The period between two consecutive wake-up events is called *check interval*, whereas the time that the node remains in the wake-up state is called *wake-up time*. Upon detecting a command from upper layers, e.g., application layer, the coordinator starts broadcasting wake-up packets. The overall duration of the network synchronization phase is called *synchronization interval*. Within the *synchronization interval*, wake-up packets are transmitted at a rate called *transmit interval* and have a duration named *transmit duration*. Wake-up packets are formed by a short preamble and payload and, among other information, contain the time at which nodes are expected to enter the data transmission phase and, also, the channel offset at which nodes are expected to start communicating. Thus, when nodes receive a wake-up packet from a coordinator they configure a time event to wake up at a specific moment in time and enter the data communication phase, which is described in the following subsection.

The parameters that describe the operation of the network synchronization phase, e.g., *check interval* and *wake-up time*, as well as the channel that nodes listen to, are configurable according to target network synchronization delay and node energy consumption. Frequent *check intervals* and long *wake-up times* lead to fast network synchronization at the expense of increasing node average energy consumption. In that sense, it is mandatory that all nodes that are part of a network share the same con-

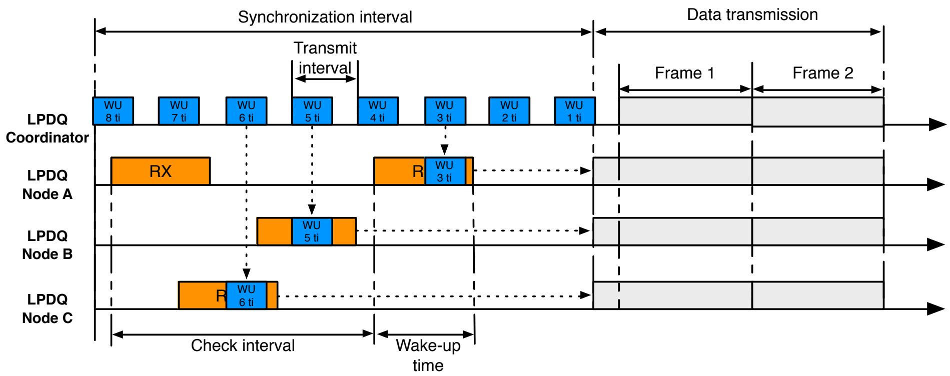

Figure 4.2: Network synchronization using low-power listening. Node C receives the wake-up packet when 6 ticks remain, whereas Node B receives it when 5 ticks remain and Node A receives it when only 3 ticks remain. However, because all nodes share the same notion of time, they will wake-up simultaneously to start the data transmission phase.

figuration parameters to be able to synchronize with a coordinator and enter the data transmission phase. To achieve such behaviour a tick is defined among all nodes as the smallest unit of time at which events can occur within the network. For example, during the synchronization phase the *check interval* can be configured to 1000 ticks and the *wake-up time* to 2 ticks, thus defining a 0.2% duty cycle. The tick unit of time is obtained by each node independently from a clock with a good resolution, e.g., 1 μs, and low drift, e.g., 10 ppm, to ensure that actions are executed at the same time. Furthermore, due to the asynchronous nature of communications, two constraints need to be met to ensure that all nodes within the coordinator communication range receive at least one wake-up packet during the *check interval* [75]. First, the coordinator *synchronization interval* has to be longer than the node *check interval*. Second, the coordinator *transmit interval* has to be shorter than the node *wake-up time*.

4.3.3. Data transmission

In LPDQ the data transmission period operates in a synchronous basis using a time-fixed frame structure that repeats over time until communications are completed, e.g., when nodes have no further data packets to be transmitted to the coordinator. At each frame, three time-fixed subperiods are defined: access request, data transmission and feedback information, as depicted in Figure 4.3. The aim of the access request subperiod is to enable nodes to request network access by means of transmitting an Access Request Packet (ARP). The aim of the data transmission subperiod is to enable nodes to transmit a data packet to the coordinator without contention. Finally, the aim of the feedback information subperiod is to enable the coordinator transmit a FeedBack Packet (FBP) that provides nodes with information regarding the status of the access request and the data transmission subperiods, e.g., data positive or negative acknowledgement. In addition, a Short Inter-Space Frame (SIFS) and Long Inter-Space Frame (LIFS) are introduced to compensate for random delays, e.g., data processing. The SIFS and LIFS differ in their duration because the time to process the data is different in each case. In the SIFS the node only requires to calculate the packet CRC and to switch the radio from reception to transmission. Contrarily, in the LIFS the coordinator has to perform more actions, e.g., it needs to compute the status of each ARP.

In order to ensure collision-free data transmission, two distributed queues are used; one to organize nodes that need to resolve their collisions during the access request subperiod (CRQ, Collision Resolution Queue) and another to organize nodes that have successfully entered the system and are awaiting to transmit their data packet to the coordinator (DTQ, Data Transmission Queue). Both queues are distributed in the sense that each node only has two integer numbers representing each queue; one number that represents the total length of the queue (same value in all nodes) and another number that represents the relative position of the node within the queue (different for each node). The resolution of collisions within the CRQ is done using a Blocked Tree Splitting Algorithm (BTSA) and a set of rules, e.g., a node can only transmit an ARP if the CRQ is empty and it does not hold any position in the DTQ. A detailed overview of the protocol operation, including the set of rules that determine how queues are managed and how nodes behave under each situation, can be found in [71].

The access request subperiod is further divided into a configurable number m of ARP

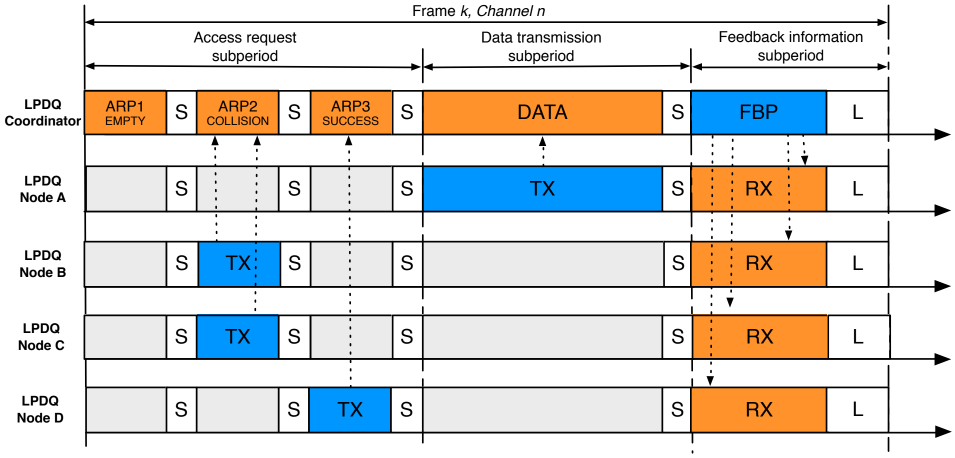

Figure 4.3: Data transmission using a time-fixed structure with access request, data transmission and feedback information subperiods. Example: in the access request subperiod the ARP1 is empty (no node transmits an ARP), the ARP2 is collision (Node B and Node C transmit an ARP, so they will join the CRQ) and ARP3 is success (only Node D transmits an ARP, so it will join the DTQ). In the data transmission subperiod Node A transmits its data packet because it is at the head of the DTQ. Finally, in the feedback information subperiod the coordinator transmits a FBP that is received by all nodes. Note that S stands for SIFS and L stands for LIFS.

slots, and it is used by the nodes to request access to the network. To do so, they select an ARP slot at random and transmit an ARP. The coordinator operates in receive mode for the complete access request subperiod and listens to the ARPs transmitted by nodes. According to the outcome of each ARP slot, the coordinator can distinguish between three states: empty, success or collision. An ARP slot is empty if no node has transmitted an ARP in that slot. An ARP slot is declared successful when a single ARP has been received and decoded. Finally, a collision occurs when two or more nodes transmit in a particular ARP slot and none can be decoded by the coordinator. The outcome of each ARP slot (empty, success or collision) is later provided by the coordinator to the nodes in the FBP subperiod. Based on the outcome, nodes that succeed in transmitting an ARP enter the DTQ, whereas nodes that collide enter the CRQ. Using such approach, nodes are progressively separated into smaller groups and the process is repeated in every frame until all nodes are queued in the DTQ. Therefore, collisions in LPDQ can only happen during the access subperiod and are used to organize nodes into the CRQ or DTQ depending on the ARP outcome. This implies that the energy wasted due to collisions is reduced in LPDQ with regard to other MAC protocols that use data packets to contend because collisions only happen with ARPs, which are shorter than data packets. Moreover, BTSA ensures that in every frame a maximum number of m nodes can solve their previous ARP collision and enter the DTQ. This approach reduces the average number of ARP transmission attempts required by each node to enter into DTQ logarithmically.

The data subperiod is used by the node at the head of the DTQ, i.e., at the first position, to transmit its data packet to the coordinator. The outcome of a data packet in the data subperiod is threefold: success, empty or error. Success indicates that the coordinator received the data packet successfully. Empty indicates that no data packet was detected in the current data subperiod. Finally, error indicates that the data packet could not be properly received, e.g., it did not pass the Cyclic Redundancy Check (CRC). As only one node can hold the first position of the DTQ at any given time, LPDQ ensures that data packets are transmitted without contention. Besides, LPDQ is protocol agnostic, meaning that the data packet is able to transport any type of upper layer protocol. For example, a data packet can have a IPv6 over Low power Wireless Personal Area Networks (6LoWPAN) header, thus allowing IP addressing. Moreover, because LPDQ is designed for one-hop communications, routing protocols at the network layer are not required, e.g., Routing Protocol for Low-Power and Lossy Networks (RPL) [76]. To enable communications with other networks, e.g., the Internet, the coordinator can actuate as a gateway implementing any address translation or routing protocol, and forwarding data accordingly.

The feedback subperiod is devoted to transmitting the feedback packet. The feedback packet is broadcast by the coordinator and must be received by all nodes that are currently part of the network. The feedback packet contains information regarding the status of each ARP slot in the access subperiod, e.g., empty, success or collision, and the data packet in the data subperiod, e.g., success, empty or error. Based on the information received in the feedback packet, nodes are able update their relative positions in the CRQ and DTQ. For example, if a node transmitted an ARP with success, it will enter the DTQ at the last position. Contrarily, if the ARP collided, the node will enter the CRQ at the last position. Also, if the data packet in the data subperiod was successful, the node will leave the DTQ, enabling the next node to transmit its data packet in the subsequent frame. The feedback packet also includes the current values of the CRQ and the DTQ to enable nodes ensure that their local values are consistent with the whole network and allow the recovery of nodes that may have lost one of the feedback packets. Finally, the feedback packet also includes a field that determines the end of the current collection period. Such condition occurs when the coordinator detects a certain number of frames without receiving any ARP and the DTQ being empty, i.e., neither new access requests nor data pending to be transmitted.

Finally, because LPDQ may operate in unlicensed bands or multiple LPDQ networks may coexist in the same location, a mechanism to provide robustness against physical layer effects, e.g., multi-path propagation and external interference, is required. To provide robustness against such physical layer effects, LPDQ uses a slow channel hopping mechanism similar to that of IEEE 802.15.4e [27]. The available bandwidth, W, is divided into a number of equispaced channels, $N_{channels}$. In the particular example of the IEEE 802.15.4e, $N_{channels} = 16$, numbered from 0 to 15. The channel to be used in frame $i + 1$ is denoted by c_{i+1} and can be computed as

$$c_{i+1} = [c_i + S_{pattern}] \pmod{N_{channels}}, \tag{4.1}$$

where c_i is the channel used in the previous frame i, and $S_{pattern}$ is a sequence pattern of integer numbers that is included by the coordinator in the wake-up packets during the synchronization phase. This sequence can be randomly generated by the coordinator for each collection round to provide the system with higher reliability. Note that a node which does not know and follow the sequence will not be able to interfere the network set by a given coordinator.

4.4. Protocol implementation

This section presents the implementation details of LPDQ, including both the hardware platform and the software stack that have been developed, as well as the configuration parameters that have been used. In addition, the section presents the implementation challenges that have been found during the implementation and discusses how these challenges have been addressed.

4.4.1. Hardware platform

To implement and evaluate LPDQ we have developed OpenMote-433, a Commercial Off-The-Shelf (COTS) low-power wireless platform. OpenMote-433, depicted in Figure 4.4, is based on a Texas Instruments CC430 System on Chip (SoC) [77], which embeds an MSP430 16-bit RISC microcontroller, running at 16 MHz with 4 kBytes of RAM and 32 kBytes of Flash memories, and a CC1101 radio-transceiver, which operates at the Sub-GHz band with data rates of up to 600 kbps and supports Amplitude Shift Keying (ASK), Frequency Shift Keying (FSK) and Minimum Shift Keying (MSK) modulations. The radio transceiver has been tuned to the 433 MHz band using a discrete balun and connected to a $\lambda/4$ monopole antenna through an SMA connector. Finally, two AAA batteries provide energy to the system (3 V, 1500 mAh).

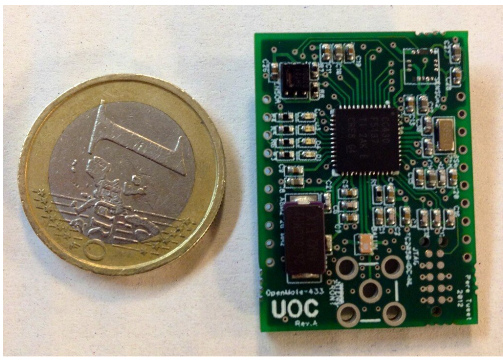

Figure 4.4: An OpenMote-433 board with a Texas Instruments CC430 SoC.

Parameter	Value
Frequency band	433 MHz
Channel number	2
Channel frequency	433.380 MHz
Channel bandwidth	540 kHz
Modulation scheme	MSK
Data rate	250 kbps
Transmit power	0 dBm
Sensitivity	-91 dBm

Table 4.1: LPDQ physical layer parameters.

4.4.2. Physical layer

LPDQ is independent of the physical layer and thus can operate in any frequency band, at any data rate, and with any modulation scheme. However, for the sake of the evaluation in this article, we have implemented LPDQ to operate at the 433 MHz band. This is the band of operation defined in the specification of the IEEE 802.15.4f amendment [13] to the IEEE 802.15.4 standard [6], which is targeted at active RFID applications, e.g., data collection scenarios.

This amendment defines three possible data rates, i.e., 31, 100 and 250 kbps, and a type of continuous phase FSK modulation called MSK. For our implementation, we have used a data rate of 250 kbps, which yields a measured sensitivity of -91 dBm for a Packet Error Rate (PER) of 1% transmitting packets of 20 bytes and using a channel bandwidth of 540 kHz. This data rate has been selected because it is equivalent to that of IEEE 802.15.4 and achieves the least energy consumption per bit while offering a range that has been measured to be 1.6 times that of the 2.4 GHz band in real conditions [78]. In case that a longer range is required, the lower data rates defined in the standard, e.g., 31 kbps or 100 kbps, can be selected at the expense of increasing the energy consumption per bit if the transmit power is kept constant.

4.4.3. Network synchronization phase

Regarding network synchronization, the implementation of low power listening on both the coordinator and the nodes has been realized using the microcontroller hardware.

The time reference has been obtained from the internal Real-Time Clock (RTC), which operates at 32.768 kHz. Therefore, the minimum time unit at which events are resolved is referred to as a tick and its duration is equal to 30.51 μs (1/(32.768 kHz)).

Upon the reception of a command from the application layer, the coordinator initiates the synchronization phase. A timer is configured to periodically generate an interrupt that wakes-up the microcontroller. Upon wake-up, the microcontroller configures the transceiver and transmits a wake-up packet that has a duration of *transmit duration*. After the wake-up packet has been transmitted the microcontroller puts the transceiver back to sleep mode until the next wake-up event defined by *transmit interval*. The process is repeated until the total duration of the synchronization phase expires, which is defined by *synchronization interval*.

On the node side, the timer is configured to periodically generate an interrupt that wakes-up the microcontroller (*check interval*). Upon wake-up, the microcontroller configures the radio transceiver and puts it in receive mode for a certain amount of time (*wake-up time*). Once the wake-up event expires, the microcontroller puts the transceiver back to sleep mode until the next wake-up event. If a wake-up packet is successfully received from the coordinator when the transceiver is in receive mode, the node schedules the beginning of the next data transmission phase (indicated in the wake-up packet) by configuring a timer interrupt and goes back to sleep. The interrupt will wake up the node to start the data transmission phase at the right time.

The network synchronization parameters that describe the operation of the coordinator and the nodes are summarized in Table 4.2. With such configuration parameters, the node radio duty cycle during the synchronization phase has a value of approximately 0.1%, which yields an average energy consumption of 30 uA on our platform. With a battery capacity of 1500 mAh, a node can remain alive in the network synchronization phase for 5 years.

Parameter	Ticks	Time
Synchronization interval	65535 ti	2 s
Transmit interval	32 ti	0.9765 ms
Transmit duration	16 ti	0.4882 ms
Check interval	32768 ti	1 s
Wake-up time	32 ti	0.9765 ms

Table 4.2: LPDQ network synchronization parameters.

4.4.4. Data transmission phase

Regarding data transmission, the implementation of the frame timing on both the coordinator and the nodes has also been realized using the microprocessor RTC, attaining the same tick resolution. As described earlier, there are three fixed-time subperiods in each frame: access request, data transmission, and feedback information. The parameters that characterize and describe the duration of each subperiod are summarized in Table 4.3. Taking into consideration these parameters, LPDQ operates at a rate of 84 frames/second.

The number of ARP slots, m, within the access subperiod can be arbitrary chosen and determines the speed at which collisions can be resolved. Xu et al. demonstrated in [79] that setting $m = 3$ is sufficient to ensure the stability of the protocol by resolving collisions in the access request subperiod faster than the actual transmission of data packets. Increasing the number of slots has minimal impact on the performance of the collision resolution mechanism but extends the duration of the frames at no gain. Therefore, we have set $m = 3$ in our implementation.

Regarding the data transmission subperiod, it is important to note that with the chosen timing configuration and selected data rate, as presented earlier, the data packet is able to transport a payload of up to 127 bytes. Such configuration makes LPDQ fully compatible with standardized protocols for the Internet of Things [51], i.e., 6LoWPAN frames and other upper layer protocols such as the Constrained Application Protocol (CoAP).

Finally, it is important to remark that all nodes must receive each FBP to maintain synchronization and properly update the values of CRQ and DTQ. Therefore, nodes

Parameter	Ticks	Time
Access subperiod	28 ti	0.85 ms
Data subperiod	168 ti	5.12 ms
Feedback subperiod	42 ti	1.28 ms
SIFS	16 ti	0.488 ms
LIFS	32 ti	0.976 ms
Total	390 ti	11.9 ms

Table 4.3: LPDQ data transmission parameters.

apply a simple mechanism to detect possible synchronization losses and to correct them, e.g., when a FBP is not received due to multi-path propagation or external interference. The mechanism makes use of a counter that is initialized to a predetermined value. This counter is decreased by one unit every time a FBP is not received. In such case, the node also resets the value of CRQ and DTQ to avoid interfering with other nodes. If the counter reaches zero, the node considers that it has lost communication with the coordinator and returns to the synchronization phase.

4.4.5. Implementation challenges

Four main challenges had to be resolved to operate LPDQ in a robust manner. These challenges are described in the next subsections.

Time synchronization

LPDQ has much stricter timing requirements than FSA as five different events occur within a frame: an ARP subperiod with $m = 3$ ARP slots, a data subperiod with a data slot and, finally, a feedback subperiod. Attaining such a granular synchronization poses a severe challenge because loosing synchronization can lead to interference in the protocol behavior, e.g., a node transmitting out of the slot bounds. There are three aspects related to time synchronization that had to be taken into account along the implementation process:

1. **Clock drift.** Due to physical characteristics of the crystals used to source the microcrontroller RTC, e.g., construction, temperature, aging, etc., the ticks of

the clock may have a relative drift between nodes. In order to compensate this drift, each node aligns its clock in the data transmission phase when it receives the feedback packet from the coordinator. With this approach it is possible to achieve a per-frame network-wide synchronization of ±1 tick or ±30.51 μs with the coordinator. This is sufficient to ensure that crystal characteristics do not interfere with the protocol timing. Other techniques to cope with clock drift due to temperature effects have been recently reported in [80].

2. **Turn-around times.** The delay to turn on and off the radio transceiver and the time it takes to change from one state to the other, e.g., from idle to receive or transmit and vice-versa. These delays are caused by the time it takes for the radio transceiver clock to stabilize. Since these delays are deterministic, or have a worst case response time, it is possible to measure the worst case condition of each delay using a logic analyzer and compensate them in the firmware. For example, in our implementation, an event that needs to change the radio transceiver state from idle to receive is compensated by 4 ticks or 122 μs, which is enough to be in accordance with the CC430 datasheet [77].

3. **Processing delays.** The time it takes the microcontroller to prepare a packet to be transmitted or to process the data received from the radio transceiver, and to take action based on it, is not deterministic. Moreover, this time is different for nodes and the coordinator because they process data differently. For instance, nodes need to execute the protocol rules after receiving a feedback packet from the coordinator. To compensate for these delays, we have included a SIFS after each ARP slot in the access subperiod and after the data packet in the data subperiod, and a LIFS after the feedback packet in the feedback subperiod. This ensures that both the coordinator and the nodes have enough processing time.

ARP selection

The collision resolution process is logarithmic because nodes are subsequently divided into sub-groups each time they collide. The base of the logarithm at which collisions are resolved depends on the number of ARP slots in each access subperiod, e.g., three ARP slots per access subperiod ensures that the collision resolution process is log_3. However, to ensure that the resolution of ARP collisions is truly logarithmic the selection of ARP slots by the nodes has to meet the following properties:

1. It has to follow a uniform distribution, e.g., all the ARP slots must have the same probability to be selected.

2. It must have no memory, e.g., the selection of the next ARP slot shall not depend on the previously selected ARP slot.

The mechanism to select the ARP in nodes is based on a Pseudo-Random Number Generator (PRNG). In order to obtain a truly random process, we obtain the seed for the PRNG by reading the noise level at input of the Analog-to-Digital Converter (ADC). Then, the pseudo-random sequence is generated using a Galois Linear-Feedback Shift Register (LFSR).

A simple experiment has been conducted to check the suitability of this approach. A single node selects an ARP slot at random within the access request subperiod and transmits an ARP to the coordinator. The process is repeated 25.000 times and the state probability, e.g., the probability of selecting each ARP, and state transition probabilities, e.g., the probability of selecting an ARP depending on the ARP previously selected, are computed. The results obtained, shown in Figure 4.5, validate the effectiveness of such mechanism.

However, it is worth noting that if two or more nodes generate the same initial seed, then all the pseudo-random numbers that will be generated using the Galois LFSR will be exactly the same. Thus, the nodes will select the same ARP slots again and again, resulting in continuous ARP collisions. This situation would lead to nodes not being able to join the DTQ and therefore, not being able to transmit their data packets. To

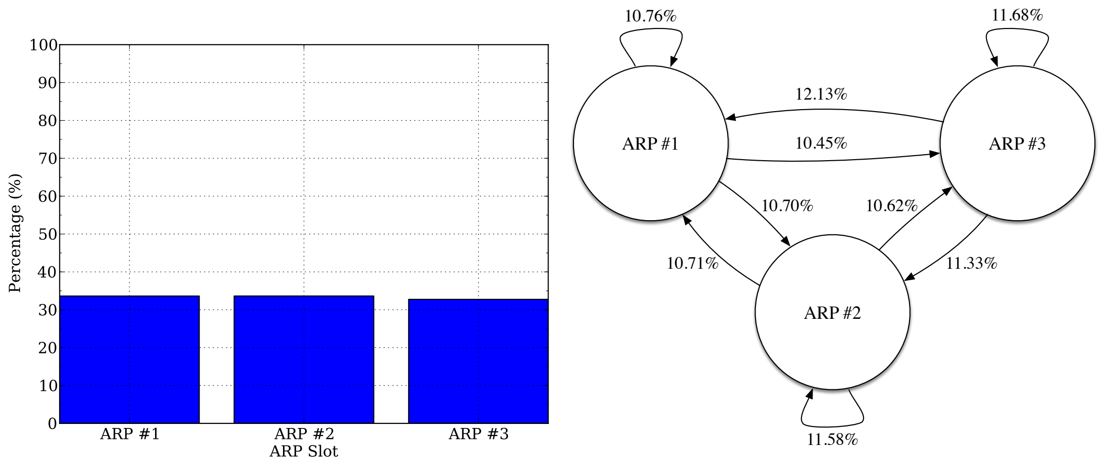

(a) (b)

Figure 4.5: Selection and transition properties of the ARP selection mechanism based on a Galois LFSR.

solve this problem our implementation ensures that a new seed is generated every time a node collides in the transmission of an ARP.

Collision detection

Detecting collisions in the access subperiod is a great challenge. Radio transceivers have not been specifically designed for such purpose, but to provide robust data transmissions. However, the proper operation of the BTSA, and thus LPDQ, depends on the successful detection of whether each ARP is either success, empty or collision, to enable nodes join the appropriate queue; the CRQ in the case of ARP collision and the DTQ in the case of ARP success.

Ideally, the state of an access request slot, e.g. idle, success, or collision could be established by determining *i)* the presence or absence of a physical layer preamble (note that all data packets must have attached a preamble to enable synchronization at the receiver side), and *ii)* the amount of energy present in the channel for the duration of an ARP, i.e., the Receiver Signal Strength (RSS). In the latter case, a threshold must be defined to determine when the channel is considered to be either occupied or idle.

According to these two criteria, the following four situations can occur:

- Preamble detected and RSS above the threshold; in this case, a success is claimed.
- Preamble detected and RSS below the threshold; in this case, a collision is claimed.
- Preamble not detected and RSS above the threshold; in this case, a collision is claimed.
- Preamble not detected and RSS below the threshold; in this case, no transmission occurred.

In our implementation, we have set the RSS threshold at -80 dBm. In order to define this value, we have analyzed the noise level present in the channel using a spectrum analyzer to ensure that the false positive rate, defined as the probability that a collision is detected when the ARP slot is actually empty because no node transmitted an ARP, is negligible.

Unfortunately, real world implementation shows that artifacts such as clock drifts, transmission delays, or propagation effects, make the status detection more difficult. In particular:

1. **Lack of synchronization**. Assuming that nodes are synchronized to a clock with a 1 tick resolution, and considering that two nodes can have a maximum relative drift of 2 ticks, e.g., 61 μs, a node can start transmitting its ARP up to 61 μs earlier than another node. Therefore, the coordinator will receive the preamble of a node before the preamble of the other, detecting a successful ARP transmission when, indeed, a collision has occurred.

2. **Capture effect** [81]. The coordinator can receive the transmissions from two nodes with different RSS values due to either their different location or the effects of multi-path propagation. Therefore, the coordinator will receive the signal from the closest node with higher RSS, treating the signal of the furthest node as noise or interference. Again, a successful ARP slot will be announced when, in reality, a collision has occurred.

In both cases the feedback provided by the coordinator will indicate that the ARP slot has been successful and the two nodes will enter the DTQ in the same position. This will lead to a collision in the data subperiod when both nodes get to the first position of DTQ simultaneously, yielding a degradation of the protocol performance.

In order to overcome these two problems, LPDQ attaches the node Unique IDentifier (UID) and a CRC to each ARP. Therefore, once an ARP is received, a CRC check is performed. If the check is successful, then the node UID of the successful ARP is included in the feedback packet. However, if a preamble is correctly detected but the CRC check fails, then the ARP is considered to be collided and a null node UID is indicated in the feedback packet by the coordinator. Therefore, the detection of the status of the ARP slots becomes very reliable, avoiding the effects of the capture effect and the lack of perfect synchronization. It is worth mentioning that assuming an ideal configuration with $m = 3$ access slots, the inclusion of 3 UIDs in the FBP has no significant impact on the performance of the protocol, even though the overhead increases slightly. As an alternative to including the UIDs and thus reduce the overhead, it would be possible to include a random number computed per node per each transmitted ARP and making sure that the probability that two or more nodes select the same random number and select the same ARP slot in the same frame is negligible.

Multi-path propagation

It has been demonstrated that channel hopping at the 2.4 GHz band is able to combat both multi-path propagation and external interference effects [82]. On the one hand, multi-path propagation is caused by reflected radio-frequency signals, which are out-of-phase with the main signal propagation path. This phenomena may lead to destructive interference that reduces Packet Delivery Ratio (PDR). On the other hand, external interferences are caused by other networks operating in the vicinity at the same frequency band. Similarly, this phenomena may lead to a reduction in the PDR when listen-before-talk mechanisms are not implemented.

However, at the Sub-GHz bands, it has been demonstrated that channel hopping can only combat the effects of external interferences. This is due to the fact that the channel coherence bandwidth at the sub-GHz bands is larger than the available bandwidth [78], which causes that all the channels of the band are highly correlated. Taking into consideration these results, other mechanisms may be required to add robustness against multi-path propagation in LPDQ implementations that operate at Sub-GHz bands. Among other alternatives, the inclusion of antenna diversity at the physical layer could help solve this problem.

4.5. Protocol evaluation

In this section, we conduct an empirical evaluation of the LPDQ protocol. The first subsection presents the results of a single experiment with 15 nodes to help understanding the operation of LPDQ with regard to the CRQ and DTQ evolution over time, as well as the transmission of data packets within each frame. The second subsection presents the results of experiments depending on the number of nodes present in the network and compares them with the simulated results of the optimal configuration of FSA, e.g., when the number of slots per frame is equal to the number of nodes present in the network [83].

4.5.1. Single experiment

In this experiment, 15 nodes and the coordinator were placed on a table at an approximate distance of 2 m, as shown in Figure 4.6. The coordinator and the nodes used the configuration parameters presented in the previous section and summarized in Table 4.1, Table 4.2 and Table 4.3. All nodes transmitted their packets with a power of 0 dBm and, with such configuration, the average RSS at the coordinator was approximately equal to -35 dBm. In each experiment nodes synchronized using the LPL mechanism described in Section 3 and transmitted data packets to the coordinator until the experiment was over. In each experiment nodes had an infinite number of data packets to be transmitted. This means that, upon successful transmission of a data packet, each node contended again for the channel by transmitting an ARP in the next available frame once the CRQ became empty and new access requests were granted. Each experiment consisted of 2 seconds for network synchronization and 3 seconds for data transmission, which translates into approximately 255 frames.

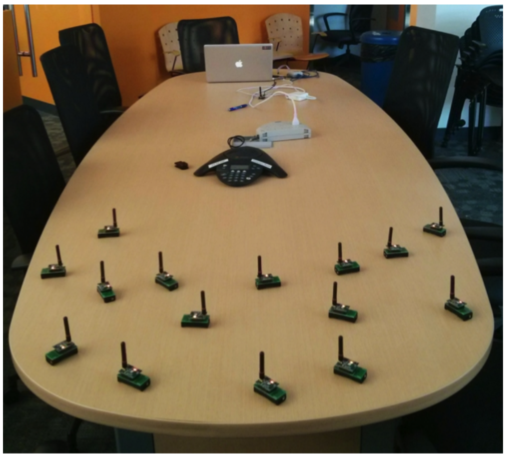

Figure 4.6: Experiment setup with a coordinator and 15 nodes.

Figure 4.7 shows the evolution over time of the total number of elements in the CRQ and the DTQ, i.e., the queue length, as well as the accumulated packet count for successful and empty frames for two independent experiments, (a) and (b). The horizontal axis represents the time evolution in terms of the absolute frame number, i.e., the number of frames that have elapsed since the start of the experiment. The left vertical axis represents the instantaneous length of the CRQ and DTQ, whereas the right vertical axis represents the count for each of the data packet states in each frame, e.g., success, empty or error. In a particular frame, the *success* event indicates the probability that a packet transmitted in the data subperiod was successfully received by the coordinator, the *empty* event indicates that there were no packet transmissions and, finally, the *error* event indicates that there was a packet transmission but it was discarded by the coordinator as it did not pass the CRC check.

In both figures, it can be observed that the CRQ and DTQ lengths evolve over the frame number and rapidly converge to their expected values. The CRQ becomes empty once all nodes have successfully resolved their collisions and, thus, have entered the DTQ. In its turn, the length of the DTQ converges to *n-1*, where n is the number of nodes in the experiment (here $n = 15$), due to the fact that there is always a node at the head of the DTQ that is transmitting its data packet. The convergence time of both queues is non-deterministic because it depends on the particular selection of ARPs made by each node independently in every experiment. For example, Figure 4.7a converges after 30 frames whereas Figure 4.7b converges after 20 frames. However, the convergence time is bounded in the sense that all collisions will be eventually resolved by virtue of the BTSA and the fact that the PRNG is compliant with the ARP selection requirements, as demonstrated in the previous section.

Another important property that can be observed in both experiments is that the success rate in the transmission of data packets is high, 99.27% and 98.53% respectively, and there are no collisions during data packet transmission. This is owing to the fact that only the node that is at the head of the DTQ is allowed to transmit in the data subperiod. However, there are some empty data packets in both experiments, 0.73% and 1.47% respectively. This phenomenon is caused by two effects. First, due to the fact that the initial data subperiods are empty because the DTQ is empty, as nodes are waiting in the CRQ to resolve their ARP collisions. Second, nodes may loose synchronization with the CRQ and DTQ values due to a corrupt FBP caused by the effects of multipath propagation or external interference. Under such circumstances, nodes are forced to reset their respective pointers to the DTQ and CRQ, e.g., the positions that they may hold in either queue, to avoid interfering with other nodes. Thus, the data subperiod assigned to these nodes will be empty. However, it is important to remark that such event does not affect the remaining nodes because they will update their pointers accordingly upon receiving the FBP.

Figure 4.8 shows the histogram for the same two experiments presented in Figure 4.7. In this case, the horizontal axis represents the unique identifier of each node that takes part of the experiment, whereas the vertical axis is the percentage of data subperiods assigned to each of these nodes. It is important to remark that the bin with Node ID zero

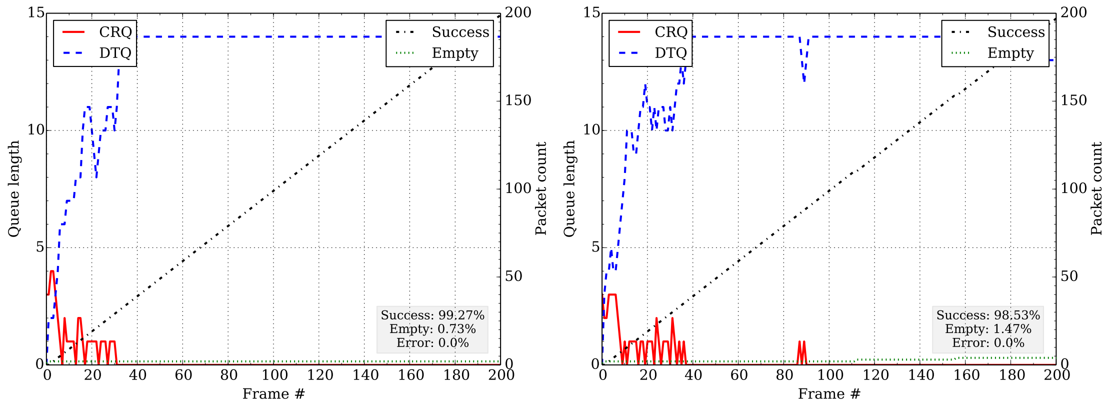

(a) Experiment 1 (b) Experiment 2

Figure 4.7: Queue Lengths and Packet Count Evolution for Two Different Experiments, (a) and (b), with 15 nodes. Note that in both experiments there are no packet collisions or error packets.

is the probability that a data subperiod is empty due to the reasons explained before.

The main aspect to observe in Figure 4.8 is how all nodes receive a fair share of the network resources despite the fact that there is no scheduler that determines which node can transmit at each frame. That is, the network is able to autonomously build a schedule using the BTSA and the information obtained from resolving the collisions in the access subperiod. In particular, each node in the network receives one out of each n data subperiods, with n being the number of nodes that are part of the network. The small differences that can be appreciated among certain nodes (below 1.0%) are due to the fact that a single experiment only lasts for approximately 255 frames and, at that point, some nodes may have had the chance to transmit an additional data packet whereas other nodes are still waiting on the DTQ to transmit their respective data packet.

4.5.2. Average performance

In this subsection, the experiment setup to evaluate the average performance of LPDQ was the same as in the previous section. Nodes synchronized using the LPL mechanism and transmitted data packets to the coordinator. Each experiment was com-

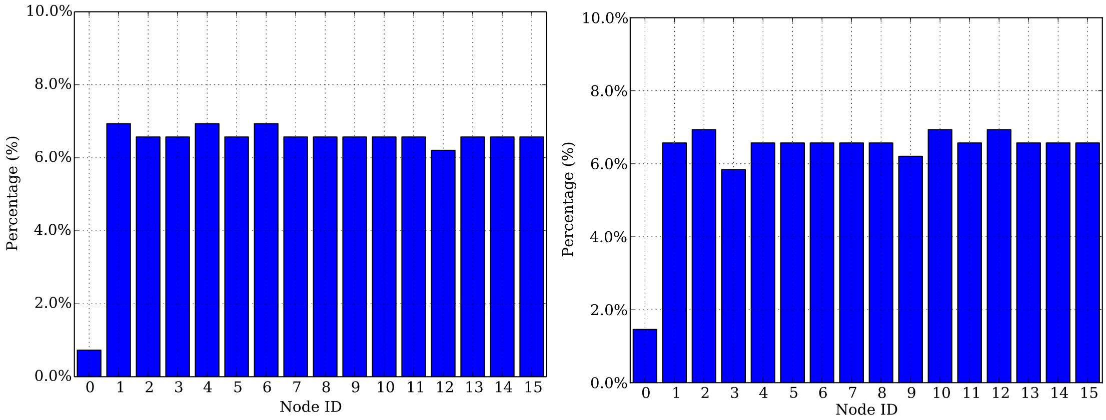

(a) Experiment 1 (b) Experiment 2

Figure 4.8: Data transmission histogram for two different experiments, (a) and (b), with 15 nodes. Note that Node ID zero represents the empty probability.

prised of 2 seconds for network synchronization and 3 seconds for data transmission, which translated into approximately 255 frames. However, here we conducted experiments with a different number of nodes (from 5 to 25 nodes, in steps of 5 nodes) to evaluate the data transmission mechanism of LPDQ. We repeated each experiment 100 times to compute the average and standard deviation and observe how LPDQ behaves on average depending on the number of nodes in each experiment.

As presented earlier, two key performance indicators of LPDQ are the evolution over time of the CRQ and the DTQ lengths depending on the number of nodes that were present in the network. Figure 4.9a shows the average evolution of the CRQ length for the different number of nodes in each experiment. Each point in the line is the average of 100 experiments and the shadowed surface above and below the average curve represents the standard deviation of the experiments. In the beginning of the experiment, the length of the CRQ grows rapidly due to the collisions occurring in the ARP slots when all the devices attempt to get access to the channel. However, the BTSA algorithm splits collisions into subgroups and allows to resolve them in subsequent frames. Once a collision is resolved, the successful nodes enter the DTQ at the last position (in any arbitrary order, for example using the chronology of the access slots), thus ensuring that no collisions exist during the transmission of data packets. Finally, after a certain number of frames, the length of the CRQ converges to zero. Since only one node can leave the DTQ at a given frame, once the network reaches steady state operation the CRQ is always empty on average. However, as described in the previous section, small deviations exist due to the fact that the collision resolution process is non-deterministic.

It is worth recalling that the BTSA is blocking; thus, nodes that have already transmitted a data packet have to wait until the CRQ is empty to be able to enter the network again. This behavior explains the sudden increase in the length of the CRQ after it starts decreasing, e.g., around frame 15 for the experiment with 25 nodes. At that point, all the nodes that have already transmitted a data packet will try to access the system again because the CRQ is empty, causing another batch of ARP collisions. However, the BTSA resolves these collisions again and the length of the CRQ converges again to zero. Note that the number of contending nodes in this second batch of collisions is lower than at the beginning because there are nodes which are still in the DTQ waiting for their turn to transmit. In this case, the collision resolution algorithm and the data transmission process are executed simultaneously, leading to an improved network performance.

Figure 4.9b shows the evolution over time of the average DTQ length for the different number of nodes in each experiment. Again, the horizontal axis represents the time evolution in terms of the frame number, where each point is the average of 100 experiments and the shadowed surface above and below the average curve represents the standard deviation of each experiment, and the vertical axis represents the average length of the DTQ. It is possible to observe how the length of the DTQ rapidly converges to $n - 1$ and the standard deviation is bounded. This is due to the fact that at each frame only one node can leave the DTQ. It is also important to remark that the time it takes for the length of the DTQ to converge is bounded. In the worst case scenario, this time is determined by the BTSA, which depends on the value of n and m.

LPDQ yields a performance that is close to the optimal that can be achieved at the MAC layer thanks to the use of the distributed queues CRQ and DTQ, and the use of the BTSA. In addition, since collisions are confined to the ARPs slots, which are

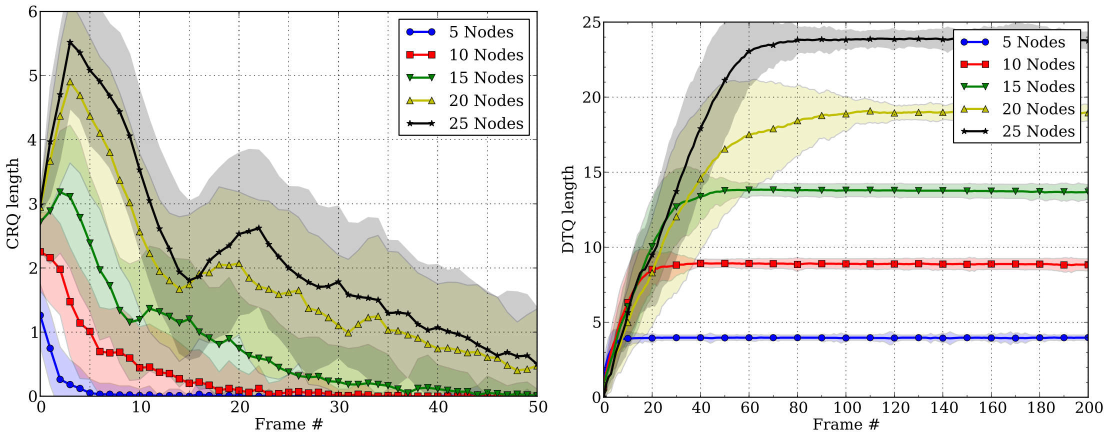

(a) (b)

Figure 4.9: Evolution of the average length of the CRQ (a) and the DTQ (b) depending on the number of nodes in the network in each experiment.

very small compared to the data subperiod, the energy required to solve collisions is smaller. Moreover, the concurrent execution of the collision resolution algorithm and the transmission of data offers a performance advantage with other MAC protocols using data packets for contention.

Finally, Figure 4.10 shows the average outcome of data packet transmissions with LPDQ, that is, the percentage of success, empty and error packets depending on the number of nodes in each experiment. Each point is the average of 100 experiments and the error bars represent the standard deviation. As it can be to observed, LPDQ achieves a MAC performance close to 99% with a typical standard deviation smaller than 5% regardless of the number of nodes. This behavior is caused by the fact that there are no data packet collisions. Instead, collisions are confined to ARP slots and, based on its outcome, nodes are organized into the CRQ and DTQ. However, there is a small probability that some data subperiods are empty, e.g., 2% for the experiment with 20 nodes. As presented earlier, this behavior may be caused by the effects of external interference or multi-path propagation, which may cause a FBP packet to not be successfully received by a node. This leads to the reset of the DTQ and CRQ pointers, which forces that particular node to re-enter the system. In that case, the data subperiod assigned to the node remains empty because no other node will be able to transmit its data packet. However, as described earlier, such event does not affect the remaining nodes in terms of throughput, latency, fairness or energy consumption, because they will update their pointers accordingly upon the reception of the FBP. The results of Figure 4.10 are also summarized in Table 4.4.

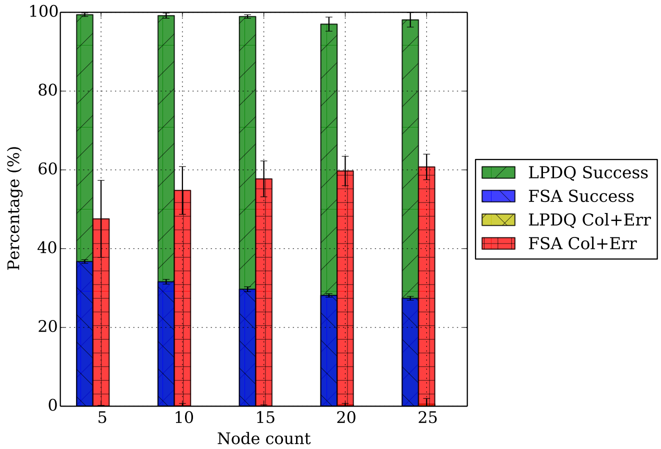

Figure 4.10: Average data packet transmission with FSA and LPDQ. Note that the *LPDQ Col+Err* bar does not appear because there are (almost) no packet collisions or error packets in the experiments.

Outcome / Nodes	**5**	**10**	**15**	**20**	**25**
LPDQ Success	99.39	99.15	98.93	96.99	98.07
LPDQ Collision	0.06	0.15	0.09	0.33	0.54
LPDQ Empty	0.55	0.7	0.98	2.68	1.39
FSA Success	36.73	31.59	29.71	28.13	27.39
FSA Collision	47.56	54.78	57.71	59.71	60.74
FSA Empty	15.71	13.63	12.58	12.16	11.87

Table 4.4: Average data packet transmission, collision and empty percentage (%) with FSA and LPDQ. Notice that the residual collision probability in LPDQ is due to external effects such as external interference or multi-path propagation.

In conclusion, LPDQ offers a clear performance advantage over FSA or any other random access packet based on contention with data packets. Even in the optimal case, e.g., when the number of slots per frame is equal to the number of nodes in the network, FSA yields a MAC performance of only 36.8%. This implies that, with FSA, approximately only 4 out of 10 packets transmitted by the nodes will be successfully received by the coordinator. This increases the amount of time required to collect information from all the nodes of the network and it also increases the average energy consumption of nodes. Note that every packet retransmission leads to additional energy charge being extracted from the battery. In addition, it is important to remark that optimum performance of FSA can be achieved when $n = m$, which implies a priori knowledge of the network. However, LPDQ operates independently of the number of devices in the network. Finally, it is worth highlighting another interesting property of LPDQ; even without a network schedule that determines how resources are assigned to nodes, the MAC protocol is fair. As nodes join the DTQ in order and only one node can leave the DTQ at a time, all nodes in the network receive the same amount of network resources, e.g., transmission opportunities.

4.6. Conclusions

This paper has introduced LPDQ as a novel efficient, fair, and low-power MAC protocol specifically suited for wireless data collection scenarios with a large number of nodes, either fixed or mobile, that generate bursty traffic. Today, such scenarios are typically addressed by MAC protocols based on FSA, which has a maximum efficiency of 36.8% due to the effects of contention. Moreover, such efficiency can only be achieved when the number of slots per frame is equal to the number of nodes in the network, which is unknown a priori. On the contrary, LPDQ is able to dynamically build and dynamically update a network schedule that enables all nodes to transmit free-of-collisions data packets, thus achieving efficiencies close to 99%. In addition, LPDQ performance is independent of the number of nodes in the network and fair in the sense that all nodes receive a similar amount of network resources. The paper has presented the design principles, operation fundamentals, implementation details of LPDQ and an experimental evaluation using real hardware. The implementation and the results presented in this paper demonstrate the suitability of the technology for low-power commercial radio transceivers and outline it as a clear candidate for upcoming IoT standards targeted at data collection scenarios with an unpredictable number of connected devices. As future work we plan to extend LPDQ to multi-hop networks, which would enable to further extend the range of the wireless network while maintaining its performance. Such an extension would be of great interest to environments where network deployment is costly or difficult, e.g. smart cities applications.

5 Experimental Energy Consumption of Frame Slotted ALOHA and Distributed Queuing for Data Collection Scenarios

***Abstract**: Data collection is a key scenario for the Internet of Things because it enables gathering sensor data from distributed nodes that use low-power and long-range wireless technologies to communicate in a single-hop approach. In such scenario the network is composed of one coordinator that covers a particular area and a large number of nodes, typically hundreds or thousands, that transmit data to the coordinator upon request. Considering this scenario, in this paper we experimentally validate the energy consumption of two Medium Access Control (MAC) protocols, Frame Slotted ALOHA (FSA) and Distributed Queuing (DQ). We model both protocols as a state machine and conduct experiments to measure the average energy consumption in each state and the average number of times that a node has to be in each state in order to transmit a data packet to the coordinator. The results show that FSA is more energy efficient than DQ if the number of nodes is known a priori because the number of slots per frame can be adjusted accordingly. However, in such scenarios the number of nodes cannot be easily anticipated, leading to additional packet collisions and a higher energy consumption due to retransmissions. Contrarily, DQ does not require to know the number of nodes in advance because it is able to efficiently construct an ad hoc network schedule for each collection round. Such schedule ensures that there are no packet collisions during data transmission, thus leading to an energy consumption reduction above 10% compared to FSA.*

5.1. Introduction

The Internet of Things (IoT) aims at making domestic, industrial and city-wide processes more efficient and sustainable by revealing real-time information to its stakeholders and enabling them to make informed decisions [58]. Until today, such information has remained hidden to them due to the lack of available infrastructure. However, this is currently changing and Wireless Sensor Networks (WSN) are a key asset because they provide the communications infrastructure that enables to collect data from distributed sensors. In that sense, there is an ongoing paradigm shift in low-power wireless communications towards using single-hop long-range technologies instead of conventional short-range mesh technologies. The rational behind such change is reducing the cost of deploying the communications infrastructure while retaining the capacity of nodes to operate for years using batteries. In practice, this paradigm shift implies that a large number of nodes can now be potentially addressed by each network coordinator, which creates new challenges that need to be investigated and addressed.

In particular, the challenges introduced by single-hop long-range wireless technologies are key in data collection scenarios because the number of nodes present in the network is unknown a priori and is dynamic between consecutive collection rounds. Moreover, since nodes in a data collection scenario only communicate when triggered by the network coordinator, either periodically or on demand, this creates bursty traffic patterns that are a potential source of network congestion and energy expenditure. Given the unknown number of devices and the bursty traffic patterns, as well as the low-power requirements described earlier, designing a low-power Medium Access Control (MAC) protocol is important for data collection scenarios. The MAC layer controls when the radio transceiver receives or transmits and, thus, it determines the average energy consumption of nodes [55]. It is well-known that the energy waste at the MAC layer comes from four sources [54]: idle listening, packet overhearing, packet collisions and protocol overhead. Thus, it is crucial to design MAC protocols that are efficient in these terms.

The MAC layer for data collection scenarios is typically based on Frame-Slotted

ALOHA (FSA) due to its simplicity. Other alternatives such as Time Division Multiple Access (TDMA) or Carrier Sense Multiple Access (CSMA) [55] are not used because the number of nodes is unknown a priori or due to the performance effects of the hidden node [84]. In FSA time is divided into frames which, in turn, are divided into a number of fixed-length slots. Each node to be collected selects one slot of the current frame at random and transmits its data packet. The outcome of each slot can be empty, success or collision. Successful nodes go back to sleep and the process is repeated until all nodes have been successfully collected. Despite its simplicity, it is well-known that the maximum performance of FSA is bounded to around 36.8% due to the effects of contention [83]. Moreover, such efficiency can only be achieved when the number of slots per frame is equal to the number of nodes [61], which is unknown a priori. Over the last decade different proposals have been made to improve the performance of FSA [85]. These approaches are either based on adapting the number of slots per frame through estimating the number of nodes from collisions or by means of building a query tree prior to collecting the data from nodes.

An alternative to FSA is Distributed Queuing (DQ), which was first presented by Xu et al. [69, 79] for the distribution of CATV (Cable TeleVision) signals and has later been adapted to wireless communications [70, 71, 72, 73]. In short, DQ is a channel access mechanism that ensures collision-free data transmissions and offers a near optimum performance that is independent of the offered traffic and the number of nodes present in the network. DQ evolves from CTA (Collision Tree Algorithm) protocols [68], where the ternary feedback (e.g., empty, collision and success) obtained from the transmission of data packets is used to subsequently split nodes into sub-groups to reduce the collision probability of future data packet transmissions. However, DQ has several advantages over CTA. First, it interleaves the contention resolution process with the transmission of data packets. Second, it uses specific packets that are shorter than data packets to obtain the ternary feedback. Third, it uses the feedback obtained to organize the nodes in two different queues, one to manage collision resolution and the other to manage data transmission. This enables to minimize the effects of contention, thus leading to an increase in network performance and a reduction in the energy consumption.

Taking that into account, in Vazquez et al. [86] we proposed an analytic energy consumption model of FSA and DQ for data collection scenarios and validated it using computer simulations. The results showed that in data collection scenarios DQ can reduce the energy consumption by more than 80% compared to FSA thanks to the way it organizes nodes into queues to ensure that there is no contention during data packet transmission. However, an implementation of DQ was not available at that time and, consequently, the results of the energy model were not empirically validated. Thus, the aim of this article is to experimentally validate the energy consumption model of FSA and DQ in a data collection scenario. To do that we build a testbed, implement both FSA and DQ, and conduct a series of experiments to evaluate its energy consumption. The results obtained show that FSA can be very energy efficient when the number of nodes is known in advance and the number of slots per frame adjusted accordingly. However, such conditions are unrealistic and additional energy consumption can be expected. Contrarily, DQ does not require to know the number of nodes in advance, as it is able to dynamically build an ad hoc network schedule to ensure collision free data transmission. On average, DQ offers a 10 % reduction in energy consumption compared to the optimal FSA. This adds to the fact that DQ has a MAC layer efficiency close to 100%, whereas FSA can only achieve a MAC layer efficiency around 36.8% [87].

The remainder of the article is organized as follows. Section 2 presents the operation of FSA and DQ. Section 3 presents the analytical energy consumption model of FSA and DQ. Section 4 presents the experiments to validate the energy consumption of FSA and DQ and a discussion of the results obtained. Finally, Section 5 concludes the article.

5.2. Background

This section presents the operation background of Frame-Slotted ALOHA (FSA) and Distributed Queuing (DQ). For a detailed operation of FSA and DQ please refer to [85] and [71] respectively.

5.2.1. Frame Slotted ALOHA

In FSA time is divided into fixed-length frames that repeat over time until data from all nodes has been successfully collected, as depicted in Figure 5.1. Each frame starts with a feedback period that enables the coordinator to provide information to nodes regarding the number of slots in the current frame, as well as the length of each slot. After the feedback period there are k fixed-length data slots that enable nodes to transmit their data packets to the coordinator. Each data slot is divided into two subperiods, data and acknowledgement. The data subperiod enables nodes to transmit its data to the interrogator, whereas the feedback subperiod enables the interrogator to acknowledge the correct reception of the data.

At the beginning of each frame nodes who have still not been successfully collected by the coordinator select at random one slot of the k slots available in the current frame and transmit their data packet. The random number is drawn from a uniform distribution to ensure that all slots have the same probability of being selected. The outcome of each slot can be threefold: empty, collision or success. Empty happens when no node selects that particular slot. Collision happens when two or more nodes select the same slot. Finally, success happens when only one node selects a given slot. Depending on the outcome of each particular slot the coordinator provides feedback to the nodes. Based on such feedback each node decides which action to take. Nodes that have been successfully collected go back to sleep until a next collection round begins. Contrarily, nodes of which packets have collided in the current frame wait until the next frame starts and repeat the process. Thus, the data collection process is repeated until the coordinator detects that all the slots of the current frame are empty.

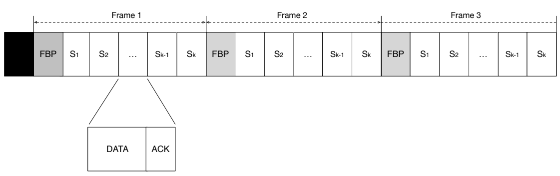

Figure 5.1: Frame Slotted ALOHA (FSA) time organization. The black square in front of the first frame represents the protocol used to wake-up and synchronize the nodes.

5.2.2. Distributed Queuing

In DQ time is divided into fixed-length slots but, contrarily to FSA, the slots are not grouped in frames. As depicted in Figure 5.2, within each slot three sub-periods are defined, the access request subperiod, the data transmission subperiod and the feedback subperiod. From a node perspective, the data and the feedback subperiods serve the same purpose as in FSA, that is, transmit a data packet to the coordinator and receive a FBP (FeedBack Packet) from the coordinator. However, the access request subperiod serves a different purpose. It enables nodes to request access to the system by transmitting an Access Request Packet (ARP) in one of the m available ARP slots. Similarly to FSA, the ARP slot is selected at random, e.g., using a uniform distribution. An ARP is a short packet, compared to a data packet, that enables the coordinator to distinguish between the three states, e.g. empty, collision or success, as described earlier. The number of ARP slots in the access request subperiod can be optimized depending on the number of nodes. A small number of ARP slots increases the network throughput, whereas a large number of ARP slots reduces the time to resolve collisions. However, it has been show in [79] that $m = 3$ is the minimum number that ensures that the system is stable.

Based on the feedback provided by the coordinator in the feedback subperiod nodes are organized into two queues, the Collision Resolution Queue (CRQ) and the Data Transmit Queue (DTQ). On the one hand, the CRQ is used to resolve collisions during the access request subperiod. Nodes that transmit in the same ARP and collide are subsequently grouped together to resolve their collisions in subsequent attempts. This policy works towards creating smaller groups with reduced collision probability at each step which, in the end, ensures a successful ARP transmission no matter the conditions, e.g., number of contending devices. On the other hand, the DTQ is used to queue devices that have successfully transmitted their ARP and are waiting to transmit their data packet to the coordinator. Because only one node can hold each position in the queue, this policy works towards ensuring that no collisions occur during the transmission of data packets. In DQ each queue is represented by two integer numbers, one that is global to the network and the other that is local to each node. The two global integer determine the overall length of each queue, whereas the two local integer determines the current position of the node in each queue.

Finally, there is a set of rules that determine two aspects of the protocol operation. First, how to update the global and local numbers that represent the CRQ and DTQ in each device based on the feedback provided by the coordinator in each slot. Second, what action can each device take in the next slot based on their current position on either of the queues. For example, a node can only hold a position in one or the other queue simultaneously, that is, it can either be waiting to resolve a collision or be waiting to transmit a data packet. Similarly, a node in the CRQ or the DTQ can only transmit if they are at the head of either queue. In contrast to FSA, the data collection process ends when the coordinator notices that both the CRQ and the DTQ are empty, that is, no further nodes are waiting to gain access to the system or have to transmit their data packet.

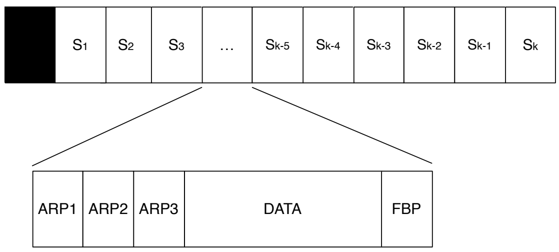

Figure 5.2: Distributed Queuing (DQ) time organization. The black square in front of the first slots represents the protocol used to wake-up and synchronize the nodes.

5.3. Energy Model

The analytic energy consumption model of FSA and DQ for a data collection scenario where a given number of nodes have to transmit a data packet to the coordinator was presented in [86]. However, the analytic model cannot be validated experimentally due to the assumptions made to develop it. Taking that into account, in this section we present a methodology to validate the energy consumption of FSA and DQ experimentally. In both cases the methodology is based on modeling the protocols as a state machine and measuring two parameters. First, the average number of times that a node has to be in each state in order to successfully transmit a data packet to the coordinator. Second, the average energy consumption that a node spends in each state due to radio transceiver activity, e.g., transmit or receive. A similar methodology has been used to evaluate other MAC protocols, such as WirelessHART [88] and IEEE 802.15.4e TSCH (Time Slotted Channel Hopping) [57, 89].

5.3.1. Frame Slotted ALOHA

In FSA a node can be in one of the following states: `FBP_LISTEN`, `DATA_WAIT`, `DATA_TRANSMIT` and `FBP_WAIT`, as depicted in Figure 5.3a. The actions that a node has to perform in each of these states are the following:

- `FBP_LISTEN`: A node is in the `FBP_LISTEN` at the beginning of each frame. In the `FBP_LISTEN` state a node has to receive the FBP from the interrogator. As described earlier, the FBP contains information regarding the number of slots of the current frame and the length of each slot. Based on that information each node independently selects one slot to transmit its data packet. The selection is made at random using a uniform distribution to ensure that all the slots have the same probability of being selected.

- `DATA_WAIT`: A node is in the `DATA_WAIT` state while it waits for the selected slot to transmit its data packet. During the `DATA_WAIT` state the node does not incur in any radio activity.

- `DATA_TRANSMIT`: A node is in the `DATA_TRANSMIT` state during the slot selected at random during in the `FBP_LISTEN` state. In the `DATA_TRANSMIT` state the node has to transmit its data packet to the coordinator and listen to the acknowledgement. If the transmission is successful the node goes back to sleep immediately. Otherwise, the node moves to the `FBP_WAIT` state, as described next.

- FBP_WAIT: A node that has collided during the transmission of its data packet enters the FBP_WAIT state, where it waits until the end of the current frame to start the process again by moving to the FBP_LISTEN state. During the FBP_WAIT state the node does not incur in any radio activity.

Given the state machine depicted in Figure 5.3a, it can be easily seen that in any given frame each node has to exactly be 1 time in the FBP_LISTEN and the DATA_TRANSMIT states and wait $N-1$ times in the DATA_WAIT and the FBP_WAIT states. Thus, in order to model the average energy consumption of FSA in a data collection scenario it is sufficient to measure the number of times that a node has to be in the DATA_TRANSMIT state, that is, the average number of times that a node has to transmit its data packet for it to be successfully received by the coordinator.

5.3.2. Distributed Queuing

In DQ there are four possible states in which a node can be: ARP_TRANSMIT, CRQ_WAIT, DTQ_WAIT and DATA_TRANSMIT. The actions that a node has to perform in each of these states are the following:

- ARP_TRANSMIT: A node is in the ARP_TRANSMIT state when it transmits an ARP to gain access to the DTQ. In the ARP_TRANSMIT state a node has to transmit an ARP to the coordinator in a randomly selected ARP slot (using a uniform distribution) and receive a FBP from the coordinator in the FBP subsection of the slot.

- CRQ_WAIT: A node is in the CRQ_WAIT state while it is waiting to become the head of the CRQ, which allows it to move back to the ARP_TRANSMIT state and transmit another ARP to gain access to the DTQ. While in the CRQ_WAIT state a node only has to receive a FBP from the coordinator in the FBP subsection of the slot.

- DTQ_WAIT: A node is in the DTQ_WAIT state while it is waiting to become the head of the DTQ, which allows it to move forward to the DATA_TRANSMIT state, as described next. Similarly to the CRQ_WAIT state, in the DTQ_WAIT state a node only has to receive a FBP from the coordinator in the FBP subsection of the slot.

- `DATA_TRANSMIT`: A node is in the `DATA_TRANSMIT` state when it becomes the head of the DTQ and is allowed to transmit its data packet. In the `DATA_TRANSMIT` state a node has to transmit a data packet packet to the coordinator in the DATA subsection of the slot and receive a FBP from the coordinator in the FBP subsection of the slot.

Given the state machine presented in Figure 5.3b, we can model the average energy consumption of DQ measuring the number of times that a node is in three states: `ARP_TRANSMIT`, `CRQ_WAIT` and `DTQ_WAIT`. We do not need to model the number of times that a node is in the `DATA_TRANSMIT` state for two reasons. First, because we assume that nodes only have one data packet to transmit. Second, because DQ ensures that there will be no collisions during the transmission of data packets, as only one node that holds the first position in the DTQ is entitled to transmit. In case of collision due to external effects, e.g., interference from another network operating nearby, the node would need to repeat the process again until the data packet is successfully transmitted to the coordinator.

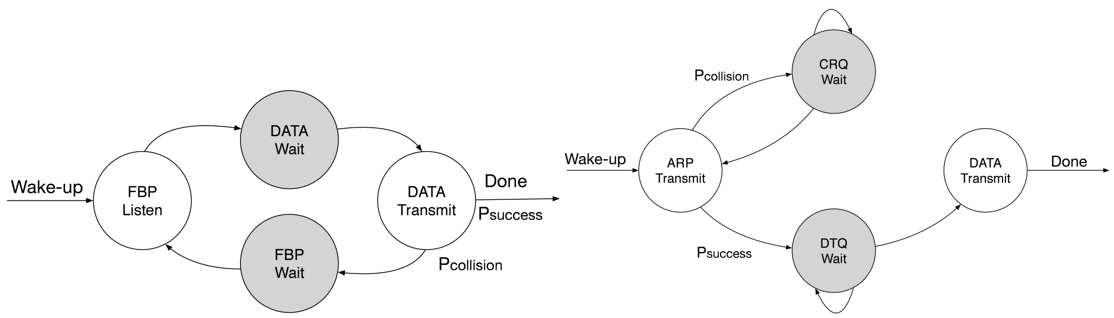

(a) Frame Slotted ALOHA (FSA) states. (b) Distributed Queuing (DQ) states.

Figure 5.3: FSA and DQ states.

5.4. Energy Consumption Evaluation

Based on the methodology to validate the energy consumption of FSA and DQ presented in the previous section, this section describes the experiments to evaluate the energy consumption of both FSA and DQ, as well as discuss the obtained results. First, we present the research platform and the parameters that have been used to conduct the experiments. Second, we present the methodology followed to conduct the experiments. Third, we present the energy consumption analysis of FSA and DQ. Finally, we discuss the obtained results.

5.4.1. Research Platform

The research platform is composed of 25 nodes and an interrogator connected to a computer that acts as the system manager, as shown in Figure 5.4. Both the interrogator and the nodes are based on OpenMote-433, a low-power wireless platform build using COTS (Commercial Off-The-Shelf) hardware. Specifically, OpenMote-433 is based on a Texas Instruments CC430 SoC (System on Chip), which embeds an MSP430 16-bit RISC microcontroller, running at 16 MHz with 4 kBytes of RAM and 32 kBytes of Flash memory, and a CC1101 radio transceiver, which operates at Sub-GHz bands with data rates of up to 600 kbps and support for amplitude and frequency modulations. In both cases the radio transceiver is tuned to the 433 MHz band using a discrete balun and connected to a $\lambda/4$ monopole antenna through an SMA connector. Since the experiments are conducted in close range, we have added a 30 dB RF (Radio Frequency) attenuator to the interrogator to ensure that the radio transceiver does not saturate due to the input power. Finally, the nodes are powered using two AAA batteries (3 V, 1500 mAh), whereas the interrogator is powered through the computer USB port.

Table 5.1 summarizes the physical layer parameters that have been used to conduct the experiments. The parameters used in the experiments are in accordance with the IEEE 802.15.4f amendment [13] to the IEEE 802.15.4 standard [6], which is targeted at active RFID (RadioFrequency IDentification) applications, e.g., data collection scenarios. IEEE 802.15.4f defines three possible data rates, i.e., 31, 100 and 250 kbps, and a type of continuous phase FSK (Frequency Shift Keying) modulation called MSK (Minimum Shift Keying). In our experiments we have used a data rate of 250 kbps, which yields a measured sensitivity of -91 dBm for a PER (Packet Error Rate) of 1%

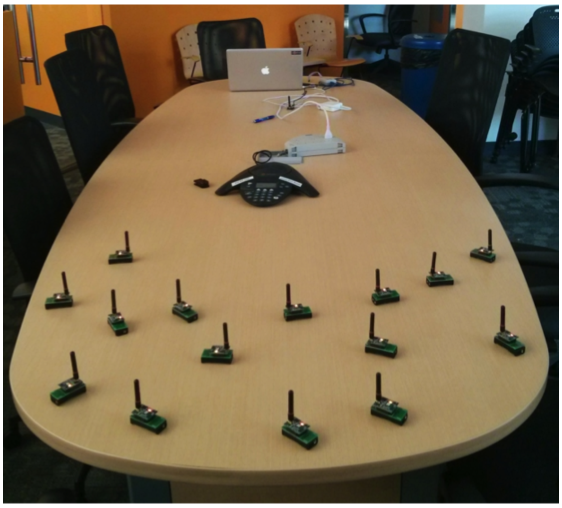

Figure 5.4: Research platform with 25 nodes, one coordinator and the system manager.

Parameter	**Value**
Frequency band	433 MHz
Channel number	2
Channel frequency	433.380 MHz
Channel bandwidth	540 kHz
Modulation scheme	MSK
Data rate	250 kbps
Transmit power	0 dBm
Sensitivity	-91 dBm

Table 5.1: Physical layer parameters according to IEEE 802.15.4f.

transmitting packets of 20 bytes and using a channel bandwidth of 540 kHz [78]. This data rate has been selected because it is equivalent to that of IEEE 802.15.4 and achieves the least energy consumption per bit while offering a range that has been measured to be 1.6 times that of the 2.4 GHz band in real conditions [78].

Table 5.2 summarizes the energy consumption of the CC1101 radio transceiver within the CC430 SoC. The CC1101 has four possible states: `OFF`, `SLEEP`, `TRANSMIT` and `RECEIVE`. Each state has a power associated taking into account that the system is supplied at 3 V. We only consider the radio transceiver consumption because the microcontroller is in sleep mode while the radio is transmitting or receiving and is only operating to process the packet.

States	Data Sheet (mW)	Measured (mW)
`OFF`	0.3	1
`SLEEP`	5.1	5.67
`TRANSMIT`	50.4	60.9
`RECEIVE`	54	54.3

Table 5.2: Power consumption of the CC430 SoC in different states. The differences in `OFF`, `SLEEP` and `RECEIVE` are due to the static consumption of other onboard peripherals, e.g., temperature, humidity and acceleration sensor. The difference in `TRANSMIT` is due to a higher transmit power to compensate for additional RF losses, e.g., balun.

5.4.2. Research Methodology

To perform the experiments and obtain the results we use the following methodology. By default nodes are in the preamble sampling state [59], where they periodically listen to the channel for a short period of time. When triggered, the interrogator sends a train of wake-up packets to synchronize the nodes present within its communication range. Upon synchronization, nodes enter the data transmit state, in which they transmit a 127 bytes data packet to the interrogator using the appropriate MAC protocol, e.g., FSA and DQ. Once a node has transmitted its data packet, it goes back to the preamble sampling state, where it remains until the next experiment begins. We perform an overall of 6 experiments with $k = 5, 10, 15, 20, 25, 30$ nodes respectively. Each experiment is repeated 100 times to obtain the average, minimum and maximum values.

FSA Experimental Results

To obtain the average energy consumption of FSA according to the model presented in Section 5.3.1, we determine the number of data packet transmissions that each node has to perform on average. To do so, we conduct an experiment where the nodes participate in a data collection scenario, that is, each node has one data packet to transmit to the coordinator. Because we know the number of nodes (n) in the experiment in advance we configure the number of slots per frame (k) to the optimal, that is, $k = n$ [61].

The results obtained in the experiments are depicted in Figure 5.5. On average, each node has to transmit its data packet twice in order for the packet to be successfully received by the coordinator. To validate the experimental results we conduct computer simulations using a Monte Carlo method. In the simulations, each of the n nodes selects one of the k slots at random to transmit a data packet. The random number follows a uniform distribution to ensure that the probability of selecting any given slot is equal. The simulations for each given k are repeated 10000 times and the average, maximum and minimum values are computed. As shown in Figure 5.5, the simulation and experimental results fit, thus validating the experimental results. The differences that can be appreciated between the simulation and experimental results can be explained by the capture effect [81], which is taking place due to the low number of nodes and the FSK modulation scheme that is used to transmit data.

Finally, in FSA the average number of data packet transmissions also determines the number of `FBP_LISTEN`, `DATA_WAIT` and `FBP_WAIT` states. For a given number of nodes n, the optimal number of slots per frame is $k = n$. Thus, if a given node has to transmit its data packet twice, it will also need to listen to two FBP, as well as remain $2k - 2$ slots waiting either prior to transmitting the data packet or waiting until the following FBP.

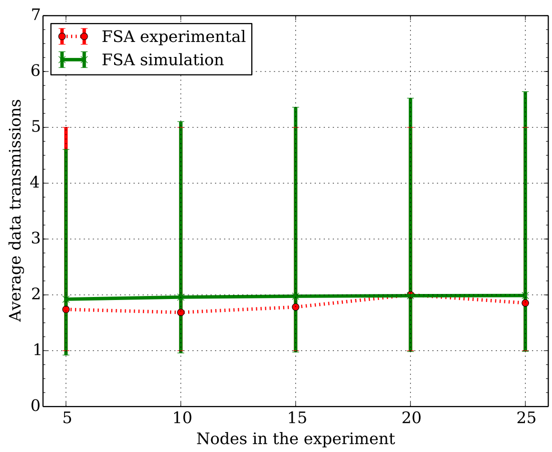

Figure 5.5: Average number of data packet transmissions using FSA. Each point is the average of 100 experiments and the error lines are the minimum and maximum values. If the number of slots per frame k is equal to the number of nodes n, on average data packets need to be retransmitted twice in order to be successful.

DQ Experimental Results

To obtain the average energy consumption of DQ according to the model presented in Section 5.3.2, we determine two things. First, the average number of ARPs that a node has to transmit in order to request access to the system. Second, the average number of slots in which a node has to wait in a queue, either the CRQ or the DTQ.

First, we validate the average number of ARP that a node needs to transmit in order to gain access to the DTQ. According to [68, 86], the number of slots in which a node tries to access the DTQ can be approximated by $d_N = log_m(n-1) + (\frac{1}{2} + \frac{\gamma}{log(m)}) + \frac{1}{2nlog(m)}$, where $\gamma = 0.5772$ (Euler constant). As depicted in Figure 5.6a, the measured data fits the theoretical data perfectly. For $m = 3$ the theoretical model can be simplified to $d_n = log_3(n-1) + 1$, which corresponds to the average number of levels in the ternary tree plus the root.

Second, we validate the average number of slots that a node has to wait in the CRQ queue in order to transmit an ARP to join the DTQ, as well as the average number of slots that a node has to wait in the DTQ queue in order to reach its head and be able to transmit the data packet. As depicted in Figure 5.6b, the number of slots waiting in the CRQ and the DTQ queues is linearly proportional to the number of nodes present in the experiment. Such result is as expected because either a priori or a posteriori nodes have to wait in a queue which average size will depend on the number of nodes within the experiment.

5.4.3. Energy Consumption Analysis

The average number of states that a given node of the network has to go through in order to transmit its data packet to the coordinator in a data collection round using FSA and DQ, as obtained in Section 5.4.2 and Section 5.4.2, is summarized in Table 5.3.

Measuring the average energy consumption in each of these states, it is now possible to obtain the average energy consumption of a given node. To do so, we first measure the time spent in each state for FSA and DQ using a logic analyzer. The timing is

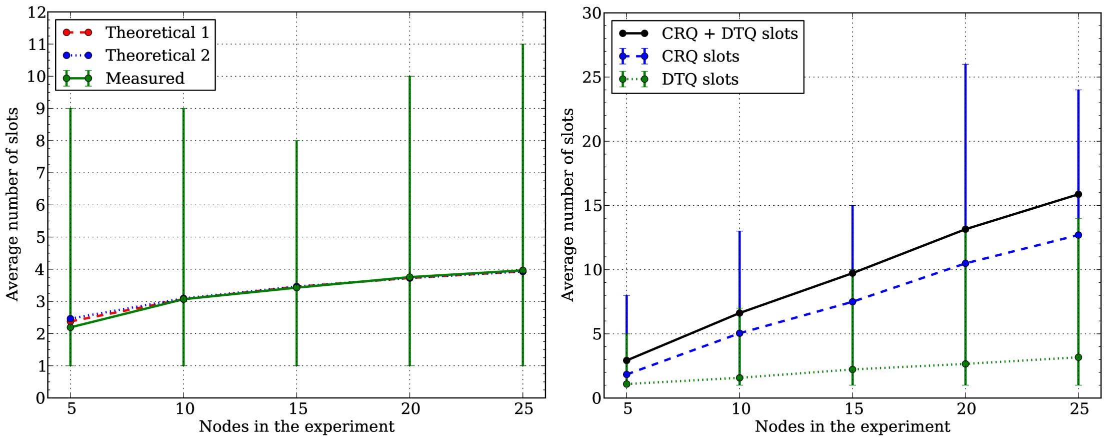

(a) ARP count.

(b) CRQ+DTQ count.

Figure 5.6: Average number of ARP and CRQ+DTQ required to be able to transmit a data packet using DQ. Each point is the average of 100 experiments and the error lines are the minimum and maximum values. The average number of ARP increases logarithmically, whereas the average number of CRQ+DTQ increases linearly.

		Nodes				
	States	**5**	**10**	**15**	**20**	**25**
FSA	`FBP_LISTEN`	2.0	2.0	2.0	2.0	2.0
	`FBP_WAIT`, `DATA_WAIT`	8.0	18.0	28.0	38.0	48.0
	`DATA_TRANSMIT`	2.0	2.0	2.0	2.0	2.0
DQ	`ARP_TRANSMIT`	2.2	3.1	3.4	3.8	4.0
	`CRQ_WAIT`, `DTQ_WAIT`	3.0	6.5	10.0	13.1	16.0
	`DATA_TRANSMIT`	1.0	1.0	1.0	1.0	1.0

Table 5.3: Average states for FSA and DQ that a node has to be in to transmit a data packet to the coordinator depending on the number of nodes in the network.

captured toggling on and off a pin when the radio enters or exits the transmit and receives modes. As stated in Section 3, in FSA a node can be in four different states: `FBP_LISTEN`, `DATA_WAIT`, `DATA_TRANSMIT` and `FBP_WAIT`. Conceptually, the `DATA_WAIT` and `FBP_WAIT` states are the same because the node remains waiting in sleep mode, e.g., no radio activity. Contrarily, the `FBP_LISTEN` and the `DATA_TRANSMIT` states are different, as a node has to execute different actions, e.g., receive a FBP or transmit a DATA packet plus receive an ACK packet. Similarly, in DQ a node also can be in four states: `ARP_TRANSMIT`, `CRQ_WAIT`, `DTQ_WAIT` and `DATA_TRANSMIT`. Here, the `CRQ_WAIT` and the DTQ_WAIT states are the same, e.g., the node remains waiting and only needs to receive a FBP. Contrarily, the ARP_TRANSMIT and the DATA_TRANSMIT are different. In the ARP_TRANSMIT state the node has to transmit an ARP packet to request access to the system and receive a FBP from the coordinator. In the DATA_TRANSMIT state the node has to transmit a DATA packet and receive a FBP from the coordinator. The timing of the radio in each state using FSA and DQ is depicted in Figure 5.7 and Figure 5.8 respectively.

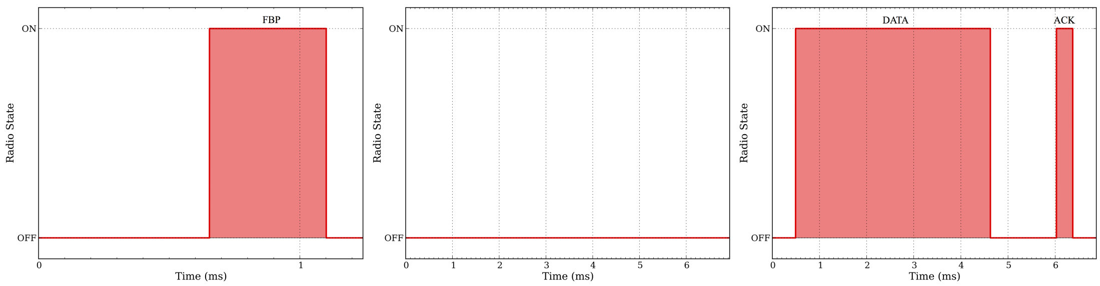

(a) FBP_LISTEN state. OFF=800 μs RX=450 μs

(b) FBP_WAIT and DATA_WAIT states. OFF=6.85 ms

(c) DATA_TRANSMIT state. OFF=2.3 ms RX=450 μs TX=4.1 ms

Figure 5.7: FSA states and radio activity. The total slot length is 6.85 ms, yielding an overall of 145 packets per second. In FSA the FBP_LISTEN state duration is shorter (1.25 ms) than other states.

Based on the timing and the radio activity in each of these states, as depicted in Figure 5.7 and Figure 5.8, and the power consumption in each radio state, summarized in Table 5.2, we can now obtain the average energy spent in each state for both FSA and DQ. Table 5.4 summarizes the energy consumption of FSA and DQ in each state.

Finally, with the energy spent in each state and the average number of times that a node has to be in each state in order to transmit a data packet, as summarized in Table 5.3, it is possible to calculate the average energy consumption of both FSA and DQ. We do so by multiplying the average number of times that a node is in each state by the energy consumption in each of these states depending on the number of nodes. The results are summarized in Table 5.5.

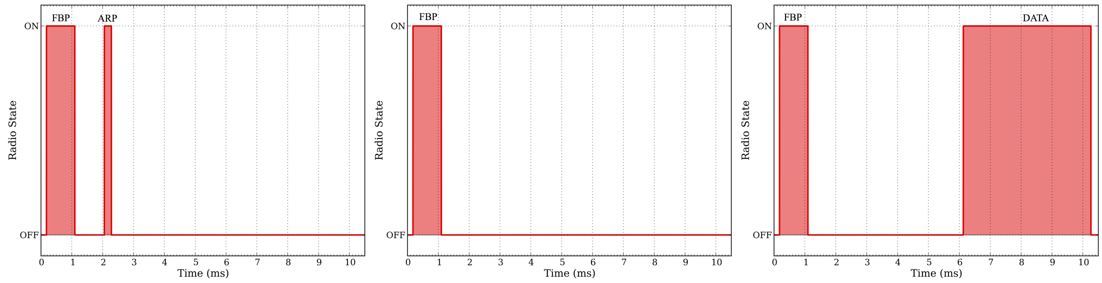

(a) `ARP_TRANSMIT`
OFF=10.6 ms
RX=1 ms
TX=300 μs

(b) `CRQ_WAIT` and `DTQ_WAIT`.
OFF=10.9 ms
RX=1 ms

(c) `DATA_TRANSMIT`.
OFF=6.8 μs
RX=1 ms
TX=4.1 ms

Figure 5.8: DQ states and radio activity. The total slot length is 11.9 ms, yielding an overall of 84 packets per second. In DQ the duration of all the states is the same (11.9 ms).

Protocol	State	Energy Consumption
FSA	`FBP_LISTEN`	25.235 μJ
	`DATA_WAIT`, `FBP_WAIT`	6.850 μJ
	`DATA_TRANSMIT`	276.425 μJ
DQ	`ARP_TRANSMIT`	83.170 μJ
	`CRQ_WAIT`,`DTQ_WAIT`	65.200 μJ
	`DATA_TRANSMIT`	310.900 μJ

Table 5.4: Average energy consumption in each of the FSA and DQ states. The energy consumption in each DQ state is larger than in FSA due to listening the FBP in each slot.

	Number of nodes				
Protocol	**5**	**10**	**15**	**20**	**25**
FSA	0.658 mJ	0.726 mJ	0.795 mJ	0.863 mJ	0.932 mJ
DQ	0.689 mJ	0.992 mJ	1.245 mJ	1.481 mJ	1.686 mJ
FSA/DQ	95.5%	73.2%	63.8%	58.3%	55.3%

Table 5.5: Energy consumption of FSA and DQ. The FSA/DQ quotient represents the energy savings of using FSA with respect to DQ. In this case, using the optimal FSA leads to a reduction in energy consumption between 5% to 45% compared to DQ.

5.4.4. Discussion

According to Table 5.5, FSA achieves a lower energy consumption than DQ regardless of the number of nodes in the network. However, the results obtained for FSA are the optimal case, that is, when the coordinator knows the number of nodes (n) in the network a priori and, thus, it is able to adjust the number of slots per frame (k) to the optimal case, e.g., $k = n$. Such assumption is not realistic in data collection scenarios because the number of nodes may change at each data collection period. In case the coordinator does not have such information in advance, an impact on the performance and energy consumption of FSA can be expected. On the one hand, if the number of slots per frame is larger than the number of nodes, e.g., $k > n$, the data collection time will be affected because a large number of slots will remain empty. On the other hand, if the number of slots per frame is smaller than the number of nodes, e.g., $k < n$, a greater energy consumption can be expected because the collision probability will be higher and, thus, the nodes will have to transmit their data packet additional times. In contrast, in DQ the coordinator does not need to know the number of nodes a priori because the collision resolution mechanism and the distributed queues work towards creating an ad hoc network schedule that ensures collision free transmission of data packets. In addition, the collision resolution process is interleaved with data transmission, thus improving the data collection delay compared to other protocols.

Another downside of FSA comes from the implementation point of view. In FSA there is no mechanism to recover the clock synchronization for the duration of a frame. Crystals clocks running at 32.768 Hz are typically used as time references to ensure proper protocol operation, e.g., at which slot should a node wake up and transmit the data packet to the coordinator. However, crystal clocks are not perfect and drift with respect to each other depending on many factors, e.g., aging and temperature. For example, two crystals that are rated at 20 *ppm*, a typical value, can drift as much as 40 ppm or 40 μs per second with respect to each other, one going *fast* and the other going *slow*. Considering a guard interval of 16 clock ticks (488.281 μs) between two consecutive slots, a node will be out of synchronization after 12 seconds. Thus, considering the current time length of a slot (6.85 ms), the maximum length of a frame is limited to 1750 slots. Despite there are temperature compensated crystals (2 ppm), drift poses a limitation to the number of nodes that a network can support using FSA. In contrast, in DQ the FBP packet can be used as a mechanism to maintain synchronization, e.g., ensure that clock drift does not lead to packet collisions because a node transmits out of its bounds. In that sense, it is worth noting that the current implementation of DQ listens to all FBP while waiting in the CRQ and the DTQ queues in order to maintain synchronization. However, from an implementation perspective it is possible to only listen to enough FBP to maintain clock synchronization within bounds. In such conditions the number of wait states in the CRQ and DTQ would be the same, but the energy consumption in such states would drop from 65.2 μJ to 10.9 μJ. Such reduction in the CRQ and DTQ wait states would lead to important savings in the overall energy consumption, as summarized in Table 5.6 and depicted in Figure 5.9.

	Number of nodes				
Protocol	**5**	**10**	**15**	**20**	**25**
FSA	0.658 mJ	0.726 mJ	0.795 mJ	0.863 mJ	0.932 mJ
DQ	0.529 mJ	0.646 mJ	0.713 mJ	0.783 mJ	0.834 mJ
FSA/DQ	24.3%	12.5%	11.6%	10.3%	11.8%

Table 5.6: Energy consumption of FSA and DQ with no synchronization. The FSA/DQ quotient represents the additional energy expenditure of using FSA with respect to DQ. Assuming perfect synchronization, the optimal FSA has an additional energy that is between 10% and 24% higher than DQ.

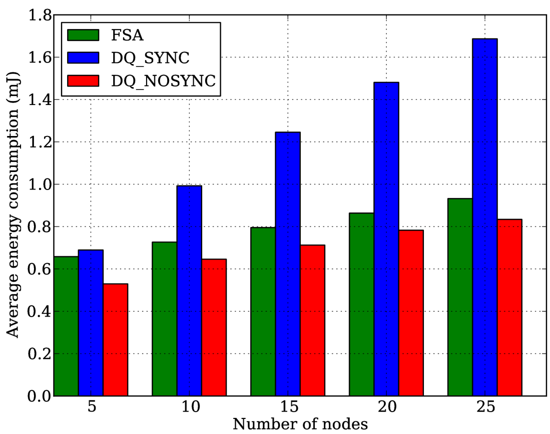

Figure 5.9: Energy consumption of FSA and DQ with and without synchronization. Reducing the number of FBP required to maintain synchronization leads to a reduction in energy consumption that makes DQ more energy efficient and easier to implement than FSA.

Finally, there are two other optimizations that can be introduced to further improve the performance and energy consumption of DQ with respect to FSA. First, it is possible to reduce the number of bytes devoted to the ARP. Currently ARP packets are 13 bytes long because it includes a radio preamble (4 bytes), synchronization word (4 bytes), payload length (1 byte), node address (2 bytes) and the payload checksum (2 bytes). Such information is included because the mechanism to decide the outcome of an ARP, e.g., empty, success or collisions, is based on the node address and the payload checksum. However, this number could be reduced implementing an advanced collision detection mechanism, e.g., using signal processing techniques. Second, it is possible to increase the number of ARP slots in the access subperiod of a slot. Currently, we use $m = 3$ because it is the minimum that ensures a stable system [79]. However, a larger m would lead to a faster collision resolution and, thus, lower energy consumption because nodes would need to transmit a lower number of ARPs to gain access to the DTQ.

5.5. Conclusions

This paper has empirically evaluated the energy consumption of two MAC protocols, Frame Slotted ALOHA (FSA) and Distributed Queuing (DQ), for data collection scenarios in smart cities. The results show that in the optimal case, that is, when the number of slots per frame is equal to the number of nodes present in the network, FSA consumes less energy than DQ. However, the optimal case for FSA is difficult to achieve in real scenarios for two reasons. First, the number of nodes is unknown a priori by the coordinator. Second, the number of nodes may change in each data collection period, thus requiring additional algorithms to adapt the number of slots per frame. Contrarily, DQ does not require to know the number of nodes in advance, yet it is capable of providing an energy consumption that is more than 10% lower than FSA if it only listens to enough FBP to maintain clock synchronization within bounds. Taking that into account, this paper concludes that DQ is an interesting alternative for data collection scenarios where the traffic is bursty and the number of nodes is dynamic.

6 Demonstrating Low-Power Distributed Queuing for Active RFID Communications At 433 MHz

***Abstract**: This paper presents a demonstrator of Low-Power Distributed Queuing (LPDQ), a MAC protocol targeted at active RFID systems operating at 433 MHz. LPDQ is based on a packet-based Preamble Sampling for network synchronization and Distributed Queuing for channel access. Compared to the MAC protocol defined in the ISO 18000- 7 standard, based on an analog Preamble Sampling and Frame Slotted ALOHA, LPDQ represents a major breakthrough in terms of system performance and energy consumption. At the MAC layer system performance is close to the optimal, e.g., no collisions during data packet transmission, and tag energy consumption can be reduced by more than 10% compared to FSA.*

6.1. Introduction

Active Radio-Frequency IDentification (RFID) systems operating at 433 MHz are standardized under ISO 18000-7 [5], which uses an analog Preamble Sampling (PS) to wake up tags and Frame Slotted ALOHA (FSA) to manage access to the medium. However, it is well-known that the analog PS is not energy efficient [59] and that the maximum performance of FSA is bounded to around 36.8% due to the effects of contention [61]. Moreover, such efficiency can only be achieved when the number of slots per frame is equal to the number of tags [61], which is unknown a priori. Over the last decade different proposals have been made to improve the performance of FSA in RFID systems [85]. The first approach is to adapt the number of slots per frame based on estimating the tag population from collisions, e.g., double the number of slots per frame if the number of collisions is high. The second approach is to build a query tree based on subsequently querying a sub-group of tags, e.g., first discover the tags and then query each tag independently to avoid collisions. However, both approaches do not achieve a high system performance and low energy consumption due to the time and energy required to estimate the number of tags from collisions or to build the query tree.

Considering that, we have designed and implemented Low-Power Distributed Queuing (LPDQ), a Medium Access Control (MAC) protocol for active RFID systems operating at the 433 MHz band. LPDQ is based on a packet-based PS [59] to achieve tag synchronization and Distributed Queuing (DQ) [79] as the channel access mechanism. In DQ time is organized into fixed-length slots, with each slot having three subperiods (e.g., access request, data transmission and feedback information), and channel access is organized using two queues, the Collision Resolution Queue (CRQ) and the Data Transmit Queue (DTQ). The CRQ ensures that tags that collide during access request subperiod are subsequently organized into sub-groups, whereas the DTQ ensures that only the tag at the head of the queue can transmit during the data transmit subperiod. Finally, a set of rules is used to manage access to both queues, e.g., a tag cannot transmit in the access request subperiod if the CRQ is not empty. For a detailed overview of the

DQ operation please refer to [71].

There are two main benefits of using LPDQ. On the one hand, the packet-based PS contains the time at which the tags are expected to wake up, so tags can go back to sleep as soon as a PS packet is received. Compared to the analog PS mechanism of ISO 18000-7, where tags have to listen for the whole duration of the analog preamble, this enables to save energy. On the other hand, the DQ channel access mechanism ensures that the system operates without contention during data packet transmission regardless of the number of tags. Compared to FSA in ISO 18000-7, this enables a system performance close to 100% and to reduce the energy consumption of tags by more than 10% [90].

6.2. Demonstrator

The demonstrator is composed of 25 active tags and a reader connected to a computer that acts as the system manager, as shown in Figure 6.1. Both the reader and the tags are based on OpenMote-433, a low-power wireless platform build using COTS (Commercial Off-The-Shelf) hardware. Specifically, OpenMote-433 is based on a Texas Instruments CC430 SoC (System on Chip), which embeds an MSP430 16-bit RISC microcontroller, running at 16 MHz with 4 kBytes of RAM and 32 kBytes of Flash memory, and a CC1101 radio transceiver, which operates at Sub-GHz bands with data rates of up to 600 kbps and support for amplitude and frequency modulations. The radio transceiver is tuned to the 433 MHz band using a discrete balun and connected to a $\lambda/4$ monopole antenna through an SMA connector. Finally, two AAA batteries provide energy (3 V, 1500 mAh) to the tags, whereas the reader is powered through the USB port.

Regarding the software, the demonstrator is build using two components. First, the firmware that runs on both the tag and the reader is written in C and provides the implementation of both FSA and LPDQ, as well as other basic functionalities (e.g., random number generation, cyclic redundancy check, etc.). Second, the software that runs in the computer is written in Python and manages the active RFID system and presents the system performance and energy consumption results, as depicted in Figure 6.2. The

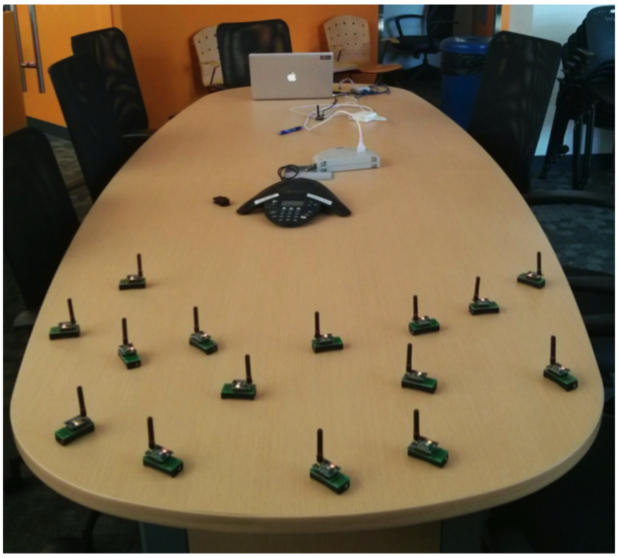

Figure 6.1: Demonstrator with 15 active tags and a reader connected to a computer, which acts as the system manager.

2744 software allows the user to select which channel access mechanism to test, e.g., FSA and
2745 LPDQ, and the duration of each test. In case of selecting FSA, the software also allows
2746 to select the number of slots per frame.

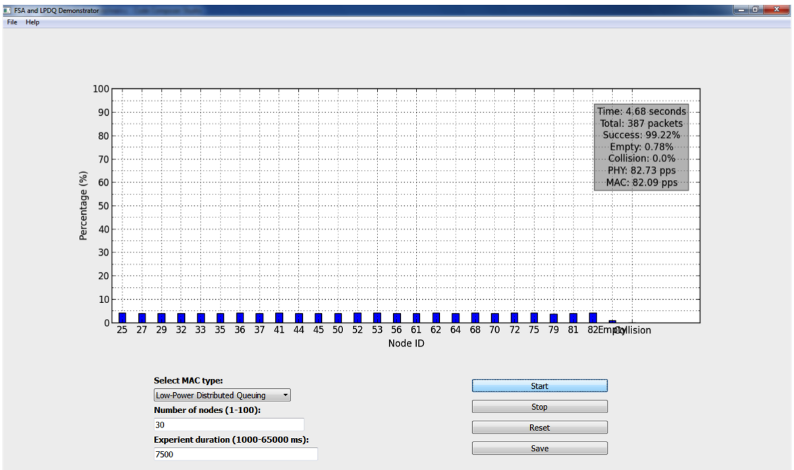

Figure 6.2: User interface to manage the active RFID system and show the system performance and energy consumption.

2747 Each test consists of two phases, network synchronization and data collection. Initially tags are in preamble sampling mode, where they periodically enter the receive mode for a short period of time to detect wake-up packets from the reader. When triggered by the manager, the reader transmits a series of wake-up packets, which allows tags to synchronize. Once tags wake up, the data collection phase begins. In the data collection phase each tag executes the configured channel access mechanism and transmits a given number of packets to the reader. Once the packets have been transmitted the tag goes back to preamble sampling mode.

The results obtained with the demonstrator, depicted in Figure 6.3, show that LPDQ outperforms FSA standard in terms of system performance, e.g., packet success and collision rates. Essentially, LPDQ achieves a system performance that is optimal at the MAC layer, as there are no collisions during data packet transmission. This, in turn, reduces the energy consumption of tags by more than 10% because no energy is wasted due to data packet retransmission. Moreover, there are two additional benefits of LPDQ compared to the mechanisms to improve FSA described earlier. First, the system performance is independent of the number of tags, e.g., it is not necessary to adjust the number of slots per frame based on the number of collisions. Second, the collection time is reduced because collision resolution and data transmission are interleaved in time, e.g., it is not necessary to wait until the query tree is completely build to start receiving data packets from tags that are already in the DTQ.

6.3. Conclusions

LPDQ is a MAC protocol for active RFID systems at 433 MHz. Given the system performance and energy consumption results, and considering the fact that it can be implemented using off-the-shelf hardware, we believe that LPDQ can have a significant impact on future active RFID systems.

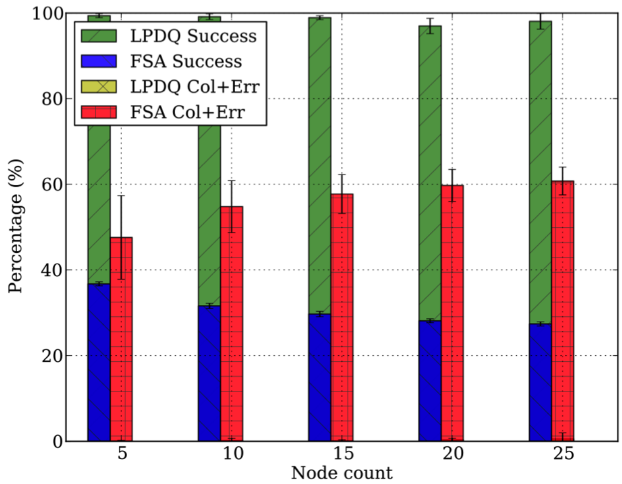

Figure 6.3: System performance of LPDQ and FSA depending on the number of tags using the active RFID demonstrator.

7 Conclusions and Future Work

This chapter summarizes the results presented in this thesis and gives some brief on future possible research. In particular, it gives insights on two specific developments: the first is related to studying the performance of LPDQ in different environments and the second is related to extending the use of LPDQ to multi-hop networks.

7.1. Conclusions and Future Work

This thesis has focused on active RFID (RadioFrequency IDentification) systems operating at the 433 MHz band. Specifically, the thesis has focused on the lowest layers of the communications stack, that is, the physical and the data-link layers.

At the physical layer the thesis has evaluated the propagation characteristics of the 433 MHz band in both indoor and outdoor environments and compared it to the 2.4 GHz band. From the results obtained it has also presented a novel propagation model for the 433 MHz and the 2.4 GHz bands depending on tag height. The results show that the 433 MHz band has better propagation characteristics than the 2.4 GHz band in both environments. This enables to reduce multi-hop communications requirements which, in turn, has a direct impact on the tag energy consumption and battery life. However, the results also show that, contrarily to the 2.4 GHz band, multipath propagation cannot be combated through channel hopping at the 433 MHz band. This is because the channel coherence bandwidth is larger than the whole channel bandwidth and, thus, all channels are highly correlated. Therefore, this results need to be taken into account when designing active RFID systems that operate at the 433 MHz band. For example, it may be required to add antenna diversity to the interrogator to improve link robustness against multi-path propagation.

At the data-link layer the thesis has presented LPDQ (Low-Power Distributed Queuing), a MAC (Medium Access Control) protocol for active RFID networks. LPDQ addresses scenarios with a large number of tags, either fixed or mobile, that generate bursty traffic patterns. Regarding network synchronization, LPDQ uses a LPL (Low-Power Listening) mechanism that allows tags to have a duty cycle close to 0.2%, thus minimizing the energy expenditure caused by idle listening. In contrast, the current synchronization mechanism standardized in ISO/IEC 18000-7 requires tags to remain awake for a minimum of 30 seconds after a wake-up command, which leads to an increased energy consumption. Regarding data transmission, LPDQ uses DQ (Distributed Queuing), which is able to dynamically create a network schedule and enables all tags to transmit data packets without collisions. This enables to achieve a packet throughput close to 99% regardless of the number of tags. In contrast FSA (Frame Slotted ALOHA), which is the channel access mechanism standardized in ISO/IEC 18000-7, only achieves 36.8% due to the effects of contention. In addition, DQ reduces tag energy consumption by more than 10% compared to the optimal version of FSA, e.g., when the number of slots per frame is equal to the number of tags.

Focusing on LPDQ, the results obtained in terms of packet throughput and energy consumption demonstrate its suitability as an alternative to current standards for active RFID systems operating at the 433 MHz band, e.g., those standardized under ISO/IEC 18000-7. Current alternatives proposed in the literature either require determining the tag population a priori by creating a binary tree or estimating the number of contending tags a posteriori based on collisions. Both alternatives, though technically feasible, lead to an increased collection time and higher energy consumption when compared to LPDQ. Thus, given these results and the fact that it has been demonstrated that LPDQ can be successfully implemented using off-the-shelf radio transceivers at the 433 MHz band, it deems interesting to present the results obtained to the international committees that standardize active RFID technology. In particular, LPDQ could be incorporated to the standard for active RFID systems operating at the Sub-GHz band that is currently being developed by the DASH7 Alliance.

In addition to that, the research conducted and the results obtained in this thesis leave a number of open questions to be studied in the future. Specifically, we consider the following as alternatives that are interesting to explore for active RFID networks.

First, it would be interesting to evaluate the performance of LPDQ in different environments. So far, the experiments have evaluated the performance of LPDQ under optimal conditions, e.g., when all the tags are at a similar distance from the interrogator. However, in a real-world scenario the tags are expected to be at different distances from the interrogator. Distance differences between tags and the interrogator may impact the performance of the protocol in various ways. For example, a tag that is located at the edge of the interrogator coverage area will be received with a lower signal strength than a tag that is located close by. Such differences in signal strength may impact the fairness of the protocol because tags with a lower signal strength may never be able to join the network due to the capture effect of nearby tags. In addition, it would also be interesting to study the impact of interference created by other networks operating in the same band. In that sense, the interference created by such networks may impact the performance of the mechanism that is used to create the network schedule.

Second, it would be interesting to study the viability of LPDQ in multi-hop networks. Currently, LPDQ is designed to operate in a single-hop scenario, that is, a scenario where tags communicate directly to the interrogator. However, in a real-world scenario tags may not be able to communicate directly with the interrogator due to propagation characteristics. For example, a tag may be placed in a location in which the received signal strength is below the radio transceiver sensitivity, thus not being able to communicate directly with the interrogator. In such cases it would be interesting to create clusters that enable tags communicate in a two-hop scenario, e.g., an intermediate tag would act as a relay and forward the information to the interrogator. Despite such an approach is technically feasible, the mechanisms needed to create it and the impact on the protocol performance need to be investigated. One particular challenge to be addressed is detecting the tags that require two-hop communications to the interrogator considering that the number of tags and its conditions are unknown a priori.

Finally, we conclude by pointing out that the contributions made in this thesis regarding the DQ channel access mechanism may also be applicable to other wireless technologies that face similar constraints. In particular, we foresee that DQ could be applied to cellular technologies which are, in part, targeted at providing M2M (Machine-to-Machine) services to a large number of devices. Current cellular technologies use a random channel access mechanism to enable terminals join the network and obtain the resources required to communicate reliably. However, such an approach makes cellular technologies unsuitable in scenarios with a high number of devices competing to join the network simultaneously. This is due to the fact that the shared resources devoted to allowing terminals join the network saturate, leading to a scenario where the network resources cannot be assigned to terminals. Leveraging DQ as the mechanism to join the cellular network would enable to quickly resolve contention and create an ad hoc schedule that allows all terminals to join the network regardless of the number of contenders.

8 Bibliography

Bibliography

[1] ISO 18000-1:2008. *Radio frequency identification for item management – Part 1: Reference architecture and definition of parameters to be standardized.* ISO, Geneva, Switzerland, 2008.

[2] ISO 18000-2:2009. *Radio frequency identification for item management – Part 2: Parameters for air interface communications at 135 kHz.* ISO, Geneva, Switzerland, 2009.

[3] ISO 18000-6:2008. *Radio frequency identification for item management – Part 6: Parameters for air interface communications at 860 MHz to 960 MHz.* ISO, Geneva, Switzerland, 2008.

[4] ISO 18000-4:2008. *Radio frequency identification for item management – Part 4: Parameters for air interface communications at 2.4 GHz.* ISO, Geneva, Switzerland, 2008.

[5] ISO 18000-7:2009. *Radio frequency identification for item management – Part 7: Parameters for active air interface communications at 433 MHz.* ISO, Geneva, Switzerland, 2009.

[6] *IEEE Standard for Information Technology- Telecommunications and Information Exchange Between Systems- Local and Metropolitan Area Networks- Specific Requirements Part 15.4: Wireless Medium Access Control (MAC) and Physical Layer (PHY) Specifications for Low-Rate Wireless Personal Area Networks (WPANs).* 2011.

[7] P Huang, L. Xiao, S Soltani, M Mutka, and N Xi. The Evolution of MAC Protocols in Wireless Sensor Networks: A Survey. *Communications Surveys & Tutorials, IEEE*, (99):1–20, 2012.

[8] *IEEE Standard for Information Technology-Telecommunications and Information Exchange Between Systems-Local and Metropolitan Area Networks-Specific Requirements - Part 11: Wireless LAN Medium Access Control (MAC) and Physical Layer (PHY) Specifications.* 2012.

[9] S. Hara, Dapeng Zhao, K. Yanagihara, J. Taketsugu, K. Fukui, S. Fukunaga, and K. Kitayama. Propagation characteristics of IEEE 802.15.4 radio signal and their application for location estimation. In *VTC 2005: 61st IEEE Vehicular Technology Conference*, volume 1, pages 97–101, 2005.

[10] Sébastien Dawans, Simon Duquennoy, and Olivier Bonaventure. On Link Estimation in Dense RPL Deployments. In *IEEE SenseApp 2012: International Workshop on Practical Issues in Building Sensor Network Applications*, 2012.

[11] M. Petrova, Lili Wu, P. Mahonen, and J. Riihijarvi. Interference Measurements on Performance Degradation between Colocated IEEE 802.11g/n and IEEE 802.15.4 Networks. In *ICN 2007: 6th International Conference on Networking*, pages 93–93, 2007.

[12] S. Aust, R.V. Prasad, and I. G M M Niemegeers. IEEE 802.11ah: Advantages in standards and further challenges for sub 1 GHz Wi-Fi. In *Communications (ICC), 2012 IEEE International Conference on*, pages 6885–6889, 2012.

[13] *IEEE Draft Standard for Local and Metropolitan Area Networks Part 15.4: Low Rate Wireless Personal Area Networks (LR-WPANs) Amendment: Active Radio Frequency Identification (RFID) System Physical Layer (PHY).* 2011.

[14] E. Tanghe, W. Joseph, P. Ruckebusch, L. Martens, and I. Moerman. Intra-, inter-, and extra-container path loss for shipping container monitoring systems. *IEEE Antennas and Wireless Propagation Letters*, 11:889–892, 2012.

[15] Texas Instruments. CC1101 Datasheet: Low-Power Sub-1 GHz RF Transceiver, 2013.

[16] Rodger E. Ziemer and William H. Tranter. *Principles of Communications*. Wiley, 6th edition, 2008.

[17] A. Goldsmith. *Wireless Communications*. Cambridge University Press, 1st edition, 2005.

[18] C Phillips, D Sicker, and D Grunwald. A Survey of Wireless Path Loss Prediction and Coverage Mapping Methods. *Communications Surveys & Tutorials, IEEE*, (99):1–16, 2012.

[19] J. Turkka and M. Renfors. Path loss measurements for a non-line-of-sight mobile-to-mobile environment. In *ITS Telecommunications, 2008. ITST 2008. 8th International Conference on*, pages 274–278, 2008.

[20] Atmel. AT86RF230: Low Power 2.4 GHz Transceiver for ZigBee, IEEE 802.15.4, 6LoWPAN, RF4CE and ISM Applications, 2009.

[21] JFW Industries. 50PA-512, Solid-State Programmable Attenuator, 2012.

[22] Rigol Technologies. DSA815, 1.5 GHz Spectrum Analyzer, 2012.

[23] P. Tuset-Peiró, A. Anglès-Vázquez, J. López-Vicario, and X. Vilajosana-Guillén. On the suitability of the 433 MHz band for M2M low-power wireless communications: propagation aspects. *Transactions on Emerging Telecommunication Technologies*, 2013. doi: 0.1002/ett.2672.

[24] V.P. Gil and A. Garcia. Field measurements and guidelines for the application of wireless sensor networks to the environment and security. *Sensors*, 9(12):10309–10325, 2009.

[25] H. Hongwei, X. Youzhi, C. Bilen, and Z. Hongke. Coexistence issues of 2.4ghz sensor networks with other rf devices at home. In *SENSORCOMM 2009, o 1st International Conference on Technologies and Applications*, 2009.

[26] T Watteyne, S. Lanziseram, A. Mehta, and K. Pister. Mitigating Multipath Fading Through Channel Hopping in Wireless Sensor Networks. In *IEEE International Conference on Communications (ICC)*, 2010.

[27] *IEEE Draft Standard for Local and Metropolitan Area Networks Part 15.4: Low Rate Wireless Personal Area Networks (LR-WPANs) Amendment to the MAC sub-layer.* 2011.

[28] T. Watteyne, X. Vilajosana, B. Kerkez, F. Chraim, K. Weekly, Q. Wang, S. Glaser, and K. Pister. OpenWSN: a standards-based low-power wireless development environment. *Transactions on Emerging Telecommunication Technologies*, 23(1):480–493, 2012.

[29] European Telecommunications Standards Institute. *Electromagnetic Compatibility and Radio Spectrum Matters (ERM); Short Range Devices (SRD); Radio equipment to be used in the 25 MHz to 1 000 MHz frequency range with power levels ranging up to 500 mW; Part 1: Technical characteristics and test methods.* EN 300 220-1, 2000.

[30] Federal Communications Commission. *Part 15 — Radio Frequency Devices; 15.231 Periodic operation in the band 40.66–40.70 MHz and above 70 MHz.* FCC Part 15.231, 2011.

[31] K. Kuladinithi, C. An, A. Timm-Giel, and C. Görg. Performance evaluation of radio disjoint multipath routing. *European Transactions on Telecommunications*, 20(7):668–678, 2009.

[32] Y. Yang, J. Hu, T. Song, and L. Shen. A Study of Near Ground Channel Model for 2.4 GHz IEEE 802.15.4 Signal in Outdoor Environment. In *1st International Conference on Information Science and Engineering (ICISE)*, 2009.

[33] J. Pardo, A. Sala, M. Delgado, E.E. Lopez, L. Llacer, and J. Haro. Channel Model at 868 MHz for Wireless Sensor Networks in Outdoor Scenarios. In *International Workshop on Wireless Ad hoc Networks*, 2005.

[34] R Sawant, Q. Liang, D. Popa, and F. Lewis. Experimental Path Loss models For Wireless Sensor Networks. In *Military Communications Conference*, 2007.

[35] S. Ghassemzadeh, L. Larry, J. Greenstein, A. Kavcic, T. Sveinsson, and V. Tarokh. An empirical indoor path loss model for ultra-wideband channels. *Communications Networks*, 5:303–308, 2003.

[36] K. Sohrabi, B. Manriquez, and G. Pottie. Near ground wideband channel measurement in 800-1000 MHz. In *IEEE 49th Vehicular Technology conference (VTC)*, 1999.

[37] J. Thelen, D. Goense, and K. Langendoen. Radio Wave Propagation in Potato Fields. In *1st Workshop on Wireless Network Measurements*, 2005.

[38] M. Holland, R. Aures, and W. Heinzelman. Experimental Investigation of Radio Performance in Wireless Sensor Networks. In *2nd IEEE Workshop on Wireless Mesh Networks (WiMesh)*, 2006.

[39] J R Hampton, N M Merheb, W L Lain, D E Paunil, R M Shuford, and W T Kasch. Urban Propagation Measurements for Ground Based Communication in the Military UHF Band. *IEEE Transactions on Antennas and Propagation*, 54(2):644–654, 2006.

[40] Wei Zhang, Yong He, Fei Liu, Congcong Miao, Shitao Sun, Chengfeng Liu, and Jianfang Jin. Research on wsn channel fading model and experimental analysis in orchard environment. *Computer and Computing Technologies in Agriculture V*, 369:326–333, 2011.

[41] H. Wennerström, F. Hermans, O. Rensfelt, C. Rohner, and L. Norden. A long-term study on the effects of meteorological conditions on 802.15.4 links. In *8th Swedish National Computer Networking Workshop*, 2012.

[42] Xiaohong Mao, Yee Hui Lee, and Boon Chong Ng. Wideband channel modelling in uhf band for urban area. In *IEEE International Symposium on Wireless Communication Systems (ISWCS 2008)*, pages 240–244, 2008.

[43] K. Phaebua, C. Phongcharoenpanich, D. Torrungrueng, and J. Chinrungrueng. Short-distance and near-ground signal measurements in a car park of wireless sensor network system at 433 mhz. In *5th International Conference on Electrical Engineering/Electronics, Computer, Telecommunications and Information Technology (ECTI-CON 2008)*, pages 241–244, 2008.

[44] Xiaohu Zhang, T.W. Burress, K.B. Albers, and W.B. Kuhn. Propagation comparisons at vhf and uhf frequencies. In *IEEE Radio and Wireless Symposium (RWS 2009)*, pages 244–247, 2009.

[45] Qiong Wu, D.W. Matolak, and R.D. Apaza. Airport surface area propagation path loss in the vhf band. In *Integrated Communications, Navigation and Surveilance Conference (ICNS 2011)*, 2011.

[46] A. Neskovic, N. Neskovic, and G. Paunovic. Modern approaches in modeling of mobile radio systems propagation environment. *IEEE Communications Surveys and Tutorials*, 3:2–12, 2000.

[47] D. Xu, X. Gao, P Zhang, and Y. Wu. Indoor Office Propagation Measurements and Path Loss Models at 5.25 GHz. In *IEEE 66th Vehicular Technology Conference (VTC)*, 2007.

[48] A. Balanis. *Antenna Theory: Analysis and Design.* John Wiley & Sons, 3rd edition, 2005.

[49] M. Pozar. *Microwave Engineering.* John Wiley & Sons, 4rd edition, 2012.

[50] Luigi Atzori, Antonio Iera, and Giacomo Morabito. The Internet of Things: A survey. *Computer Networks*, 54(15):2787 – 2805, 2010.

[51] M.R. Palattella, N Accettura, X. Vilajosana, T. Watteyne, L.A. Grieco, G. Boggia, and M. Dohler. Standardized Protocol Stack for the Internet of (Important) Things. *Communications Surveys & Tutorials, IEEE*, 15(3):1389–1406, 2013.

[52] Michele Zorzi, Alexander Gluhak, Sebastian Lange, and Alessandro Bassi. From today's intranet of things to a future internet of things: a wireless-and mobility-related view. *Wireless Communications, IEEE*, 17(6):44–51, 2010.

[53] Nicolas Fourty, Adrien van den Bossche, and Thierry Val. An advanced study of energy consumption in an IEEE 802.15.4 based network: Everything but the truth on 802.15.4 node lifetime. *Computer Communications*, 35(14):1759–1767, 2012.

[54] Wee Lum Tan, Wing Cheong Lau, and OnChing Yue. Performance analysis of an adaptive, energy-efficient MAC protocol for wireless sensor networks. *Journal of Parallel and Distributed Computing*, 72(4):504 – 514, 2012.

[55] A Bachir, M. Dohler, T. Watteyne, and K K Leung. MAC essentials for wireless sensor networks. *Communications Surveys & Tutorials, IEEE*, 12(2):222–248, 2010.

[56] L. Doherty, W. Lindsay, and J. Simon. Channel-specific wireless sensor network path data. In *Computer Communications and Networks (ICCCN), 16th International Conference on*, pages 89–94, 2007.

[57] Thomas Watteyne, Xavier Vilajosana, Branko Kerkez, Fabien Chraim, Kevin Weekly, Qin Wang, Steven Glaser, and Kris Pister. OpenWSN: a standards-based low-power wireless development environment. *Transactions on Emerging Telecommunications Technologies*, 23(5):480–493, 2012.

[58] Ignasi Vilajosana, Xavier Vilajosana, Jordi LLosa, Albert Angles, Marc Domingo, and Borja Martinez. Bootstrapping smart cities through a self-sustainable model based on big data flows. *Communications Magazine, IEEE*, 51(6):128–134, jun 2013.

[59] Cristina Cano, Boris Bellalta, Anna Sfairopoulou, and Miquel Oliver. Low energy operation in WSNs: A survey of preamble sampling MAC protocols. *Computer Networks*, 55(15):3351–3363, 2011.

[60] J. Yick, B. Mukherjee, and D. Ghosal. Wireless sensor network survey. *Computer Networks*, 52(12):2292–2330, 2008.

[61] Vinod Namboodiri, Maheesha DeSilva, Kavindya Deegala, and Suresh Ramamoorthy. An extensive study of slotted Aloha-based RFID anti-collision protocols. *Computer Communications*, 35(16):1955 – 1966, 2012.

[62] Won-Ju Yoon, Sang-Hwa Chung, and Seong-Joon Lee. Implementation and performance evaluation of an active RFID system for fast tag collection. *Computer Communications*, 31(17):4107 – 4116, 2008.

[63] Ming-Kuei Yeh, Jehn-Ruey Jiang, and Shing-Tsaan Huang. Adaptive splitting and pre-signaling for RFID tag anti-collision. *Computer Communications*, 32(17):1862–1870, 2009.

[64] B. Lars and S. Bertil. An Energy and Application Scenario Aware Active RFID Protocol. *EURASIP Journal on Wireless Communications and Networking*, 2010, 2011.

[65] Kwan-Wu Chin and Dheeraj Klair. E2MAC: An energy efficient MAC for RFID-enhanced wireless sensor networks. *Pervasive and Mobile Computing*, 7(2):241–255, April 2011.

[66] Chen Qian, Yunhuai Liu, R H Ngan, and L M Ni. ASAP: Scalable Collision Arbitration for Large RFID Systems. *Parallel and Distributed Systems, IEEE Transactions on*, 24(7):1277–1288, 2013.

[67] Haifeng Wu, Yu Zeng, Jihua Feng, and Yu Gu. Binary Tree Slotted ALOHA for Passive RFID Tag Anticollision. *Parallel and Distributed Systems, IEEE Transactions on*, 24(1):19–31, 2013.

[68] A J E M Janssen and M J de Jong. Analysis of contention tree algorithms. *Information Theory, IEEE Transactions on*, 46(6):2163–2172, 2000.

[69] W. Xu and G. Campbell. A near perfect stable random access protocol for a broadcast channel. In *Communications (ICC), 1992 IEEE International Conference on*, pages 370–374, 1992.

[70] L. Alonso, R. Agusti, and O. Sallent. A near-optimum MAC protocol based on the distributed queueing random access protocol (DQRAP) for a CDMA mobile communication system. *Selected Areas in Communications, IEEE Journal on*, 18(9):1701–1718, 2000.

[71] J. Alonso-Zarate, C. Verikoukis, E. Kartsakli, A. Cateura, and L. Alonso. A near-optimum cross-layered distributed queuing protocol for wireless LAN. *Wireless Communications, IEEE*, 15(1):48–55, 2008.

[72] E. Kartsakli, A. Cateura, L. Alonso, J. Alonso-Zarate, and C. Verikoukis. Cross-layer enhancement for WLAN systems with heterogeneous traffic based on DQCA. *Communications Magazine, IEEE*, 46(6):60–66, 2008.

[73] J. Alonso-Zarate, E. Kartsakli, L. Alonso, and C. Verikoukis. Performance analysis of a cluster-based MAC protocol for wireless ad hoc networks. *EURASIP Journal on Wireless Communications and Networking*, 2010, 2010.

[74] B. Otal, L. Alonso, and C. Verikoukis. Highly reliable energy-saving MAC for wireless body sensor networks in healthcare systems. *Selected Areas in Communications, IEEE Journal on*, 27(4):553–565, 2009.

[75] Giuseppe Anastasi, Marco Conti, Mario Di Francesco, and Andrea Passarella. Energy conservation in wireless sensor networks: A survey. *Ad Hoc Netw.*, 7(3):537–568, May 2009.

[76] T. Winter, P. Thubert, A. Brandt, J. Hui, R. Kelsey, P. Levis, K. Pister, R. Struik, JP. Vasseur, and R. Alexander. RPL: IPv6 Routing Protocol for Low-Power and Lossy Networks. RFC 6550 (Proposed Standard), 2012.

[77] Texas Instruments. CC430 Datasheet: MSP430 SoC With RF Core, 2013.

[78] Pere Tuset-Peiró, Albert Anglès-Vazquez, José López-Vicario, and Xavier Vilajosana-Guillén. On the suitability of the 433 MHz band for M2M low-power wireless communications: propagation aspects. *Transactions on Emerging Telecommunications Technologies*, 2013.

[79] Wenxin Xu and Graham Campbell. A distributed queueing random access protocol for a broadcast channel. *SIGCOMM Comput. Commun. Rev.*, 23(4):270–278, 1993.

[80] D Stanislowski, X. Vilajosana, Q. Wang, T. Watteyne, and K. Pister. Adaptive Synchronization in IEEE802.15.4e Networks. *Industrial Informatics, IEEE Transactions on*, (99):1, 2013.

[81] K. Whitehouse, A. Woo, F. Jiang, J. Polastre, and D. Culler. Exploiting the capture effect for collision detection and recovery. In *Embedded Networked Sensors, 2005. EmNetS-II. The Second IEEE Workshop on*, pages 45–52, 2005.

[82] T. Watteyne, S. Lanzisera, A. Mehta, and K.S.J. Pister. Mitigating multipath fading through channel hopping in wireless sensor networks. In *Communications (ICC), 2010 IEEE International Conference on*, pages 1–5, 2010.

[83] Zornitza Genova Prodanoff. Optimal frame size analysis for framed slotted ALOHA based RFID networks. *Computer Communications*, 33(5):648–653, mar 2010.

[84] G. Zhou, T. He, S. Krishnamurthy, and J.A. Stankovic. Models and solutions for radio irregularity in wireless sensor networks. *ACM Transactions on Sensor Networks (TOSN)*, 2(2):221–262, 2006.

[85] Dheeraj K Klair, Kwan-Wu Chin, and Raad Raad. A survey and tutorial of RFID anti-collision protocols. *Communications Surveys & Tutorials, IEEE*, 12(3):400–421, 2010.

[86] Francisco Vazquez-Gallego, Jesus Alonso-Zarate, Pere Tuset-Peiro, and Luis Alonso. Energy analysis of a contention tree-based access protocol for machine-to-machine networks with idle-to-saturation traffic transitions. In *Communications (ICC), 2014 IEEE International Conference on*, 2014.

[87] Pere Tuset-Peiro, Luis Alonso, Francisco Vezquez-Gallego, Jesus Alonso-Zarate, and Xavier Vilajosana-Guillen. Demonstrating low-power distributed queuing for active rfid communications at 433 mhz. In *Computer Communications Workshops (INFOCOM WKSHPS), 2014 IEEE Conference on*, pages 157–158, April 2014.

[88] Osama Khader and Andreas Willig. An energy consumption analysis of the WirelessHART TDMA protocol. *Computer Communications*, 36(7):804 – 816, 2013.

[89] X. Vilajosana, Q. Wang, F Chraim, T. Watteyne, T Chang, and K. Pister. A Realistic Energy Consumption Model for TSCH Networks. *Sensors Journal, IEEE*, (99):1, 2013.

[90] F. Vazquez Gallego, J. Alonso-Zarate, and L. Alonso. Energy and delay analysis of contention resolution mechanisms for machine-to-machine networks based on low-power wifi. In *Communications (ICC), 2013 IEEE International Conference on*, pages 2235–2240, June 2013.

Appendices

A List of Papers

This appendix includes the first page of all the papers that have been published as part of this thesis. In particular it includes:

- ***Pere Tuset**, Ferran Adelantado, Xavier Vilajosana, Francisco Vázquez, Jesús Alonso. "On the use of the 433 MHz band to Improve the Energy Efficiency of M2M Communications". 24th Anual IEEE Symposium on Personal, Indoor and Mobile Radio Communications (PIMRC 2013). London, United Kingdom. September, 2013.*

- ***Pere Tuset**, Albert Anglès, José López, Xavier Vilajosana. "On the suitability of the the 433 MHz band for M2M wireless communications: propagation aspects". Transactions on Emerging Telecommunications Technologies. April 2013.*

- ***Pere Tuset**, Francisco Vázquez, Jesus Alonso, Luis Alonso, Xavier Vilajosana. "LPDQ: a self-scheduled TDMA MAC protocol for one-hop dynamic low-power wireless networks". Special Issue on "Internet of Things". Elsevier Pervasive and Mobile Computing. November 2013.*

- ***Pere Tuset***, *Francisco Vázquez, Jesus Alonso, Luis Alonso, Xavier Vilajosana. "Experimental energy consumption of FSA and DQ for data collection scenarios". Special Issue on "Wireless Sensor Networks and the Internet of Things". MDPI Sensors. June 2014.*

- ***Pere Tuset***, *Francisco Vázquez, Jesus Alonso, Luis Alonso, Xavier Vilajosana. "Demonstrating Low-Power Distributed Queuing for Active RFID Communications at 433 MHz". IEEE International Conference on Computer Communications (INFOCOM 2014). Toronto, Canada. May, 2014.*

2013 IEEE 24th International Symposium on Personal, Indoor and Mobile Radio Communications: Mobile and Wireless Networks

3164 On the use of the 433 MHz band to Improve the Energy Efficiency of M2M Communications

Pere Tuset, Ferran Adelantado, Xavier Vilajosana
Universitat Oberta de Catalunya (UOC)
Barcelona, E08013 Spain
Email: {peretuset, ferranadelantado,xvilajosana}@uoc.edu

Francisco Vázquez-Gallego, Jesús Alonso-Zárate
Centre Tecnològic de Telecomunicacions de Catalunya (CTTC)
Castelldefels, E08860 Spain
Email: {francisco.vazquez, jesus.alonso}@cttc.es

***Abstract*—Due to propagation and interference effects at the 2.4 GHz band, Machine-to-Machine (M2M) wireless communications based on the IEEE 802.15.4 standard typically need multi-hop communications to connect end devices with a gateway. Unfortunately, multi-hop transmissions pose some challenges that are not trivial to solve and may slow down the deployment of M2M networks. For this reason, the IEEE 802.15.4f Working Group (WG) is currently defining the specifications of a new physical layer operating at the 433 MHz band, which offers better propagation conditions and suffers from lower interference levels. In this paper, we analyze the energy consumption of single-hop and multi-hop communications at both 433 MHz and 2.4 GHz. We use realistic propagation models and accurate energy consumption models to conduct a comprehensive assessment of the energy performance at the two frequency bands. The results presented in this paper show that operating at 433 MHz instead of 2.4 GHz can significantly reduce the number of hops between the end device and the gateway, which can be translated into a reduction of the overall network energy consumption.**

I. Introduction

The main factor that determines the lifespan of a battery-operated end device in Machine-to-Machine (M2M) wireless communications is the time that the radio transceiver is on, either to transmit or receive a packet, or in idle listening. This time depends basically on two factors: the application requirements, i.e., how often does the device need to communicate, and the Medium Access Control (MAC) protocol, which manages the access to the shared physical medium [1]. While the amount of M2M applications are very diverse and pose a great variety of requirements, the MAC protocols suitable for M2M deployments rely on a small subset of technologies. Among other candidate technologies, both the IEEE 802.15.4 Standard for Low-Rate Wireless Personal Area Networks (WPAN) [2] and the IEEE 802.11 Standard for Wireless Local Area Networks (WLAN) [3] are becoming very strong players into the M2M area. These standards define the specifications of the physical (PHY) and MAC layers for short and medium-range wireless communications and, although they can operate in different license-free bands, they typically operate at the worldwide license-free 2.4 GHz band.

Unfortunately, real-life experience has shown that radio propagation conditions at 2.4 GHz are heavily influenced by the environment, and thus the strength of a transmitted radio signal is severely degraded with the distance and the presence of obstacles [4]. For this reason, wireless M2M networks operating at 2.4 GHz typically require multi-hop communications to connect an end device with its intended destination, e.g., an M2M gateway. Unfortunately, multi-hop links are complex to manage because: i) they require some degree of synchronization among the involved devices, and ii) the execution of routing protocols to determine and update the routes between any end device and its intended destination becomes necessary [5]. Moreover, multi-hop transmissions also lead to lower effective data rates and longer transmission delays. In addition, the amount of networks that today use the 2.4 GHz band with very different transmission power profiles is growing every day, leading to unacceptable cross-standard interference levels that limit their performance [6] and can even block each other.

For all these reasons, the world-wide available license-free Sub-1 GHz bands, i.e., 433 MHz and 868/915 MHz, are gaining interest for M2M Applications as an alternative to overcome the propagation and interferences issues at the 2.4 GHz [7]. Particularly, the path-loss at 433MHz is lower than at 2.4 GHz, and thus transmissions at 433 MHz can be typically done in a single-hop fashion. This makes communications simpler, faster, and more energy-efficient. For this reason, the IEEE 802.15.4f Working Group (WG) has started to define a new amendment to the legacy IEEE 802.15.4 standard that includes a narrowband PHY layer for the 433 MHz band [8]. Several authors have already studied the 433 MHz and 2.4 GHz bands focusing on its propagation properties in different environments. For instance, Tanghe et al. [9] present empirical path loss models at 433 MHz, 868 MHz and 2.4 GHz in a stacked shipping containers environment. However, to the best of our knowledge, there is no study available that focuses on the suitability of the 433 MHz band for M2M communications from an energy perspective. This is the main motivation for the work presented in this paper.

The main contribution of this paper is the analytical comparison between the energy efficiency of wireless communications at 433 MHz and 2.4 GHz bands using single-hop and multi-hop communications. Towards this end, we use two well-known channel propagation and realistic energy consumption models. The results presented in this paper show that the reduction of the number of hops at 433 MHz translate into a reduction of the overall network energy consumption. In addition, in harsh radio environments, i.e., where the path-

978-1-4577-1348-4/13/$31.00 ©2013 IEEE

TRANSACTIONS ON EMERGING TELECOMMUNICATIONS TECHNOLOGIES
Trans. Emerging Tel. Tech. (2013)
Published online in Wiley Online Library (wileyonlinelibrary.com). DOI: 10.1002/ett.2672

RESEARCH ARTICLE

On the suitability of the 433 MHz band for M2M low-power wireless communications: propagation aspects

Pere Tuset-Peiró[1,5]*, Albert Anglès-Vazquez[2], José López-Vicario [3] and Xavier Vilajosana-Guillén[1,2,4]

[1] Distributed, Parallel and Collaborative Systems Group, Universitat Oberta de Catalunya, Barcelona, Spain
[2] Worldsensing S.L., Barcelona, Spain
[3] Signal Processing for Communications and Navigation Group, Universitat Autònoma de Barcelona, Cerdanyola del Vallès, Spain
[4] Berkeley Sensor and Actuator Center, University of California, Berkeley, CA, USA
[5] Centre Tecnològic de Telecomunicacions de Catalunya, Castelldefels, Spain

ABSTRACT

The 433 MHz band is gaining relevance as an alternative to the 2.4 GHz band for machine-to-machine communications using low-power wireless technologies. Currently, two standards are being developed that use the 433 MHz band, DASH7 Mode 2 and IEEE 802.15.4f. The article presents propagation models based on measurements conducted at the 433 MHz and 2.4 GHz bands that can be used for link budget calculations in both outdoor and indoor environments depending on node height. The results obtained show that the 433 MHz band has a larger communication range in both indoor and outdoor environments despite the negative effects of having a larger Fresnel zone. In addition, indoor propagation measurements are conducted in line-of-sight and nonline-of-sight conditions to determine the suitability of channel hopping to combat the effects of multipath propagation. Contrary to the 2.4 GHz band, the results show that channel hopping at 433 MHz does not provide any link robustness advantage because the channel coherence bandwidth is larger than the whole band bandwidth, and thus, all channels are highly correlated. Copyright © 2013 John Wiley & Sons, Ltd.

***Correspondence**
P. Tuset-Peiró, Internet Interdisciplinary Institute (IN3), Universitat Oberta de Catalunya (UOC), C/ Roc Boronat 117, E08018 Barcelona, Spain.
E-mail: peretuset@uoc.edu.

Received 21 January 2013; Revised 22 April 2013; Accepted 11 May 2013

1. INTRODUCTION

Machine-to-machine (M2M) communications refer to the set of technologies that are used to connect systems for the purpose of remote monitoring and control without human intervention. To connect end devices with the surrounding infrastructure, M2M communications typically rely on cellular or low-power wireless technologies. For low-power wireless technologies the 2.4 GHz band is commonly used for two main reasons. First, the 2.4 GHz band is part of the Industrial, Scientific and Medical (ISM) bands meaning that it is available worldwide without requiring a license. Second, the IEEE 802.15.4 standard [1] defines the use of the 2.4 GHz band for low-rate wireless personal area networks, and thus, many off-the-shelf transceivers are readily available from different manufacturers. Today, IEEE 802.15.4 networks have already been successfully deployed in various environments, for example, industrial monitoring, but there are several factors that may limit its suitability. For example, in industrial environments, IEEE 802.15.4 suffers from high attenuations caused by concrete walls and metallic surfaces. In addition, in such scenarios, IEEE 802.15.4 networks have to cope with interferences coming from other narrowband and broadband wireless technologies operating at the same band with higher transmit power [2,3], for example, IEEE 802.11 and IEEE 802.15.1.

To overcome these limitations, two approaches are used in IEEE 802.15.4 networks. First, the use of direct-sequence spread spectrum helps improving coexistence with narrowband and broadband interferences. Second, channel hopping also contributes to mitigate the effects of interferences, either narrowband or broadband, and also combats the effects of multipath propagation [4]. In that

ARTICLE IN PRESS

Pervasive and Mobile Computing ▮ (▮▮▮▮) ▮▮▮–▮▮▮

Contents lists available at ScienceDirect

Pervasive and Mobile Computing

journal homepage: www.elsevier.com/locate/pmc

LPDQ: A self-scheduled TDMA MAC protocol for one-hop dynamic low-power wireless networks

Pere Tuset-Peiro [a,d,∗], Francisco Vazquez-Gallego [b], Jesus Alonso-Zarate [b], Luis Alonso [c], Xavier Vilajosana [a,d]

[a] Internet Interdisciplinary Institute, Universitat Oberta de Catalunya, C/ Roc Boronat 117, 08018 Barcelona, Spain

[b] M2M Department, Centre Tecnològic de Telecomunicacions de Catalunya, Av. Carl Friedrich Gauss 7, 08860 Castelldefels, Spain

[c] Signal Theory and Communications Department, Universitat Politècnica de Catalunya, Av. Esteve Terradas 7, C4-204, 08860 Castelldefels, Spain

[d] Berkeley Sensors and Actuators Center, University of California Berkeley, 403 Cory Hall #1774, 94720 Berkeley, United States

ARTICLE INFO

Article history:
Available online xxxx

Keywords:
Internet of Things
Machine-to-Machine communications
Medium Access Control
Frame Slotted ALOHA
Distributed Queuing

ABSTRACT

Current Medium Access Control (MAC) protocols for data collection scenarios with a large number of nodes that generate bursty traffic are based on Low-Power Listening (LPL) for network synchronization and Frame Slotted ALOHA (FSA) as the channel access mechanism. However, FSA has an efficiency bounded to 36.8% due to contention effects, which reduces packet throughput and increases energy consumption. In this paper, we target such scenarios by presenting Low-Power Distributed Queuing (LPDQ), a highly efficient and low-power MAC protocol. LPDQ is able to self-schedule data transmissions, acting as a FSA MAC under light traffic and seamlessly converging to a Time Division Multiple Access (TDMA) MAC under congestion. The paper presents the design principles and the implementation details of LPDQ using low-power commercial radio transceivers. Experiments demonstrate an efficiency close to 99% that is independent of the number of nodes and is fair in terms of resource allocation.

1. Introduction

The Internet of Things (IoT) [1] is a paradigm in which objects are augmented with sensors and actuators and integrated to the Internet through low-power wireless communications and standardized protocols [2] to enable interaction with humans and other machines in a Machine to Machine (M2M) context. Integrating objects with the Internet may be challenging due to available energy constraints and the need to have long-lasting network deployments [3]. It is widely known that the radio transceiver is the element that dominates energy consumption in wireless communication devices [4]. In particular, it is the Medium Access Control (MAC) layer that controls when the radio transceiver has to be powered on, either to transmit or receive, and thus determines the overall energy consumption. According to [5], the energy waste at the MAC layer comes from four sources: packet collisions, packet overhearing, idle listening, and protocol overhead. For that reason, it is key to design MAC protocols that are efficient in these terms.

Two aspects need to be tackled in the design of an efficient MAC protocol [6]: network synchronization and channel access. Regarding the former, MAC protocols can be classified into synchronous or asynchronous depending on whether nodes

∗ Corresponding author at: Internet Interdisciplinary Institute, Universitat Oberta de Catalunya, C/ Roc Boronat 117, 08018 Barcelona, Spain. Tel.: +34 655570294.

E-mail address: peretuset@uoc.edu (P. Tuset-Peiro).

http://dx.doi.org/10.1016/j.pmcj.2014.09.004
1574-1192/© 2014 Elsevier B.V. All rights reserved.

Sensors **2014**, *14*, 13416-13436; doi:10.3390/s140813416

OPEN ACCESS
sensors
ISSN 1424-8220
www.mdpi.com/journal/sensors

3167

Article

Experimental Energy Consumption of Frame Slotted ALOHA and Distributed Queuing for Data Collection Scenarios

Pere Tuset-Peiro [1,*], Francisco Vazquez-Gallego [2], Jesus Alonso-Zarate [2], Luis Alonso [3] and Xavier Vilajosana [1]

[1] Internet Interdisciplinary Institute (IN3), Universitat Oberta de Catalunya (UOC) C/Roc Boronat 117, Barcelona 08018, Spain; E-Mail: xvilajosana@uoc.edu

[2] M2M Department, Centre Tecnologic de Telecomunicacions de Catalunya (CTTC) Av. Carl Friedrich Gauss 7, Castelldefels 08860, Spain; E-Mails: francisco.vazquez@cttc.es (F.V.-G.); jesus.alonso@cttc.es (J.A.-Z.)

[3] Signal Theory and Communications Group, Universitat Politecnica de Catalunya (UPC) Av. Esteve Terradas 7, C4-204, Castelldefels 08860, Spain; E-Mail: luisg@tsc.upc.edu

* Author to whom correspondence should be addressed; E-Mail: peretuset@uoc.edu; Tel.: +34-630-30-34-40 (ext. 5413).

Received: 21 June 2014; in revised form: 16 July 2014 / Accepted: 17 July 2014 / Published: 24 July 2014

Abstract: Data collection is a key scenario for the Internet of Things because it enables gathering sensor data from distributed nodes that use low-power and long-range wireless technologies to communicate in a single-hop approach. In this kind of scenario, the network is composed of one coordinator that covers a particular area and a large number of nodes, typically hundreds or thousands, that transmit data to the coordinator upon request. Considering this scenario, in this paper we experimentally validate the energy consumption of two Medium Access Control (MAC) protocols, Frame Slotted ALOHA (FSA) and Distributed Queuing (DQ). We model both protocols as a state machine and conduct experiments to measure the average energy consumption in each state and the average number of times that a node has to be in each state in order to transmit a data packet to the coordinator. The results show that FSA is more energy efficient than DQ if the number of nodes is known a priori because the number of slots per frame can be adjusted accordingly. However, in such scenarios the number of nodes cannot be easily anticipated, leading to additional packet collisions and a higher energy consumption due to retransmissions. Contrarily, DQ does not require to know the number of nodes in advance

3168

Demonstrating Low-Power Distributed Queuing for Active RFID Communications At 433 MHz

Pere Tuset-Peiro
Universitat Oberta de Catalunya (UOC)
C/ Roc Boronat 117, 08018 Barcelona, Spain
Email: {peretuset}@uoc.edu

Francisco Vázquez-Gallego, Jesus Alonso-Zarate
Centre Tecnològic de Telecomunicacions de Catalunya (CTTC)
Av. Carl Friedrich Gauss 7, 08860 Castelldefels, Spain
Email: {francisco.vazquez, jesus.alonso}@cttc.es

Luis Alonso
Universitat Politècnica de Catalunya (UPC)
Av. Esteve Terradas 7, C4-204, 08860 Castelldefels, Spain
Email: {luisg}@tsc.upc.edu

Xavier Vilajosana-Guillen
University of California Berkeley (UCB)
403 Cory Hall #1774, 94720 Berkeley, United States
Email: {xvilajosana}@eecs.berkeley.edu

Abstract—**This paper presents a demonstrator of Low-Power Distributed Queuing (LPDQ), a MAC protocol targeted at active RFID systems operating at 433 MHz. LPDQ is based on a packet-based Preamble Sampling for network synchronization and Distributed Queuing for channel access. Compared to the MAC protocol defined in the ISO 18000- 7 standard, based on an analog Preamble Sampling and Frame Slotted ALOHA, LPDQ represents a major breakthrough in terms of system performance and energy consumption. At the MAC layer system performance is close to the optimal, e.g., no collisions during data packet transmission, and tag energy consumption can be reduced by more than 10% compared to FSA.**

I. Introduction

Active Radio-Frequency IDentification (RFID) systems operating at 433 MHz are standardized under ISO 18000-7 [1], which uses an analog Preamble Sampling (PS) to wake up tags and Frame Slotted ALOHA (FSA) to manage access to the medium. However, it is well-known that the analog PS is not energy efficient [2] and that the maximum performance of FSA is bounded to around 36.8% due to the effects of contention [3]. Moreover, such efficiency can only be achieved when the number of slots per frame is equal to the number of tags [3], which is unknown a priori. Over the last decade different proposals have been made to improve the performance of FSA in RFID systems [4]. The first approach is to adapt the number of slots per frame based on estimating the tag population from collisions, e.g., double the number of slots per frame if the number of collisions is high. The second approach is to build a query tree based on subsequently querying a sub-group of tags, e.g., first discover the tags and then query each tag independently to avoid collisions. However, both approaches do not achieve a high system performance and low energy consumption due to the time and energy required to estimate the number of tags from collisions or to build the query tree.

Considering that, we have designed and implemented Low-Power Distributed Queuing (LPDQ), a Medium Access Control (MAC) protocol for active RFID systems operating at the 433 MHz band. LPDQ is based on a packet-based PS [2] to achieve tag synchronization and Distributed Queuing (DQ) [5] as the channel access mechanism. In DQ time is organized into fixed-length slots, with each slot having three subperiods (e.g., access request, data transmission and feedback information), and channel access is organized using two queues, the Collision Resolution Queue (CRQ) and the Data Transmit Queue (DTQ). The CRQ ensures that tags that collide during access request subperiod are subsequently organized into sub-groups, whereas the DTQ ensures that only the tag at the head of the queue can transmit during the data transmit subperiod. Finally, a set of rules is used to manage access to both queues, e.g., a tag cannot transmit in the access request subperiod if the CRQ is not empty. For a detailed overview of the DQ operation please refer to [6].

There are two main benefits of using LPDQ. On the one hand, the packet-based PS contains the time at which the tags are expected to wake up, so tags can go back to sleep as soon as a PS packet is received. Compared to the analog PS mechanism of ISO 18000-7, where tags have to listen for the whole duration of the analog preamble, this enables to save energy. On the other hand, the DQ channel access mechanism ensures that the system operates without contention during data packet transmission regardless of the number of tags. Compared to FSA in ISO 18000-7, this enables a system performance close to 100% and to reduce the energy consumption of tags by more than 10% [7].

II. Demonstrator

The demonstrator is composed of 25 active tags and a reader connected to a computer that acts as the system manager, as shown in Figure 1. Both the reader and the tags are based on OpenMote-433, a low-power wireless platform build using COTS (Commercial Off-The-Shelf) hardware. Specifically, OpenMote-433 is based on a Texas Instruments CC430 SoC (System on Chip), which embeds an MSP430 16-bit RISC microcontroller, running at 16 MHz with 4 kBytes of RAM and 32 kBytes of Flash memory, and a CC1101 radio transceiver, which operates at Sub-GHz bands with data rates of up to 600 kbps and support for amplitude and

978-1-4799-3088-3/14/$31.00 ©2014 IEEE